Spatial Variability of Snowmelt Water Balances in a Subarctic Catchment, Wolf Creek, Yukon

A Thesis Submitted to the College of
Graduate Studies and Research
in Partial Fulfilment of the Requirements
for the Degree of Master of Science
in the Department of Geography
Centre for Hydrology
University of Saskatchewan
Saskatoon

By Stephen Edward McCartney

In presenting this thesis in partial fulfilment of the requirements for a Postgraduate degree from the University of Saskatchewan, I agree that the Libraries of this University may make it freely available for inspection. I further agree that permission for copying of this thesis in any manner, in whole or in part, for scholarly purposes may be granted by the professor or professors who supervised my thesis work or, in their absence, by the Head of the Department or the Dean of the College in which my thesis work was done. It is understood that any copying or publication or use of this thesis or parts thereof for financial gain shall not be allowed without my written permission. It is also understood that due recognition shall be given to me and to the University of Saskatchewan in any scholarly use which may be made of any material in my thesis.

Requests for permission to copy or to make other use of material in this thesis in whole or part should be addressed to:

Head of the Department of Geography
University of Saskatchewan
Saskatoon, Saskatchewan (S7N 5A5)

ABSTRACT

The intra-basin variability of snowmelt and meltwater runoff hydrology in an 8 km^2 subarctic alpine tundra catchment was examined for the 2003 melt period. The catchment, Granger Creek, is within the Wolf Creek Research Basin, Yukon which is typical of mountain subarctic landscapes in north-western Canada. The study catchment was segmented into nine internally uniform zones termed Landscape Units (LUs) based on their similar hydrological, physiographic, vegetation and soil properties. Snow accumulation exhibited significant variability among the LUs, with greatest snow water equivalent in areas of tall shrub vegetation. Melt began first on southerly exposures and at lower elevations, yet average melt rates for the study period varied little among LUs with the exception of those with strong aspects. In LUs with capping organic soils, meltwater first infiltrated this surface horizon, satisfying its storage capacity and then percolated into the frozen mineral substrate. Infiltration and percolation into frozen mineral soils was restricted where melt occurred rapidly and organic soils were thin; in this case meltwater delivery rates exceeded the frozen mineral soil infiltration rate, resulting in high runoff rates. In contrast, where there were slower meltrates and thick organic soils, infiltration was unlimited and runoff was suppressed. The snow water equivalent had a large impact on runoff generation as soil storage capacity was quickly surpassed in areas of deep snow, diverting the bulk of meltwater laterally to the drainage network. A spatially distributed water balance indicated that snowmelt freshet was primarily controlled by areas with tall shrub vegetation that accumulate large quantities of snow and by alpine areas with no capping

organic soils. The intra-basin water balance variability has important implications for modeling freshet in hydrological models.

ACKNOWLEDGEMENTS

I wish to thank my supervisor Dr. Sean Carey for his continued guidance, support, and patience. Also, thanks are owed to Dr. John Pomeroy and Dr. Phil Marsh for their assistance

I would also like to thank everyone who helped me in the field.

CONTENTS

List of Tables

List of Figures

List of symbols

ε	emissivity of the snow
σ	Stephan-Boltzmann constant (W m^{-2} K^{-4})
C	coefficient for infiltration equation
DO	dissolved oxygen
INF	infiltration
K	Kelvin degrees
K↓	incoming shortwave radiation to snow (W m^{-2})
L↓	incoming longwave radiation to snow (W m^{-2})
LWC	liquid water content
LX	lower basin landscape unit
NF	north face landscape unit
ORG	organic layer water
ORP	oxidation reduction potential
Q	streamflow discharge (mm) or (m^3 s)
Q_d	energy transported to the snowpack by deposited snow or rain
Q_E	latent heat flux due to sublimation from the snow surface (W m^{-2})
Q_H	sensible heat flux (W m^{-2})
Q_m	energy available for snowmelt (W m^{-2}),
Q_g	ground heat flux
S_0	surface saturation moisture content at soil surface (mm^3/mm^3)
S_I	average soil saturation (water and ice) of the top 0.4 m soil layer at the start of infiltration (mm^3/mm^3)

SCA snow covered area

List of symbols cont'd

SpC specific electrical conductivity (mS)

SS1 short shrub 1 landscape unit

SS2 short shrub 2 landscape unit

SUB sublimation

SWE snow water equivalent (mm)

t time

T_0 infiltration opportunity time (hours)

T_I average soil temperature for a 0.4 m soil layer at start of infiltration (K)

T_s surface temperature of the snow (K)

TS1 tall shrub 1 landscape unit

TS2 tall shrub 2 landscape unit

TS3 tall shrub 3 landscape unit

U internal energy of the snowpack

UX upper basin landscape unit

CHAPTER 1
1.0 INTRODUCTION

Cold region hydrology involves the investigation of water in all its phases and places a particular emphasis on the role of snow and ice within the hydrological cycle. Large parts of Canada and other high-latitude countries remain cold for long periods of time, and hydrological issues related to snow, ice, permafrost and seasonally frozen ground have significant scientific and societal importance (Marsh 1999). Globally, an improved understanding of cold region hydrology is necessary in order to understand the role of the cryosphere in controlling climate and in quantifying global-scale water and energy cycles (Woo et al. 2000) and in the freshwater contribution to the Arctic Ocean (Curry et al. 2003; Wu et al. 2005). In the Canadian context, key scientific issues that remain the focus of investigation are the determination of water balances, scaling of hydrological processes for modeling purposes, runoff generation, chemical transport and transformations, and atmospheric exchange as well as policy issues related to the preservation of cold regions, promoting sustainable land-use, and understanding the impacts of climate and land-use change on water resources (Woo et al. 2000). Of particular interest is the timing, magnitude, and the duration of streamflow as climate change may alter the springtime runoff regimes of snow-dominated basins (Stewart et al. 2004)

The subarctic comprises approximately 30 % of Canada's landmass, lying between the closed canopy boreal forest in the south and the treeless arctic tundra in

the north. Permafrost is widespread in subarctic soils, and vegetation ranges from open canopied boreal forests at lower elevations or latitudes to alpine vegetation at higher elevations or latitudes (Zoltai et al. 1988). In alpine and topographically complex areas, there exists a strong heterogeneity in soils, vegetation, and microclimate that affect the magnitude, direction and timing of hydrological processes (Carey and Woo 2001a). This variability complicates our understanding of these basins, particularly as scale increases from the plot and hillslope scale (where the majority of process-based research is conducted) to the basin-scale where hydrological processes integrate and are manifested in the runoff hydrograph.

Snowmelt is the dominant hydrological event in subarctic catchments. Approximately one-third to one-half of the yearly precipitation is released as snowmelt over the course of three to six weeks, resulting in the largest seasonal flows (Woo 1986). In these catchments, end-of-winter snow water equivalent is highly variable resulting from differential accumulation and redistribution throughout the winter (Benson and Sturm 1993; Pomeroy et al. 1997). Topographic depressions, leeward slopes and shrub vegetation all accumulate additional redistributed blowing snow by reducing wind speeds (Benson and Sturm 1993; Kane et al. 1991; Liston and Sturm 1998; Liston et al. 2002). Over-winter differences in sublimation within basins complicate the snow accumulation regime (Pomeroy et al. 1997; Pomeroy et al. 1999b). After the accumulation phase, the processes governing available energy to melt the snow are highly variable and dependant in part upon: i) topographic influences on radiation and energy receipt (Pomeroy et al. 2003) ii) vegetation effects controlling surface-atmosphere

exchange (Faria et al. 2000; Giesbrecht and Woo 2000; Liston et al. 2002), and iii) landscape heterogeneity and local advection (Granger et al. 2002; Neumann and Marsh 1998). This combination of non-uniform accumulation and melt results in variable quantities of water delivered from different places at different times to the catchment each spring.

During snowmelt, meltwater infiltrates and percolates into frozen soils where it either enters storage and/or is transferred to the stream as near-surface runoff (Carey and Woo 1998; 2001b; Carey and Quinton 2004; Chacho and Bredthauer 1983; Kane et al. 1981; Kane and Stein 1983; Quinton et al. 2004). The presence of ice-rich layers and the organic-mineral soil interface in permafrost soils restricts percolation during melt, enhancing near-surface wetness and runoff (Kane et al. 1981; Carey and Woo 2001b). In contrast, the absence of ice-rich layers in seasonally frozen soils and slopes has typically been cited to explain their limited streamflow contribution during freshet (Slaughter and Kane 1979; Carey and Woo 1998; 2001b). The high storage capacity and transmittance properties of near-surface organic soils has received particular attention in subarctic and tundra environments during melt as saturated horizontal hydraulic conductivity is orders of magnitude greater than the underlying mineral soils and provides a rapid runoff pathway for meltwater (Hinzman et al. 1993; McNamara et al. 1998; Quinton and Marsh 1999; Carey and Woo 2001b).

Research in the subarctic and discontinuous permafrost environments that have focused on processes operating at the plot and hillslope scale may yield detailed process descriptions, but it likely provides more information on site-

specific idiosyncrasies than dominant hydrological controls. As individual hillslopes are smaller than the representative element area of a basin, above which processes scale with increasing area and below which variability does not reflect basin response (Beven 2001), the practice of studying intensively instrumented plots and slopes may not reveal processes operating at larger scales and basin-wide controls on runoff. Ideally, processes should be observed at the scale in which they occur (Blöschl and Sivapalan 1995), and the effect of different scales on hydrological variables is one of the major unresolved issues in hydrological science (McGlynn et al. 2004). While both field and modelling approaches are necessary to increase understanding, future advances in hydrological prediction will grow most rapidly if grounded in observation, physically based relations, and process understanding (Blöschl 2001; Seibert and McDonnell 2002; Sivapalan 2003).

In light of these issues, the general objective of this thesis is to characterize the snowmelt hydrology at the basin scale (8 km^2) and how this variability manifests in the timing and magnitude of meltwater delivery to a discontinuous permafrost headwater stream that drains this basin. This study deviates from previous process research in permafrost catchments in that it attempts to move beyond the application of point-scale data to describe catchment scale hydrology through incorporating a basin-wide investigation emphasizing the spatial variability of water balance components and its impact on freshet streamflow. By defining distinct geographical areas termed Landscape Units (LUs), the specific objectives of this thesis are to:

1. Compare and contrast the magnitude and timing of snowmelt water balance components among LUs and identify the key factors responsible for water balance variability at the catchment scale.

2. Identify the LUs responsible for streamflow generation during the snowmelt period.
3. Establish a distributed snowmelt water balance for the basin incorporating the area-weighted contribution of each LU.

This research will advance cold region hydrology directly by improving understanding of process variability and how this variability at the basin scale integrates to control catchment response. By observing processes at the scale that they operate, it is anticipated that an improved understanding of freshet response will be obtained.

CHAPTER 2
2.0 BACKGROUND

2.1 SNOW ACCUMULATION

Understanding the physical processes controlling snow accumulation and melt is essential for the modeling and/or prediction of snow and runoff hydrology in cold regions (Marsh 1999). Accumulation, which is highly heterogeneous due to the variability in precipitation and redistribution of snow (Benson and Sturm 1993; Pomeroy and Goodison 1997), involves the deposition and temporal storage of snow on the landscape, whereas melt processes involve phase change and the depletion of the accumulated solid precipitation.

Snow deposition and transport are coupled processes that determine the end-of-winter accumulation pattern. Variability in snowcover occurs at a range of scales from micro (<1 m to 50 m), to meso (50 m to a few km), to macro (> a few km) (Pomeroy and Gray 1995). Blowing snow, topography, vegetation and precipitation patterns all influence the end of season accumulation pattern, which in turn impacts the surface albedo, melt and runoff (Benson and Sturm 1993; Liston and Sturm 1998; Liston et al. 2002; Pomeroy et al. 1997).

Snow transported by wind typically accumulates in topographic depressions, on the leeward side of ridges (Kane et al. 1991) and in stands of vegetation which trap snow by reducing surface wind speeds and at larger scales patterns of accumulation are attributed to the redistribution of snow rather than spatial

variability of precipitation (Benson and Sturm 1993; Liston and Sturm 1998; Liston et al. 2002; Pomeroy et al. 1997). For example, from data collected over four seasons in the Wolf Creek Research Basin, Yukon, Pomeroy et al. (1998) determined that snowfall, corrected for under-catch, was near uniform regardless of elevation and that most landscape types received the same amount of snow. However, the end-of-season accumulation variability was large and attributed to the redistribution of snow from one landscape type to another. In the boreal forest, 38-45% of the seasonal snowfall was sublimated from intercepted snow, while 39-79% of snowfall was blown off the alpine tundra. The shrub tundra acted as both a source and a sink where drifts gained 191% and non-drift areas lost 17-46% of the seasonal snowpack to blowing snow and sublimation.

End-of-season snowcover is highly variable in depth in the high arctic (i.e. Woo 1983, Marsh and Pomeroy 1996), in the sub-arctic (i.e. Pomeroy et al 1999a, Carey and Woo 1998) and alpine atchments (i.e. Anderton et al 2003, Pomeroy et al 2004). Thinner snowcovers tend to disappear from the landscape sooner, while deeper snowcovers typically persist longer, and in some cases endure into the next season (i.e. Marsh and Woo 1981; Sturm et al. 2001) resulting in a mosaic pattern of snow and snow-free areas that strongly influence the exchange of energy and mass between the atmosphere and ground, and the subsequent timing, volume and spatial variability of runoff. Snow accumulation not only provides an indication of potential runoff volumes, but has important implications for techniques to estimate areal snow-cover depletion, melt rates and mass balance of snowpacks (Liston 1999; Luce et al 1999; Pomeroy et al 2004).

2.2 SNOWMELT

Snowmelt, one of the most important processes of the hydrological cycle of cold regions (Kane et al. 1992), is a thermodynamic reaction involving phase change in which the amount of melt produced is dependent on the net heat and energy exchange between the snowpack and the environment (Davar 1970). For an idealized plane, the energy equation for the flux of snowmelt from a unit area of snowpack is expressed as (Pomeroy et al 2003):

$$Q_m = (1-\alpha)K\downarrow + \varepsilon(L\downarrow - \sigma T_s^4) - Q_E - Q_H + Q_d + Q_G - \tfrac{dU}{dt}, \qquad [2.1]$$

where (Q_m) is the energy available for snowmelt (W m^{-2}), K↓ is the incoming shortwave radiation to snow (W m^{-2}), ε is the emissivity of the snow, L↓ is the incoming longwave radiation to snow (W m^{-2}), σ is the Stephan-Boltzmann constant (W m^{-2} K^{-4}), T_s is the surface temperature of the snow (K), Q_E is the latent heat flux due to sublimation from or condensation to the snow surface (W m^{-2}), Q_H is the sensible heat flux, Q_d is the energy transported to the snowpack by deposited snow or rain, Q_g is the ground heat flux, and U is internal energy of the snowpack changing over time t.

As the accumulation season ends and the melt season begins, the snowpack temperature typically rises due to increased energy inputs, and the internal energy change is then small (Male 1980). Once the temperature is isothermal at 0°C and the energy deficit of the snowpack is overcome, additional energy inputs will result in phase change from solid to liquid. This is a generalization of the temporal period prior to the onset of snowmelt however as meltwater from cold snowpacks can occur at the surface and move down the snowpack through preferential flow paths

before an isothermal state is reached (Marsh and Woo 1984, Marsh and Pomeroy 1996).

Difficulties in the application of the energy balance equation arise as it is most easily solved at the point scale (i.e. at one given location within a catchment). The relative contribution of the individual components and transfer mechanisms vary greatly with climate, vegetation, topography and other factors (Gray and Landine 1987) and have been the focus of much research over the past several decades (i.e. de la Casiniere 1974; Marsh and Pomeroy 1996; Shook and Gray 1997; Neumann and Marsh 1998; Essery 1999; Tarboton et al. 2000; Granger et al. 2002; Liston et al. 2002; Pohl et al. 2005, Pohl et al. 2006a, 2006b, 2006c). Snowmelt variability exists because atmospheric conditions (i.e. temperatures, radiation regimes, wind patterns) or surface properties (slope, aspect, vegetation, pre-melt SWE) within a catchment are non-uniform, yet complete assessments of snowmelt requires the combined consideration of all these variables if process understanding and prediction is to be achieved (Marsh 1999).

Non-uniform snowmelt leads to spatially variable surface water inputs which affect soil moisture, runoff and ultimately the streamflow regime (Soulsby et al. 1997). Adequate representation of accumulation and melt factors is essential if the timing and magnitude of snowmelt is to be modeled accurately (Bloschl 1999). However, modeling snowmelt at a point, which can be done with great accuracy, differs from modeling snowmelt at the basin scale. Ultimately, spatial variability due to topography largely controls snowmelt dynamics and hence subsequent infiltration, soil water recharge, and streamflow (Seyfried and Wilcox 1995).

Investigating snowmelt at larger scales, Marsh and Pomeroy (1996) working in the transition zone of forest and tundra in the arctic divided a basin into four different classes; 1) drifts, 2) shrub tundra, 3) tundra, and 4) sparse forests. Each area had a unique accumulation and melt regime and comprised different fractions of the basin. As such, each area influenced spring runoff differently in terms of timing and magnitude. Additionally, the role of advected energy from bare ground was analyzed and determined to be a critical factor that influences melt dynamics. By considering the distribution of SWE as it pertained to vegetation and relief and the role of advection, the implementation of these data in a distributed hydrological model produced a more accurate portrayal of basin-scale snowmelt hydrology (Marsh and Pomeroy 1996).

Carey and Woo (2001) described snowmelt and its relation to aspect in sub-arctic, Yukon. The sequence of melt began with the south-facing slope followed by the east and west-facing slopes at approximately the same time, followed by the north-facing slope which was delayed nearly two months after the south. Each cardinal slope differed with respect to vegetation and soils which when combined with the ablation regime, varied and combined to control snowmelt runoff and spring-time streamflow.

Knowledge of snowmelt dynamics in a continuous snowcover is of only partial use in heterogeneous terrain. Snowmelt investigations in forested areas have highlighted the complications associated with describing combined or aggregate energy fluxes for snow-covered and vegetated surfaces (i.e. Harding and Pomeroy 1996; Woo and Giesbrecht 2000). Pomeroy et al. (2003) considered the energy and

atmospheric exchanges from snow-covered hillslopes to be more complex than a continuous snowcover because the hillslope contained a mixture of snow, bare ground, shrubs, rocks, and trees. While formulating an approach to model the energy exchange with varying slope angle by means of geometric corrections, they found a dramatic difference in energetics and rates of snow ablation over roughly similar shrub-tundra surfaces that are level. During the early melt season, with warm and sunny conditions, the south face rate of ablation was three times higher than the valley bottom, which itself underwent ablation twice as fast as the north-facing slope. Later, once the south face had completely become snow free the rate of ablation for the north face and valley bottom were nearly identical. Shrub exposure and subsequent albedo decay was thought to have played a role in the rapid ablation found on the south face.

In the snowmelt period, the surface temperatures of bare ground areas have been reported to exceed 40ºC (Liston 1995), while melting snow surfaces do not exceed 0ºC. Combined with differences in albedo and surface roughness between snow-free and snow-covered areas, locally-advected energy can significantly enhance melt (i.e. Weisman 1977; Neumann and Marsh 1998). Quantifying the advection of sensible heat from field investigations is complicated because of an evolving surface state with respect to the changing shape and size of snow-covered and snow-free surfaces, and highly variable meteorological conditions (Shook 1995). In light of these difficulties, Neumann and Marsh (1998) found the portion of sensible heat advected to snow patches declined with decreasing snowcover. Modeling studies (i.e. Essery 1997; Liston 1995; Shook 1995; Marsh et al. 1999)

have shown that local advection increases meltrates with the greatest effect just downwind of the snow patch edge. Recently, Granger et al. (2002) developed a parametric expression to calculate the amount of energy removed by a snow patch as warm air moves over it; however applications of this expression have not been reported.

2.3 FROZEN SOIL INFILTRATION

Infiltration into frozen soils has been investigated globally (i.e. Kuzic and Bezmenov 1963; Komarov and Makarova 1973; Kane and Stein 1983; Granger et al. 1984; Gray et al. 2001) and involves the combined heat and mass transfer through porous media with phase change. Zhao et al. (1997) describes the heat and mass transfer processes as having two forms; transient and quasi-steady state. The transient period occurs immediately after the addition of water when both the infiltration rate and heat transfer rate decline rapidly. During this period, liquid permeability increases while the capillary pressure gradient decreases and energy is added to the system primarily by conduction to increase soil temperature and melt ice. The quasi-steady-state period follows the transient period in which the infiltration rate gradually decreases with time and the rate of heat transfer reaches a steady state. Additional theoretical modeling investigations of frozen soil infiltration have been conducted by Engelmark and Svensson (1993) and Flerchinger and Saxton (1989a, 1989b), highlighting the complexities of phase change, and heat and mass transport and hydraulic property changes.

For agricultural prairie soils, Granger et al. (1984) categorized frozen soil infiltration into three classes based primarily on soil type; 1) *restricted-impervious*

where most of the SWE goes to runoff, 2) *unlimited* where the soil is capable of infiltrating the entire SWE and, 3) *limited* where infiltration is governed primarily by the SWE and the ice content of the soil at the time of melt. Using these classes, Granger et al. (1984) successfully developed and applied an empirically based equation to estimate cumulative frozen soil infiltration based on the degree of air-filled pores and the SWE into a 0.3 m column of soil.

Advancing on the work of Gray et al. (1985), Zhao and Gray (1999) and Gray et al. (2001) showed the sensitivity frozen soil infiltration to specific soil and hydrological parameters. Soil moisture content, soil texture, soil temperature, SWE, and snowmelt rates were all identified as key factors in controlling infiltration into limited class frozen soils. Zhao and Gray (1999) estimated areal snowmelt infiltration as:

$$INF = CS_0^{2.92}(1 - S_i)^{1.64}\,[(273.15 - T_I)/273.15]^{-0.45} t_0^{0.44} \qquad [2.2]$$

where C is a correction coefficient, S_0 is surface saturation moisture content at soil surface (mm^3/mm^3), S_I is average soil saturation (water and ice) of the top 0.4 m soil layer at the start of infiltration (mm^3/mm^3), T_I is average soil temperature for the 0.4 m soil layer at the start of infiltration (K), and T_0 is infiltration opportunity time (hours). The amount of water available for infiltration is taken as SWE.

In a uniform soil profile, assuming the absence of large-macropores or cracks, there is an inverse relationship between infiltration and the total water content prior to infiltration (Kuzic and Bezmenov 1963; Shipak 1969; Kane and Stein 1983; Zhao and Gray 2001) making it the major property of a frozen soil governing its ability to absorb and transmit water (Granger et al. 1984; Gray et al.

2001; Zhao and Gray 1999). Zhao et al. (1997) present initial saturation, or average soil saturation, S_I, as the average volumetric soil moisture (water and ice) divided by the soil porosity, which describes the total pre-melt soil water content for the top 400 mm of the soil profile. This initial saturation serves two functions in controlling infiltration: 1) when initial saturation is high, the capillary pressure gradient is decreased leading to lower amounts of infiltration, and 2) when initial saturation is quantified as a fraction of total porosity; a measure of the available air-filled pore space for infiltration water is given. In their expression, lower initial saturation yields a larger effective porosity and greater amounts of infiltration.

Moisture content at the soil surface is an additional control on frozen soil infiltration as greater amounts of water at the surface result in a larger hydraulic pressure gradient, increasing total infiltration (Zhao and Gray 1999). During ablation, the rate of meltwater delivery to the soil affects the moisture content at the surface and subsequently total infiltration (Gray et al. 2001). It is suggested that because the infiltration rate of most frozen soils is low, it can be assumed that a saturated surface exists when a snowcover ablates rapidly (melt rate > infiltration), yet when ablation is slow or when there are large fluctuations, the surface is unsaturated (melt rate < infiltration).

The coefficient (C) is applied to account for the difference between model and natural systems and varies between 1.14 and 2.10 for constant surface saturations as shown in the original studies (Gray et al 2001; Zhao and Gray 1999). The coefficient can be adjusted for a decrease in surface saturation.

Soil temperature has been identified as secondary influence on frozen soil infiltration (Granger et al 1984; Gray et al 2001; Komarov and Makarova 1973; Zhao et al 1997). Zhao et al. 1997 showed that a higher initial soil temperature was associated with a greater volume of cumulative infiltration. Additionally, it was identified that the liquid permeability of the soil declined as a greater ice content was found with lower temperatures. Part or all of the water infiltrating a soil below freezing will refreeze, the amount being a function of the energy status of the soil and the water, the mass of free water available, and the energy exchanges between the media (Mackay 1983).

In Eq. 2.2 snow water equivalent acts as a control on infiltration as it and the ablation rate determines the infiltration opportunity time (t_0) and the rate of meltwater delivery to the soil surface, influencing surface saturation.

In some literature, frozen soil is considered a largely impermeable barrier (Williams and Smith 1989), yet field investigations demonstrated that flow through frozen soils both vertical and laterally is an important processes during freshet (Kane and Stein 1983; Marsh 1988; 1993). The fraction of vertical and lateral flow influences the timing and magnitude runoff and the energy regime of the soil (Marsh 1993), making the determination of frozen ground infiltration essential to hydrometric investigations in cold regions. In the Mackenzie Delta region, Marsh (1988) measured 75 mm of infiltration in a 400 mm soil profile described as silts with 15 to 30% organic matter. In the Yukon, Burn (1990) found infiltration ranged between 10 and 70% of the pre-melt SWE. Greater amounts of infiltration were documented in the coarsest-grained soils that were unsaturated during the preceding

fall, providing evidence that low moisture contents enhance frozen soil infiltration. Also in the Yukon, Carey and Woo (1998) highlighted the importance of impermeable frozen layers on vertical versus lateral flow processes during melt. On an ice-rich organic-covered permafrost hillslope, approximately 155 mm of the 187 mm pre-melt SWE (83%) was runoff, whereas across the river valley in seasonally frozen unsaturated mineral soils, 100 % of SWE (137 mm) infiltrated frozen soils. In the high arctic, Marsh and Woo (1993) measured between 9 and 12 mm of infiltration which represented only 6% of each initial snowpack. This study applied the equation developed by Granger et al. (1984) in the prairie region, in a permafrost region to estimate infiltration. The equation over-predicted infiltration considerably. It was suggested this over-prediction was because the soil temperature was colder and the SWE, which ranged from 150 to 289 mm, was much larger than where the equation was developed.

Despite this work, there remains some uncertainty as to the applicability of the classification of Granger et al. (1984) to cold regions where different soil types exist from those in temperate environments. Organic soils, which are ubiquitous to permafrost regions, would initially be classified as unlimited due to their large porosity and unsaturated condition prior to melt. However, these soils are typically only 0.1 – 0.3 m thick, whereupon a sharp transition in permeability exists at the organic/mineral interface (Carey and Woo 2001; Quinton and Marsh 1999; Slaughter and Kane 1979). Field studies indicate that at some point after infiltration occurs into these soils, it becomes more restricted, shifting soils towards the limited and restricted class. It can therefore be hypothesized that the overlying organic

layer should be classified as an unrestricted soil overlying mineral soil of limited class. In this way, the equation of Zhao and Gray (1999) may be applied to percolation from the organic to mineral substrate as the rate of meltwater delivery to this interface has been shown to approximate the rate of meltwater delivery to the surface (Carey and Woo 1998; Hinzman et al. 1993).

Upscaling point infiltration estimates to larger areas has only recently been explored. Gray et al. (2001) presented conceptual model for scaling infiltration during ablation and suggests that macro and meso scale infiltration can be estimated based on the spatial distribution of soil moisture and SWE. Janowicz et al. (2002) attempted to characterize the primary governing parameters of snowmelt infiltration, SWE and pre-melt soil moisture, in a northern boreal forest, shrub-tundra, and alpine tundra landscapes with respect to topography and vegetation. Results showed little relation between vegetation, topography and the patterns of snow accumulation and soil moisture, yet reasonable success was achieved in field-testing the parametric estimate of frozen soil infiltration of Zhao and Gray (1999).

2.4 RUNOFF GENERATION

In nival basins snow comprises a large proportion of the total annual precipitation (Kane et al. 1991; Woo et al. 1983), and snowmelt water dominates the annual streamflow hydrograph, moving much of the annual precipitation from the catchment to the stream over a short period of time (Carey and Woo 2001b; Marsh and Woo 1981; McCann and Cogely 1972; McNamara et al. 1998; Woo 1986). Although large summer rainfall events occur that may exceed snowmelt rates, the increased active layer storage from thaw and higher summer

evapotranspiration rates reduce the fraction of rainfall reaching the stream (Kane et al. 1992).

Runoff mechanisms and pathways during the snowmelt season vary geographically but depend largely on the characteristics of melt and soil antecedent conditions (Dunne and Black 1971; Marsh and Woo 1981; Shanley and Chalmers 1999). The infiltration capacity of frozen ground (see section 2.2) has been cited as a key to determining snowmelt runoff timing and volume (Westerstrom and Singh 2000), which is influenced by the thermal and physical properties of the ground, soil water status (both solid and liquid), soil temperature, and the amount and rate of meltwater release (Gray et al. 2001).

With the exception of the high arctic, most permafrost and discontinuous permafrost regions have a distinct soil profile where an organic soil layer of variable thickness overlies a mineral substrate (NRC 1995). These two layers contrast each other with regard to their hydraulic properties, greatly affecting runoff. Typically, the organic soil can vary in thickness from a few centimetres to more than half a metre (Carey and Woo 1998; Dingman 1973; Quinton and Marsh 1999; Slaughter and Kane 1979) and is highly porous and with hydraulic properties (ie. conductivity, specific yield, retention) that vary sharply with depth. Below the organic layer, mineral soils exhibit reduced porosities and trasmissivities, impeding deep percolation and promoting a perched water table and lateral flow. Additionally, ice-rich layers preferentially form at the organic-mineral interface, further restricting percolation and enhancing saturation during melt (Carey and Woo 1998; Price and Dunne 1976). This characteristic soil profile results in a two-

layer flow system that is defined by the depth and properties of the organic and mineral soils, which controls the rate, volume and pathway of water flow to the drainage network (Carey and Woo 2001a; Quinton and Marsh 1999).

Within the organic layer, hydraulic conductivity declines several orders of magnitude from hundreds of metres per day to several metres per day within the top 0.3 m (Quinton et al 2000; Quinton et al. 2004). When the water table lies within the organic layer, this range of conductivities results in the rapid delivery of water via preferential flow and matrix flow (Carey and Woo 1999; Quinton et al. 2000) which give rise to flashier responses in the streamflow at the basin scale (Dingman 1973). Within the organic horizon, layers are often distinguished between a hydrologically active acrotelm and a humified and compacted catotelm (Carey and Woo 2001a; Woo and Marsh 2005). These definitions are adopted from Russian literature on the variation in hydrological functioning of peat wetland soils (Ivanov 1959). The differentiation in hydraulic properties provides a reference point to distinguish between quick and slow flow pathways within the organic layer. As the saturated thickness decreases and water tables descend following melt atop the frost, the amount of quickflow declines while slow flow within the catotelm continues. Quickflow and slowflow are broad terms used to describe runoff that is conveyed to the stream over short or long periods of time that occur via different mechanisms. Preferential flow, which can contribute to quickflow, is the uneven and often rapid movement of water through porous media, characterized by regions of enhanced flux such that a small fraction of media (such as macro-pores, soil pipes, root holes, cracks) participates in most of the flow. When snowmelt exceeds

the infiltration capacity of the soil (termed infiltration excess), overland flow results or when the water table rises to the surface and additional melt generates saturated overland flow. In areas with organic soils, saturated overland flow is the predominant method of surface runoff generation as porous near-surface organic soils are typically able to infiltrate meltwater (Burns 1990; Quinton and Marsh 1999; Quinton and Gray 2000). As the water table continues to descend following melt, it falls into mineral soils, where slow runoff pathways also predominate. This system of quick and slow flow based on depth-dependent saturated hydraulic conductivities predominates the cold-regions runoff literature, and the majority of runoff is attributed to organic layer quickflow (Carey and Woo 2001a; Quinton et al 2000).

One of the more frequent causes of overland flow found in high latitude areas are due to the presence of large snowpacks or drifts that persist well into the summer or last year-round (Lewkowicz and Young 1990; Marsh and Woo 1981; Woo and Steer 1982). As these drifts melt, the large volume of water released saturates the slope beneath the drift, causing additional melt to leading to overland flow to the stream. Additionally, because of the persistence of these drifts, flow can be sustained well after the main melt period. Dunne et al. (1976) documented overland flow in areas where a thin organic layer (less than 0.1 m) caps a mineral soil with concrete frost. Meltwater not being able to infiltrate into the frost layer resulted in lateral flow through a saturated layer at the base of the snowpack. This process is analogous to both infiltration excess and saturated overland flow as

subsurface layers impede percolations while saturation occurs up from the impermeable organic/mineral interface.

Carey and Woo (1999) studied the hydrology of two slopes in subarctic Canada, contrasting runoff regimes of a north slope underlain with permafrost and south facing slope with seasonal frost only. No runoff was observed on the south-facing slope because of the high infiltration capacity of the underlying soils allowing meltwater to percolate deep into the frozen soil column. On the north-facing slope, vertical drainage quickly led to saturation of the frozen organic layer since a high ice-content at the organic/mineral interface prevented deeper drainage. This promoted lateral flow in rills, gullies and small depressions that originated from the saturated layer in the organic mat above the mineral soil. The behaviour of the south-facing slopes is consistent for other northern regions (Slaughter and Kane 1979; Chacho and Bredthauer 1982). Where an extensive organic cover exists, overland flow is suppressed due to high infiltration capacities (Carey and Woo 2001; Quinton 1997).

Preferential flow is observed to be ubiquitous in high-latitude catchments. Quinton and Marsh (1999) studied subsurface flow in the tundra region of the Canadian arctic and found that flow predominates in the peat of the inter-hummock channels and soil pipes and may occasionally reach velocities similar to surface runoff (Quinton and Marsh 1999). In hummocky permafrost terrain, mineral earth hummocks are segregated by peat filled inter-hummock channels. Because of the large difference in hydraulic conductivity, preferential flow within the inter-hummock channels becomes the dominant runoff-mechanism capable of delivering

0.1 to 1.0 m^3 day^{-1} per unit length via matrix flow (even movement of water through the soil matrix while following an average flow path through soil) and pipeflow in the upper organic layer (Quinton and Marsh 1999).

Soil pipes have also been observed in the sub-arctic (Carey and Woo 1998; 2000; Gibson et al. 1993), and Carey and Woo (2000) present a conceptual model of pipeflow of greatest contributions during snowmelt (*ca.* 20 % of runoff) when the water table is near the surface interacting with soil pipes and enhanced hydrological connectivity allows soil pipes to drain the saturated thaw zone.

Investigations at the plot or hillslope scale have been helpful in describing runoff processes and mechanisms in a two-dimensional form. Difficulties arise in the application of runoff processes across an area. Investigations of snowmelt and runoff document the dynamic response of runoff volumes and subsequent streamflow in response to a changing water table which is largely controlled by the rate of snowmelt input, hillslope length, and the slope (Quinton and Marsh 1999). However, non-uniformity in catchment properties plays a role in determining the areal coverage of meltwater available for runoff. As a result, the size of the contributing area and subsequent volume of water available for runoff is the integration of the SWE and rate of snowmelt, the organic layer thickness controlling storage and conductivity, the antecedent hydrologic and physical conditions of the underlying mineral soil which also control infiltration, storage, and transmission and the effective linkages of the contributing area to the stream. In an attempt to model subsurface flow in a permafrost environment, Quinton and Marsh (1999) divided the study area into two zones based on the organic layer thickness; 1) the

near-stream area (10% area), characterized by thicker peat, but decreasing in thickness away from the channel and 2) uplands (90% area), where the peat is relatively thin. Their field investigations showed that streamflow response was largely controlled by the elevation of the water table, and the lateral extent of the saturated layer. When the water table is in the highly conductive organic layer, subsurface flow from areas further away in the uplands was able to reach the channel quite rapidly because of the shortened lag time. However, the streamflow response to runoff is minimal when the water table is low as water is only entering the stream as slow-seepage in the poorly conducting layers of the soil. It is not until the saturated layer increases in thickness to a level where rapid subsurface flow could occur through the highly conductive upper layers, or soil pipes did the hydrograph show a much larger response. The width of the near-stream area comes into play as the water storage capacity increases with increasing width and results in a greater lag time because of the greater attenuation of runoff from upslope areas. The authors suggest that the variability of the near-stream area width should be accounted for when attempting to model runoff from basins similar to their field site. Quinton and Marsh (1999) model results were shown to capture the primary features of the measured hydrograph, but accurate quantification of the areal extent of the saturated layer, the elevation of the water table in the near-stream area, and the spatial variation in the width of the near stream area was difficult to obtain above the hillslope scale.

2.5 WATER BALANCES

Mass balances combine the various hydrologic processes active in a given catchment and in the simplest form can be expressed as (Woo 1986):

$$P - E - Q = \Delta S \qquad [2.3]$$

where P is precipitation (rain and snow), E is evaporation and snow sublimation, Q is discharge and ΔS is change in basin storage. Woo (1986) suggests that when quantifying the water balance components errors may arise because of precipitation inaccuracies and underestimates, runoff cannot always be accurately determined due to a large volume of water leaving in a short period of time through what may be a less than ideal channel for measurement, and evaporation is difficult to measure during the melt period because the ground is mixed with patches of snow, standing water and bare ground. Process studies (i.e. melt, runoff, infiltration etc) in northern regions have had a long history of investigation while the examination of spatial and temporal variability of the water-cycle and water-balance has received less examination.

Metcalfe and Buttle (1999) analyzed sub-basin water balance in a boreal forest catchment with discontinuous permafrost and described large differences in fluxes controlled by snow accumulation, rainfall characteristics, thaw depths and storage properties. Two other mass balance studies have been carried out within the Wolf Creek Research Basin. Carey and Woo (2001) conducted a study in the subalpine open woodland assessing the water balance variability of 4 slopes for the snowmelt and summer period. For the snowmelt period the largest mass balance contrast was observed between the north and south-facing slope, where nearly three

quarters (155 mm) of the north facing snow and ice mass was attributed to runoff, while no runoff occurred on the south face. Just over one-half and one-fifth of the snowmass was attributed to runoff on the east and west slope respectively. Sublimation was greatest on the north face as snow persisted much longer. At the end of the snowmelt period the change in storage, calculated as the residual, compared well with measurements of soil moisture recharge. Evapotranspiration was the largest water loss from all hillslopes which exceeded the summer rainfall inputs and depleted the soil moisture recharged by snowmelt.

Additional work in the Wolf Creek Research Basin (Pomeroy et al. 1998) documented the snow mass balance of sites representative of a white spruce forest, an alpine tundra plateau, and a shrub-tundra valley bottom with specific reference to blowing snow. This study enforced the notion that snowfall does not equal accumulation due to the losses attributed to sublimation and blowing snow resulting in a decrease in potential runoff.

CHAPTER 3
3.0 STUDY AREA
3.1 GENERAL DESCRIPTION

The location of this study was in the west-central region of the Wolf Creek Research Basin, 15 km south-east of Whitehorse, Yukon, Canada. Existing on the eastern fringe of the Coast Mountains in the zone of discontinuous permafrost, the area represents snow regimes found in the northern boreal cordillera of western Canada (Pomeroy et al. 1998). Ranging in elevation of 750 to 2550 m and draining approximately 195 km^2, it forms part of the headwater region for the Yukon River and is generally comprised of three main land-cover types of similar proportions; alpine tundra, shrub taiga, and boreal forest with mixed spruce, pine and poplar stands (Granger 1998). Climatically the area is described as subarctic-continental and climate normals (1971-2000) from the Whitehorse airport, approximately 20 km to the north, indicate a large annual temperature range with average January and July temperatures of -17.7 ˚C and +14.1 ˚C respectively. Mean annual precipitation is 267.4 mm, of which 145 mm falls as rain (Environment Canada). Investigations in this area however suggest that precipitation may be upwards of 25-35% greater than the city of Whitehorse itself.

Geographically, the investigation was contained within the informally named Granger Basin. Lying slightly to the north by north-east of Mt. Granger (2080 m), Granger Basin was selected as the study basin due to its representativeness of the subarctic cordilleran landscape. The geological

composition is primarily sedimentary consisting of sandstone, siltstone, limestone and conglomerate. A mantle of glacial till overlays this and ranges from centimeters to up to 10 m in thickness. The lower elevations of the basin are covered with fine textured alluvium while higher elevations have shallow colluvial deposits with frequent bedrock outcrops (Mougeout and Smith 1994). Permafrost is found under the north-facing slopes and higher elevation areas while seasonal frost occurs on the southerly aspects. Lewkowicz and Ednie (2004) indicate that approximately 70-80 % of the basin is underlain with permafrost. In the lower elevations, a surface organic layer exists varying between 0.15 and 0.3 m based on aspect and catchment position (Quinton et al. 2004).

The headwater of the stream originates at the base of Mt. Granger and drains a creek in a northeasterly direction for nearly 3 km (Figure 3.1). To the west of the creek lies a large valley slope with a gentle gradient of approximately 15˚ and to the east is a large plateau. Vegetation is typically thickest in the stream channel and consists predominantly of assorted Willow (S*alix spp*) and Alder (*Aldus spp*.) On the eastern plateau, a tundra surface exists with interspersed hummocks, grasses, sedges and the occasional shrub stand. On the western slope, vegetation decreases with elevation, and at higher elevations near the catchment fringe the rocky ground is primarily lichen-covered tundra littered with only small areas of grasses and sedges. About two-thirds down the valley the stream turns easterly producing a contrasting valley with north and south facing slopes. Lower in elevation there is an increase in the presence of shrubs and in some places the creek is not discernable through the dense vegetative cover. It is in this valley where only a few sub-alpine

fir trees (*Abies lasiocarpa*) exist on the south facing slope. The catchment outlet drains approximately 8.01 km^2.

3.2 LANDSCAPE UNIT DESCRIPTION

Within Granger Basin 6 distinct areas, termed Landscape Units (LUs), were selected in the field based on accessibility and contrasting properties such as vegetation, aspect, pre-melt accumulation, and elevation (Figure 3.1). The first two LUs, one south-facing (SF) and one north-facing (NF) slope, were selected for their contrasting aspect, close proximity, and because they had been used in previous investigations. The third LU was the short-shrub plateau (SS) selected for its low-lying vegetation or lack there-of and the small pre-melt accumulation. The fourth LU was the tall shrub tributary (TS) selected for the large accumulation, presence of taller vegetation, connectivity to the main Granger Creek via water-tracks or very small tributary channels, and its contrasting properties to the SS LU. There were three tall shrub tributaries selected for study; TS1, TS2, and TS3. The fifth LU was the upper basin tundra, UX, which was selected for its cooler temperatures, larger accumulation, and the large area it comprised. The sixth landscape unit was the lower basin shrub tundra, LX. This LU contrasted the UX because of its warmer temperatures, lower accumulation and the presence of shrub vegetation. The location of the transects representing each LU is shown in Figure 3.1, while geographic co-ordinates for measurement transects within the LUs are listed in APPENDIX A and photographs of individual Landscape Units are listed in APPENDIX B.

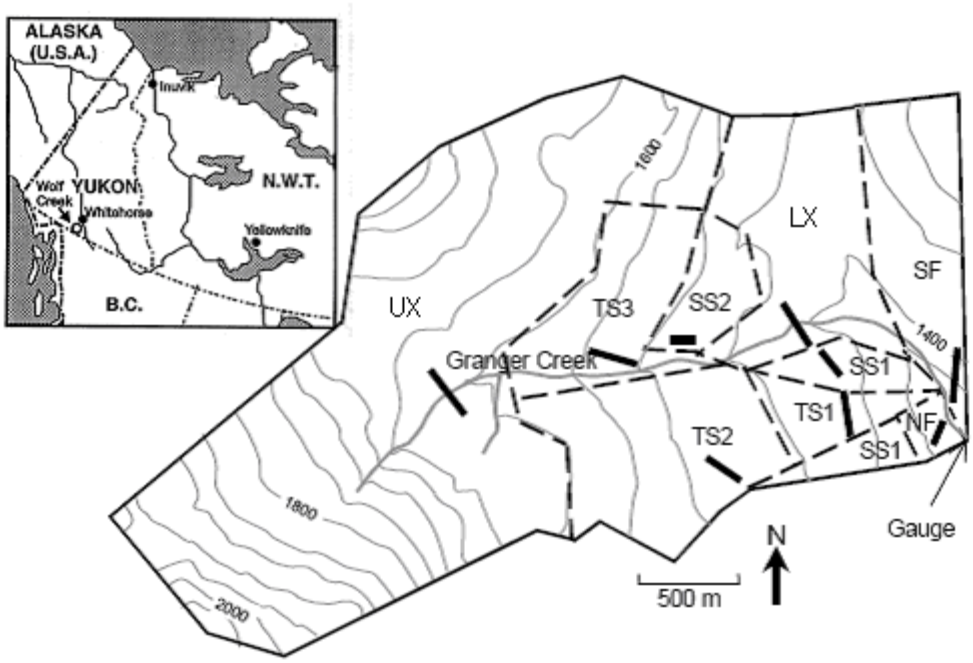

Figure 3.1 Study catchment (Granger Basin). LUs are demarcated with dashed lines and heavy solid lines are the measurement transects.
Inset shows location in Canada.

Table 2.1 Landscape Unit Characteristics. Percentage area, elevation range, organic layer thickness and vegetation height for LUs. Organic layer thickness and vegetation height values represent the mean +/- one standard deviation.

	Area (%)	Elevation Range	ORG (thickness m)	Veg (height m)
SS1	5	1440-1480	n/a	0.38 (+/- .16)
SS2	6	1500-1540		0.39 (+/- 0.38)
TS1	4	1400-1480	0.14 (+/- 0.07)	0.78 (+/- 0.45)
TS2	7	1500-1600	0.12 (+/- 0.09)	0.62 (+/- 0.67)
TS3	7	1540-1600	0.16 (+/- 0.08)	0.70 (+/- 0.74)
UX	46	1600-2080	n/a	0.12 (+/- 0.12)
LX	13	1440-1500	0.06 (+/- 0.09)	0.59 (+/-0.19)
SF	9	1350-1480	0.12 (+/- 0.12)	0.43 (+/- 0.26)
NF	2	1350-1440	0.26 (+/- 0.1)	1.1 (+/- 0.46)

3.2.1 NORTH AND SOUTH

The north (NF) and south-facing (SF) slopes located near the stream outlet, separated by the creek and a thin riparian zone had been utilized in previous investigations (e.g. Pomeroy et al. 2003; Carey 2003, Carey and Quinton, 2004; 2005; Quinton et al. 2004). The north-face underlain by permafrost had a slope of 17.5º (Pomeroy et al. 2003) with sandy textured till soils covered by an organic layer containing peat, lichens and mosses. Average organic layer thickness of 0.26 +/- 0.1 m (n=30), and the active layer ranges from several decimeters to over 1 m near the base of the slope. The average height of shrub vegetation was 1.1 +/- 0.46 m (n=20). The north-face represented approximately 2% of the basin area. The south-face had a slope of 13º and is underlain by seasonal frost (Carey and Quinton 2004). The organic layer was thinner than that of the north-face with an average of 0.12 +/- 0.09 m (n=20) and decreased in thickness upslope. The south-face LU represents approximately 9 % of the basin.

3.2.2 SHORT SHRUB

Short shrub LUs (SS1, SS2) were selected for areas representing generally flat tundra, with minimal amounts of tall vegetation and ordered with increasing elevation basin position. SS1 was located on a level plateau in the lower third of the basin to the south above the creek. SS2 was in the upper third of the basin on a slightly inclined plateau facing to the east. The vegetation in these areas was dominated by lichens, grass and sedges. Short willows were found in isolated areas as only 30% of the surveyed area contained vegetation greater than 0.35 m. The

organic layer is estimated at less than 0.05 m. SS1 and SS2 each represented 6% of the basin.

3.2.3 TALL SHRUBS

Tall shrub areas were selected as low-lying depressions filled with taller shrub vegetation. They combined to cover 18 % of the study basin area. Within these low-lying areas were small tributary streams or perennial channels termed water tracks (i.e. Hinzman et al. 1993, McNamara et al 1998) that drain into Granger Creek. TS1, located due east of SS1, was located closest to the outlet, while TS2 and TS3 were located further upstream respectively. Ground cover was hummocks and taller shrubs with an average height of 0.78 +/-0.4 m (n=48). Organic layer thickness for all three LUs was 0.14, 0.12, and 0.16 m respectively for TS1, TS2 and TS3. TS1 represented 4% of the basin. TS2 was also in a small depression with an ephemeral stream, yet located near the middle of the basin to the south of TS1. The average height of the shrub vegetation was 0.61 m +/-0.6 m (n= 36) and covered 7% of the total area. TS3 was in an area of shrubs highest in the basin and represented 7% of basin area. The contributing channel was not as incised as the others but was prone to significant over-land and inter-hummock flow. The average shrub height was 0.74 m +/- 0.7 m (n= 36).

3.2.4 UPPER AND LOWER BASIN

The upper-basin tundra, UX, in the headwater region of the catchment, was located at a higher elevation than all other transects and represented an area of the basin influenced by cooler conditions. Little shrub vegetation exists and the

groundcover is composed of grass, lichens and mosses with much exposed soil. The average vegetation height was 0.12 +/-0.2 m (n=56) m. This area, the largest of all land-cover types, was approximately 46 % of Granger Basin. The lower-basin shrub tundra, LX, represented 13% of total basin area and was located immediately before the stream turned east toward the outlet. This area was warmer than the UX LU and contained shrubs with an average height of 0.59 +/- 0.19 m (n= 45).

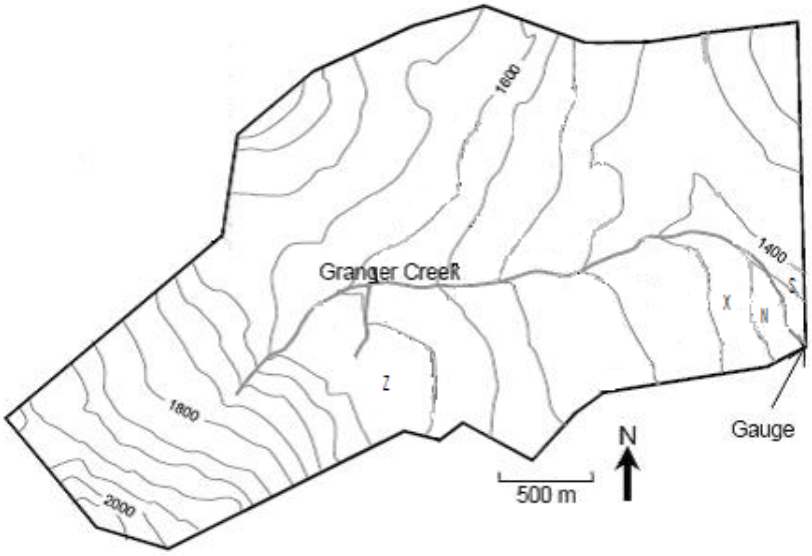

Figure 3.2 Study catchment (Granger Basin) and pre-existing meteorological stations. S is the south-facing slope station, N is the north-facing slope station, X is the plateau station and Z is the upper-basin station.

CHAPTER 4

4.0 METHODS

The timeframe for this investigation was from 1 April to 29 June, 2003 (Julian Day 100 to 180). During this time a number of methods and measurements were utilized and are described in detail below.

4.1 SNOW SURVEYS

Manual surveys provided snow depth and density data for all LUs throughout the study period. The objective of these surveys was to collect information to enable the estimation of: i) the quantity of snow that had accumulated prior to spring melt; ii) its spatial distribution within the catchment, and iii) the rates of melt and changes in the spatial distribution of SWE over the melt season.

Snow depth was measured using a G3 2.40 m Avalanche Tech Probe and snow density was determined using a Canadian MSC Aluminum snow-corer (I.D. 7.05 cm). Two snow-pits were dug in the drift on the north-facing slope and approximately twice weekly, measurements of density were obtained by weighing a control volume (143 cm^3) of snow at 10 to 20 cm intervals for the entire drift profile. Each time the pits were sampled the old pit face was sheared off, exposing the un-weathered snow. A large solar blanket was placed over the pit in between sampling periods to minimize melting. These values were then averaged and used

in the SWE calculations for depths beyond the capacity of the MSC sampler. Surveys were carried out along specific transect locations for each land-cover type. The start and end points of each transect were clearly established with large stakes and flagged for easy location and geo-referenced with a Garmin Etrex Global Positioning System. Depth measurements were carried out at 5 m intervals established using a tape measure and marked with a small fluorescent flag to assist in the relocation of each point for each subsequent measurement. When possible the same hole was used for successive measurements. Transect length varied from 120 m to 275 m and the average snow depth for each transect was determined after every survey and included 0 m (snow-free) depths in the calculation when applicable. Sampling frequency varied among land-cover types based on logistical constraints. Not including 0 m snow depths, 2990 manual depth measurements and 937 SWE measurements were obtained.

4.2 SWE ESTIMATES

A linear relationship was established between depth and density to estimate SWE for the each transect. The MSC snow sampler gave units of SWE in centimetres, which was converted to density. For each available point, where both a depth and density measurement was obtained, depth was plotted against density and a least-squares linear regression was used to estimate density for all depths. Transect SWE was then estimated by multiplying the density from the regression equation by the depth of snow and divided by the density of water. The same depth/density relationship was applied to all transect points for each particular day of measurement (Figure 4.1).

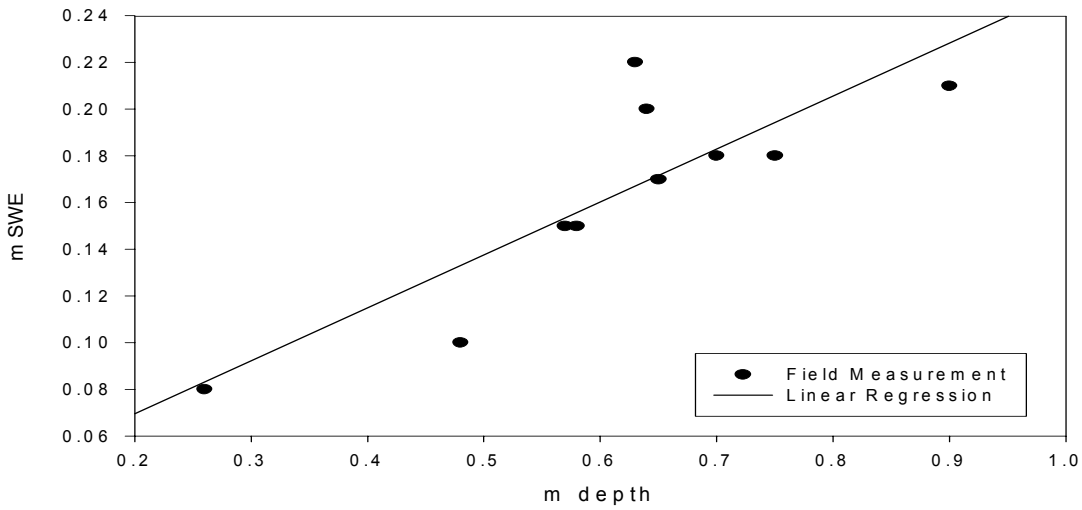

Figure 4.1 Example regression of depth and SWE relationship.

4.3 SNOW-COVERED AREA

Each snow-survey transect was considered representative of the physical properties of the snow pack within the LU, and these values were used to provide an estimate of SCA. As each point represented a fraction of the total number of points for an individual transect, when a point became snow-free, it was assumed that *SCA* declined by that percentage.

$$SCA = {n_s}/{n} \qquad [4.1]$$

where n_s was the total number of transect points with snow, and n was the total number of transect points. Additionally, a snow-cover depletion curve approximation (Essery and Pomeroy 2004) was used to compare against the above method.

$$SCA = \tan\left(1.26 SWE / CV\right) \qquad [4.2]$$

where CV is the coefficient of variation.

4.4 STREAMFLOW DISCHARGE

All discharge measurements were made at the basin outlet. At the beginning of the investigation when flow was beneath ice, salt dilution (as outlined in Dingman 2002) was used to determine baseflow discharge. Two hundred grams of salt was dissolved into 1 L of streamwater and then injected into the creek 20 m upstream of the point of measurement. Using a portable HydroLab Quanta water quality sonde, conductivity was measured at 5 second intervals. Beginning on JD 110, salt dilution was carried out until a sufficient channel reach had developed for manual gauging on JD 129. Following this, discharge was measured at least twice daily with few exceptions using a Swoffer current meter until JD 166. This procedure involved the measurement of water velocity at a height of 60% of the streamflow depth. Velocity was measured for 30 seconds then the average was determined and recorded for that location. This was repeated at the midpoint of 0.1 m increments across the channel width. Discharge was then determined from the summed cross sectional areas multiplied by the average velocity for each midpoint. Salt dilution was continued into the early open-water season whereby measurements were compared to current-metering and to the stage-discharge relationships. During the early periods of increased flow, velocity and stage was measured continuously with a Unidata Starflow ultrasonic current meter. Programmed to record stream stage (mm) and velocity ($m\ s^{-1}$) every 15 minutes, it provided data for construction a discharge-stage relationship until the channel opened completely. This stage-discharge relationship was employed from day JD 110 to JD 141. Although the ultrasonic current meter remained active for the entire

study period, discharge was calculated using a second stage-discharge relationship for the open water period consisting of a stilling well with a float attached to an electronic logger. Maintained by the Yukon Territorial Government, a stable stage-discharge relationship has existed at this gauge since 1998. This data was used to calculated discharge until the end of the summer. In total 25 discharge measurements using salt-dilution and 92 current meterings were conducted at the outlet between JD 109 and JD 166. A comparison of discharge data for the salt-dilution and current metering methods and a comparison of the measured discharge versus the modeled discharge using the stage discharge relationship is included in APPENDIX C.

The TS1 landscape unit had the advantage of being a small contained sub-catchment within Granger Basin, and was used to further understand linkages in the melt hydrology. A second Unidata Starflow ultrasonic current meter was installed very close to where TS1 drained into the primary Granger Creek. Between JD 119 and 151, 22 discharge measurements were made, 9 using salt-dilution and 13 current meterings. Using the data collected at 15 minute intervals from the ultrasonic current meter, a stage-discharge relationship was established for this sub-catchment.

4.5 STREAMFLOW CHEMISTRY

A Hydrolab 4a Datasonde located near the Department of Northern Affairs stilling well was used for continuous measurement of pH, specific electrical conductivity (SpC), water temperature, dissolved oxygen (DO), oxidation-reduction

potential (ORP). The duration of use was JD 115 to its removal at the end of the summer.

4.6 MINERAL AND ORGANIC SOIL MOISTURE

As the ground surface became exposed through the melt season, near-surface soil moisture measurements were made with a Campbell Scientific Hydrosense (0.12 m length probes) water content reflectometer. For each transect point, between 3 and 10 measurements were recorded and averaged for analysis. The device became inoperative early in the study, creating a three-week span where no manual soil moisture measurements were made. Thus, the majority of the soil moisture surveys were done between JD 142 and JD 166. The south and north-facing transects were surveyed 15 times. UX and LX were surveyed 7 and 6 times respectively. TS1, TS2, and TS3 were surveyed 11, 7, and 7 times respectively. SS2 was surveyed 6 times. A number of gravimetric soil samples were obtained in a metal cylinder of known volume for calibration of the Hydrosense. Immediately after collection in the field, they were weighed and sealed. Upon return to the lab, the samples were dried in an oven for 48 hours. Adjacent measurements of volumetric soil moisture content using the Hydrosense were then compared to the gravimetric samples for accuracy. The hydrosense slightly overestimated the moisture content of the soil, and a coefficient based on the relationship between the two methods was established and applied to the data. Organic layer depth was measured where soil samples were removed.

Three Campbell Scientific CS-615 water content reflectometers have been operating within the WCRB for several years. The first was located on north-facing

slope near the North site snow survey transect. The other two CS-615s, although slightly outside Granger Basin, were in representative areas similar to the geography of TS1, and UX. The data from these probes were used as proxy indicators of the soil moisture behaviour for this study. Because CS 615 measuremtents are questionable without a site-specific calibration (Seyfried and Murdock 2001) a linear calibration was developed covering a volumetric soil moisture range of 0.4 to 0.7%. For soil moistures below 0.4%, the calibration estimates soil moisture values close to the stanadard response curve provided by the manufacturer (Quinton 2005 personal communication).

4.7 SUBLIMATION (SUB)

Sublimation losses were determined by applying a daily rate to each area for the individual LUs duration of melt. Granger Basin has been the site of continuous meteorological measurement for sometime, and a sublimation rate of 0.2 mm/day was applied to all areas based on Pomeroy et al. (2003).

4.8 INFILTRATION (INF)

To estimate infiltration into the frozen mineral substrate between JD 110 and JD 165, Zhao and Gray's (1999) parametric equation for determining cumulative infiltration into a frozen soil of limited class was used (Eq 2.2). This component was calculated separately for each LU.

The coefficient (C) in (Eq. 2.2) used to account for the difference between model and natural systems and varied between 1.14 and 2.10 in Gray et al. (2001) it was observed that C can changed be to account for variable surface saturations

(Zhao and Gray 1999). This study assumed a C value of 1.14 because it was the smallest coefficient and it was derived from a soil type more similar to that of the present study. Zhao and Gray (1999) state that initial surface saturation (S_0), varies between 0.75 and 1, and in this study $S_0 = 1$ was used as in most situations the infiltration rate of a frozen soil is low and a value of $S_0 \cong 1$ should be assumed (especially when a snowcover ablates rapidly) (Zhao and Gray, 1999).

S_I, determined as the average volumetric soil moisture (water and ice) divided by the soil porosity, describes the pre-melt soil water content for the top 400 mm of the mineral soil profile. This value was established by utilizing the preceding fall (2002) mineral soil moisture profile data prior to freeze-back. Winter mineral soil moisture data was examined to assess if precipitation events and/or significant thaw occurred over-winter that increased soil moisture storage. In 2002, there were no over-winter rain or melt events, and the fall volumetric moisture content was considered as the most accurate representation of S_I. Soil moisture data was available for the North site, and was extrapolated from nearby sensors to the Tall Shrub Sites and the UX site. Values were then applied to the other sites based on soil characteristics and their relation to the measurement sites (Table 4.1).

Soil porosity of the mineral soils was obtained from measurements taken in previous studies within the basin (Carey and Quinton 2004; Quinton et al. 2004) and an average value of 0.49 was used in all calculations. This value compares well with porosity values for other mineral soils with similar texture (Dingman 2002).

The average temperature at the start of infiltration (T_I) was obtained from buried thermisters installed in 2001. The thermisters at the TS1 proxy were 0.15 m

below the start of the mineral horizon, 0.05 and 0.15 m below the mineral surface at the UX proxy, 0.10 below the mineral horizon surface at the NF and SF LU. The average temperature in the 0.40 m mineral soil profile prior to any meltwater passing through lysimeters was used for T_I. Temperature values before any melt took place were obtained directly for the South, and North Landscape Units. Instruments that served as a proxy site to the Tall Shrub and UX LU provided temperature values for the remaining sites.

If melt was a continuous event, the infiltration opportunity time, $T_{0,}$ is the SWE divided by the meltrate, giving the number of hours ablation resulted in water being delivered to the mineral soil assuming negligible evaporation or storages. However, a continuous melt event is rare in most natural systems and this study utilized a similar method tested by Gray et al. (2001). Where applicable, T_0 was taken as the total number of hours when air temperature and net radiation was positive and the snow pack was isothermal at 0ºC. This was done with increased precision for the NF and SF sites because of the nearby weather stations. Meteorological variables were collected at a site near the TS1, SS1, and LX sites, but were less precise because of equipment removal during part of the study period. For UX, TS3, TS2, and SS2 the total hours when air temperature was positive and the snowpack was known to be ripe were used because radiation data was not available.

Table 4.1 Equation 2.2 Parameters for each LU

	SS1	SS2	TS1	TS2	TS3	SF	NF	LX	UX
T_0 (hours)	220	252	498	656	795	299	953	598	627
mm/hr meltrate (SWE/T_0)	0.44	0.43	0.41	0.32	0.35	0.55	0.21	0.28	0.33
S_I (VMC)	0.2	0.2	0.21	0.21	0.21	0.25	0.34	0.2	0.25
T_I (°C)	-0.4	-0.4	-0.45	-0.45	-0.75	-0.4	-0.4	-0.5	-1

4.9 SEMI-DISTRIBUTED WATER BALANCE

To estimate the basin water balance during the snowmelt period a semi-distributed water balance was completed. For the melt period, the semi-distributed water balance (expressed in mm equivalent) is:

$$SWE - SUB = INF + ORG + Q \quad [4.3],$$

where SWE is the initial snow water equivalent of the snowpack, SUB is sublimation, INF is infiltration into frozen mineral soils, ORG is organic soil storage and Q is discharge. Surface storage was quantified from Granger Lake and is discussed separately. For every Landscape Unit, each water balance component was weighted by area and summed for each of the above terms.

4.10 METEOROLOGICAL DATA

Pre-existing instruments gathering a complete meteorological data set were used to obtain information for this study for the SF, NF, UX and SS LUs. Instruments were mounted 1.5–2.0 m above the top of vegetation, and oriented such that fluxes and snow depth were measured normal to the slope and aspect at the station. Turbulent fluxes and wind speed were measured using Campbell Scientific

CSAT3 three-axis sonic anemometers, coupled with fine-wire thermocouples and Krypton hygrometers. Net radiation was measured with Radiation Energy Balance Systems Q7 aspirated radiometers, again oriented to measure fluxes normal to the slope. Air temperature and humidity were measured with Vaisala HMP35CF hygrothermometers in Gill Instruments radiation shields. The stations were controlled by Campbell Scientific 23X dataloggers powered by solar panels. A more complete description is available in Pomeroy et al (1999b) and Pomeroy et al. (2003).

4.11 LANDSCAPE UNIT AND BASIN AREA

Each transect was chosen to represent a unique area of the basin. Numerous geographic co-ordinates were obtained transposed to a NTS 1:50000 map where the representative area was extrapolated. The summation of all LU areas was 8.01 km^2. This value was used in all subsequent calculations. Using co-ordinates marking the boundary of Granger Basin, the total drainage area was determined using Garmin MapSource software.

4.12 TIMING AND MAGNITUDE OF SNOWMELT EVENTS

The spatial variability of snowmelt hydrology for Granger Basin was analyzed in conjunction with measured basin discharge. The cumulative decline in spatially weighted SWE for each LU was compared to the basin hydrograph to isolate the most likely LUs contributing to spring flows. Used to identify potential source areas by the detailed examination of the timing and magnitude of ablation, it was the first analytical component in this investigation. In addition to timing and

magnitude, runoff pathways were visually monitored as an indicator of contribution.

CHAPTER 5
5.0 RESULTS

5.1 FIELD RESULTS

5.1.1 NET RADIATION

Net radiation data was available for the SF, NF, SS1 and the TS1 proxy site. Data presented consists of daily net-radiation and cumulative net radiation to the ground surface from JD 100 to JD 170 (Figure 5.1, 5.2). See APPENDIX D for detailed discsussion. During this time, SF, TS1 Proxy and SS1 each had similar daily mean net radiation values. Net radiation was positive much earlier for these three sites compared to NF. SS1 followed a pattern similar to that of the SF and TS1 proxy site but did not have the same high daily peaks exhibited by SF. After JD 110, daily average net radiation approximately tripled from less than 5 MJ day^{-1} to nearly 15 MJ day^{-1} by JD 115. Although the north and south towers were less than 300 meters apart, their contrasting aspects yielded pronounced differences with respect to net radiation (Figure 5.1), which had implications on the total energy available for melt. For each of the four sites there were similar patterns in the day to day radiation regimes, but the large contrast in the early part of the snowmelt season had implications on the cumulative radiation. By the time the NF cumulative net radiation was no longer negative (JD 123) the other sites had already accumulated more than *ca* 100 MJ (Figure 5.2).

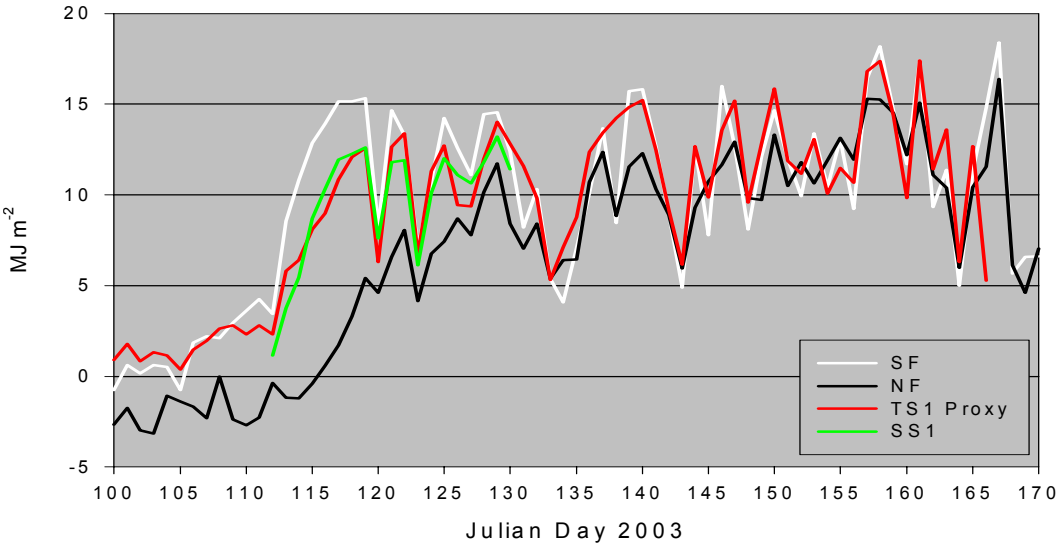

Figure 5.1 Daily net radiation flux to ground surface (MJ) for the NF, SF, SS1 and TS1 Proxy sites.

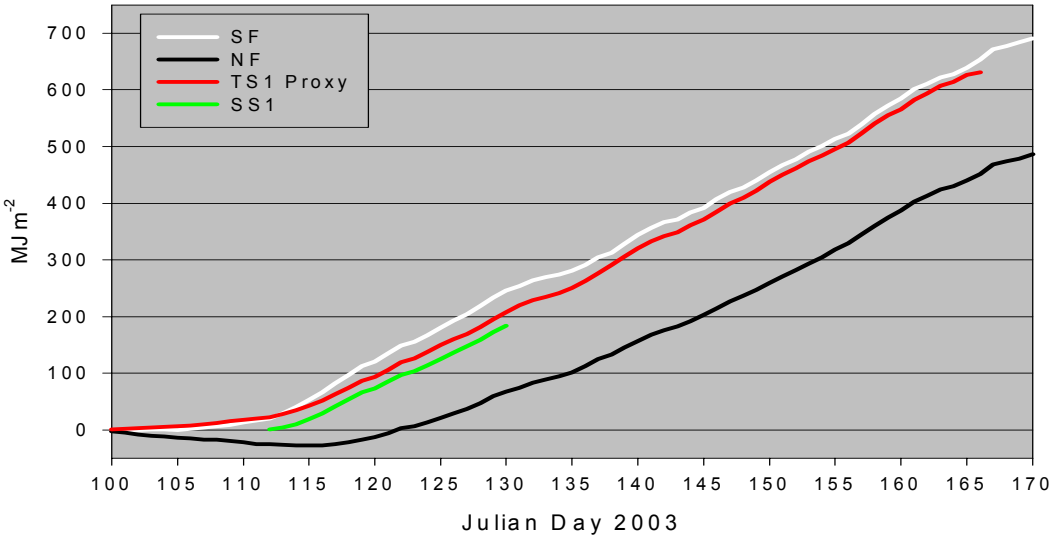

Figure 5.2 Cumulative net radiation energy to the surface (MJ) forthe SF, NF, SS1, and TS1 Proxy sites.

5.1.2 AIR TEMPERATURE

Mean daily air temperatures were available for the SF, NF, SS1, UX, and the TS1 Proxy sites. See APPENDIX E for a more detailed description. All sites followed a similar trend in temperature patterns throughout the study period (Figure 5.3). The only exception was that UX was on average 2.1 ºC (+/- 1.01 ºC) colder than the other sites in the basin for the duration of study.

With respect to NF and SF, the SF LU typically had a slightly higher mean daily temperature and was on average 0.45 ºC (+/- 0.28) greater on all but 13 days after JD 125. This similarity in air temperature despite large differences in net radiation has been observed previously at this site and elsewhere within the basin (Carey and Woo 1998; Pomeroy et al. 2003).

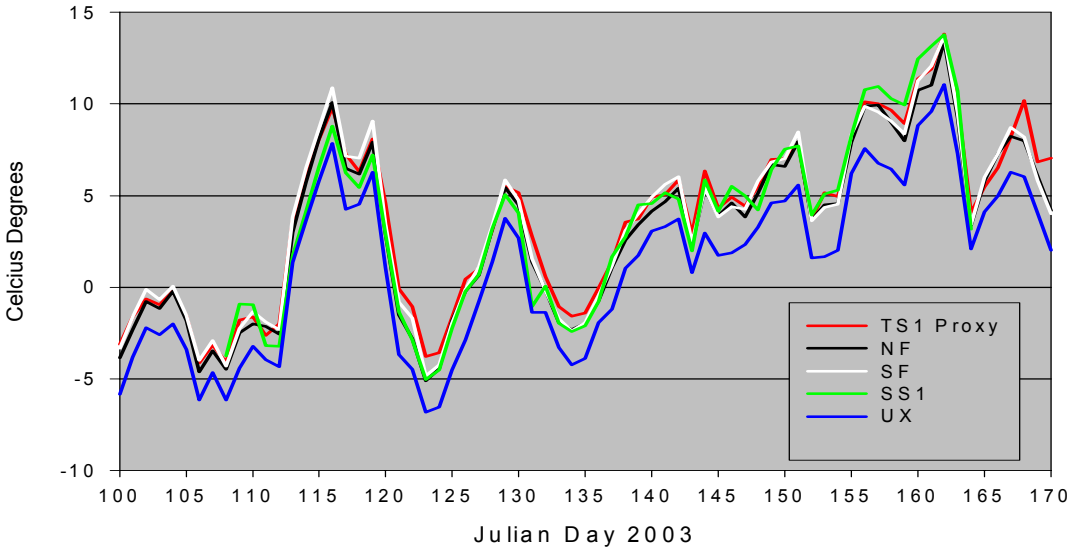

Figure 5.3 Daily mean air temperature for the NF, SF, UX, SS1, and TS1 Proxy sites.

5.1.3 SOIL MOISTURE AND GROUND TEMPERATURE

Near surface liquid water content (LWC) measurements with the CS Hydrosense for both mineral and organic soil began immediately after bare ground appeared (Figure 5.4). There is significant within-LU variability in liquid water content as evidenced by the large standard deviations (Figure 5.4). At the SF and SS LUs, values increase from *ca* 20% to *ca* 40% between early May (JD 125 +/- 5 days) and late May (JD 145 +/- 5 days). Other LUs, show consistent near-surface soil moistures that range between 35% and 40% by volume. The notable exception is the TS3 area whose mean values are *ca* 45% throughout the study period. CS 615 measurements were directly available for the NF LU and two other TDR stations located elsewhere in the Wolf Creek Research Basin (all within 4 km or less of Granger Basin) and were used as proxy data and extrapolated to all Tall Shrub sites and the UX site. There was no instrumentation in the short shrub LU. CS-615 measurements were available for the NF LU and extrapolated to the TS and UX LUs from other sites nearby. However, given the possible inaccuracies of liquid water content measurements prior to thaw some of the results during this time were considered dubious. All results are nonetheless included here.

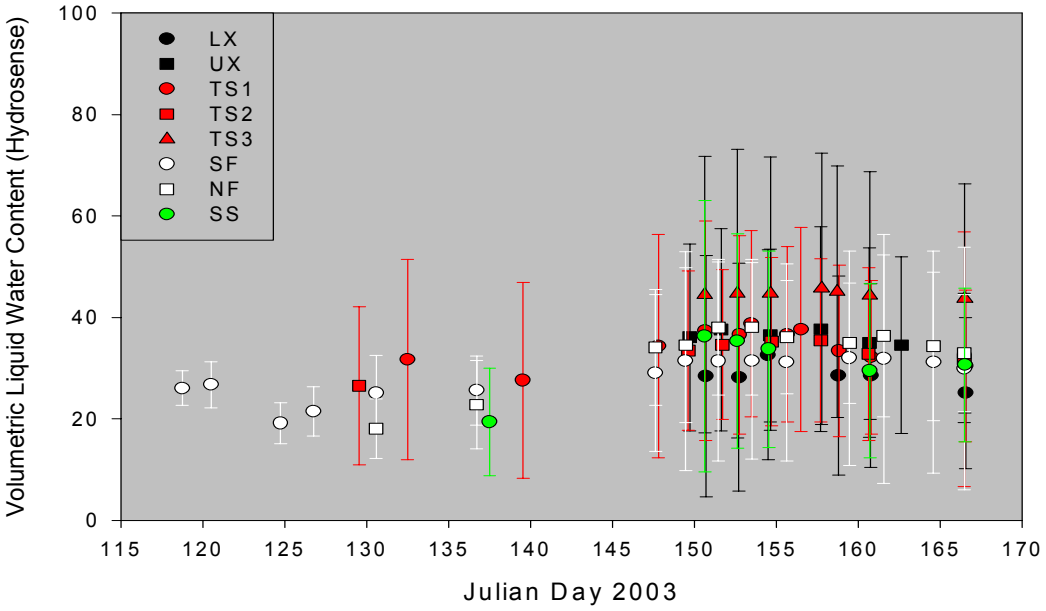

Figure 5.4 Volumetric Liquid Water Content. Points are means and bars are standard deviations of all measurements taken within an LU on the sampling date and represent liquid water content for the top 0.12 m.

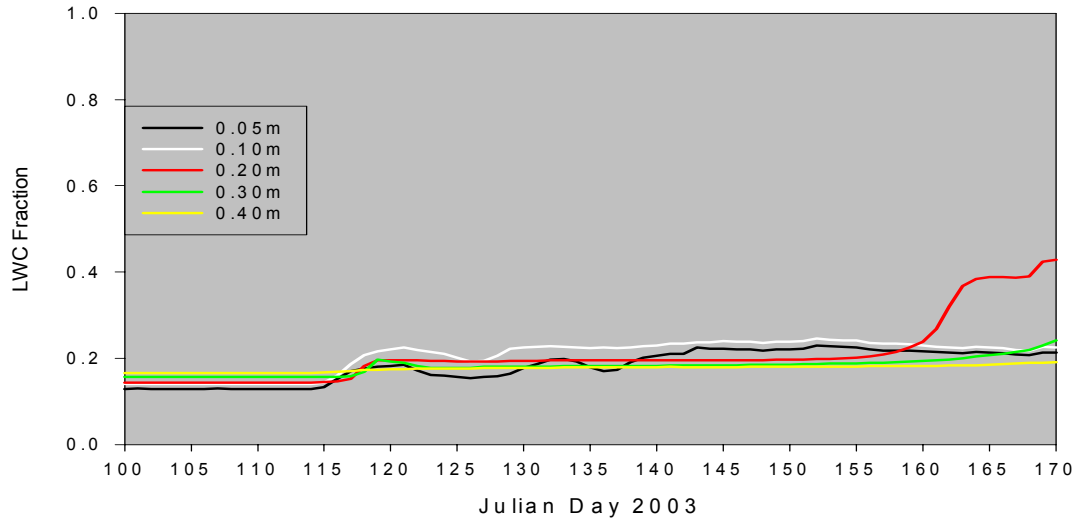

Figure 5.5 NF Mean Daily Liquid Soil Moisture Content (CS 615).

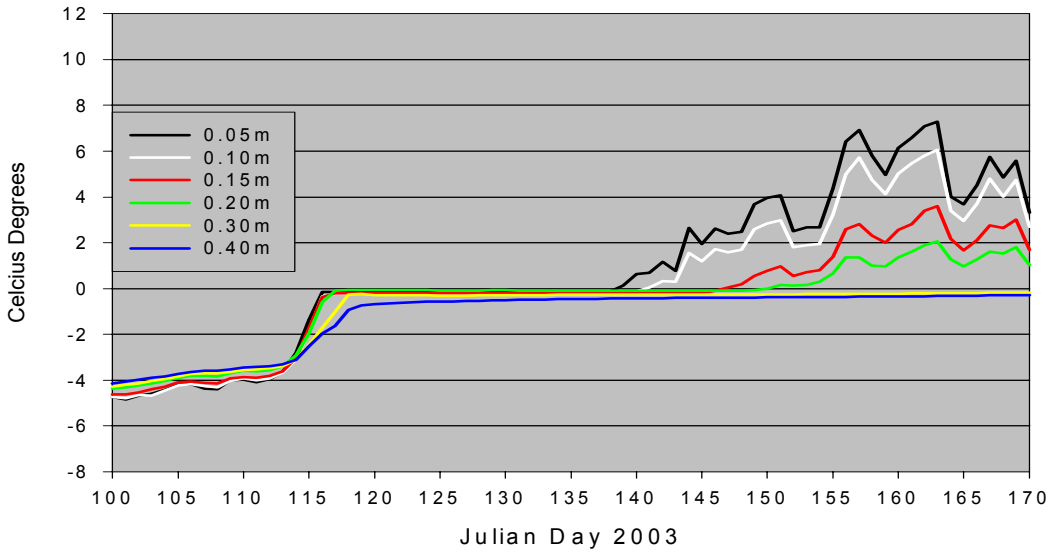

Figure 5.6 NF Mean Daily Soil Temperature

Soil temperatures at NF approached 0°C at 0.05 m around JD 115, yet did not rise significantly above freezing until JD 140 (Figure 5.6). Deeper horizons of the NF soil, 0.1 m, 0.15 m, 0.2 m, did not rise above freezing until JD 142, 147, 150 respectively, while temperatures below 0.3 m and 0.4 m remained very close to freezing for the entire study period. SF soil temperatures at 0.03 and 0.10 m depth rose above 0°C around JD 107 after the slope became snow-free and remained above freezing for the duration of the study period (Figure 5.7).

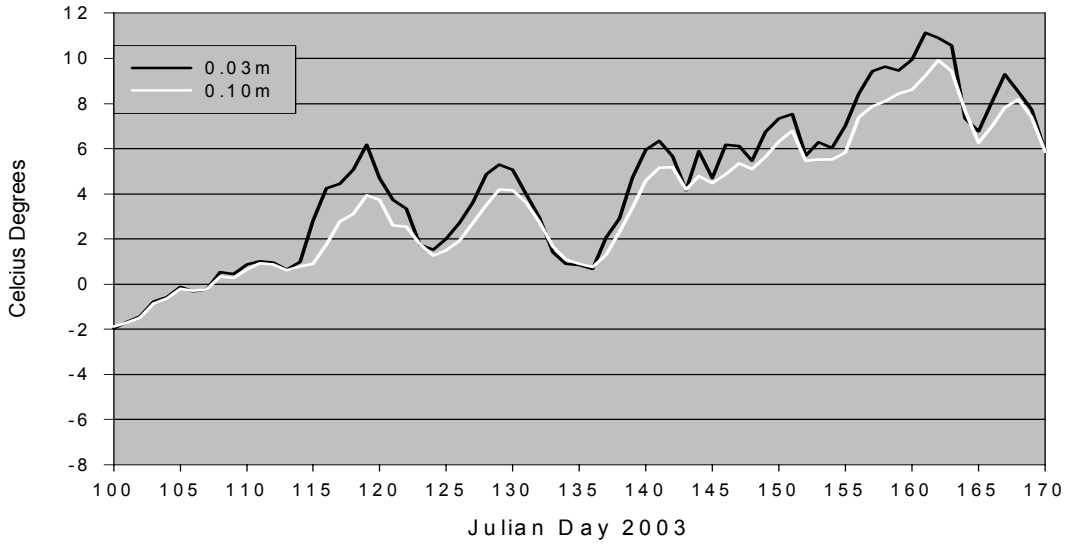

Figure 5.7 SF Mean Daily Soil Temperatures.

Soil temperature and liquid water content data obtained from a shrub tundra site just outside of Granger Basin was used to examine the likely sub-surface thermal and moisture patterns of the 2003 spring season for the TS1 site and data from the Hydrosense was used for comparison. Soil temperature at the TS1 Proxy site rapidly increased shortly after JD 110 (Figure 5.8). The greatest thaw depth, 0.80 m, observed in the TS1 proxy site occurred approximately 2 weeks before thaw 0.40 m below the surface occurred at NF.

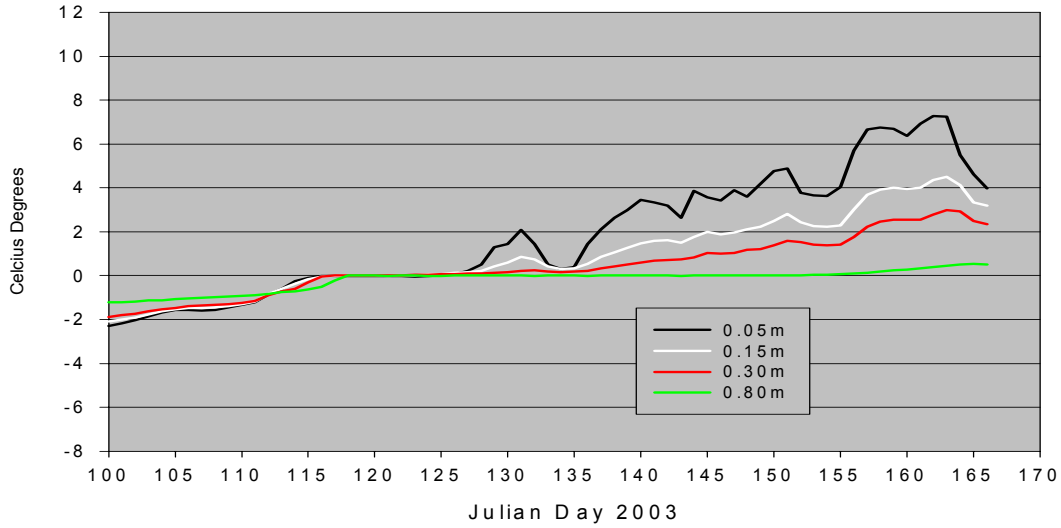

Figure 5.8 TS1 Proxy Mean Daily Soil Temperature.

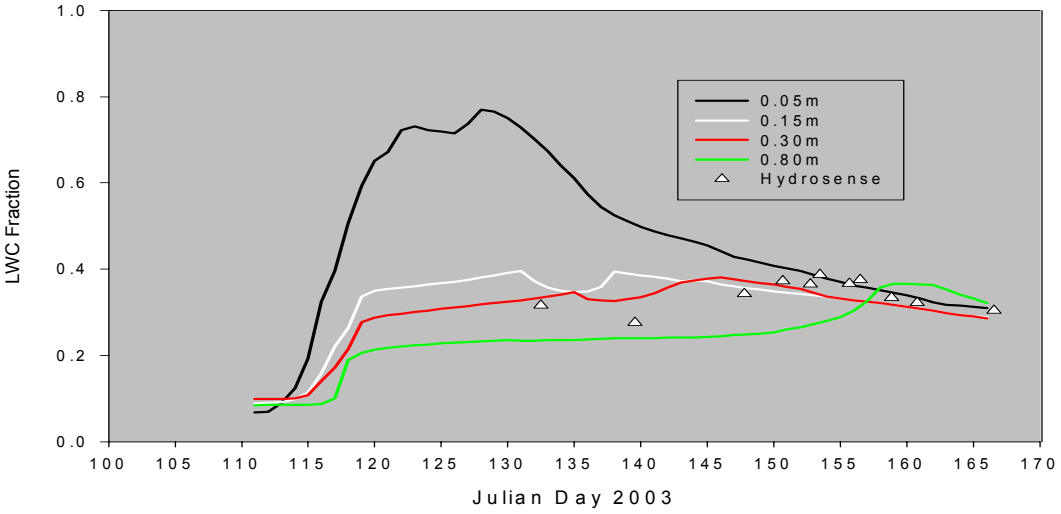

Figure 5.9 TS1 Proxy Mean Daily Liquid Soil Moisture Fraction. Hydrosense measurements represent the top 0.12 m.

The soil thawed at the TS1 Proxy to a depth of 0.15 m shortly after JD 130 and remained so for the duration of the study period. LWC rose significantly higher than NF and SF and peaked much earlier at 0.05 m just before JD 130 and peaked at 0.15 m just after JD 130 (Figure 5.9). Shortly after JD 131 the weather cooled and snowmelt was suppressed. As a result the soil temperature declined and meltwater

delivery to the soil ceased as evidenced by the rapid decline in LWC at 0.05 m and 0.15 m depth. By JD 145, the soil moisture content at 0.30 m reached its maxima and began to decline similar to other layers of the soil (Figure 5.9). At the TS1 proxy site, the soil thawed to a depth of 0.80 m more than three weeks before NF thawed to a depth of 0.40 m. Manual soil moisture measurements for the upper 0.15 m profile for TS1 are within 5% of the TDR values of the proxy site.

The UX proxy site indicated that soil temperature approached 0ºC as early as JD 120 (Figure 5.10), but did not completely thaw below 0.15 m until JD 140. At the onset of infiltration and melt, there was a distinct period of high liquid moisture content in the upper soil profile followed by a delayed peak in the lower profile (Figure 5.11). Following the peak, soil moisture declined gradually and levelled off near JD 170. The SWE at the proxy site although not measured, is known to have been less than at UX. Volumetric moisture content of the UX transect was measured several times manually (Figure 5.11) and exhibited a slow decline in the top 0.15 m of the soil profile.

No TDR data was available for or extrapolated to the LX LU. For the time measurements were obtained, the soil moisture record was relatively static and the LWC average varied between 25 and 32% (Figure 5.4). There were no stations recording soil temperature or soil moisture in the short shrub LUs, but measurements with the Hydrosense were obtained for SS2 (Figure 5.4).

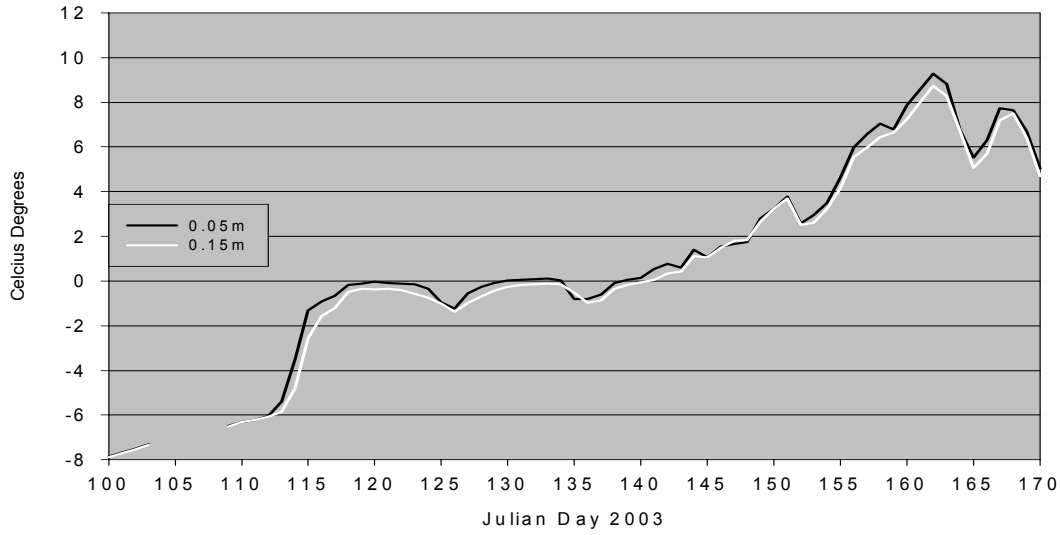

Figure 5.10 UX Proxy Mean Daily Soil Temperature.

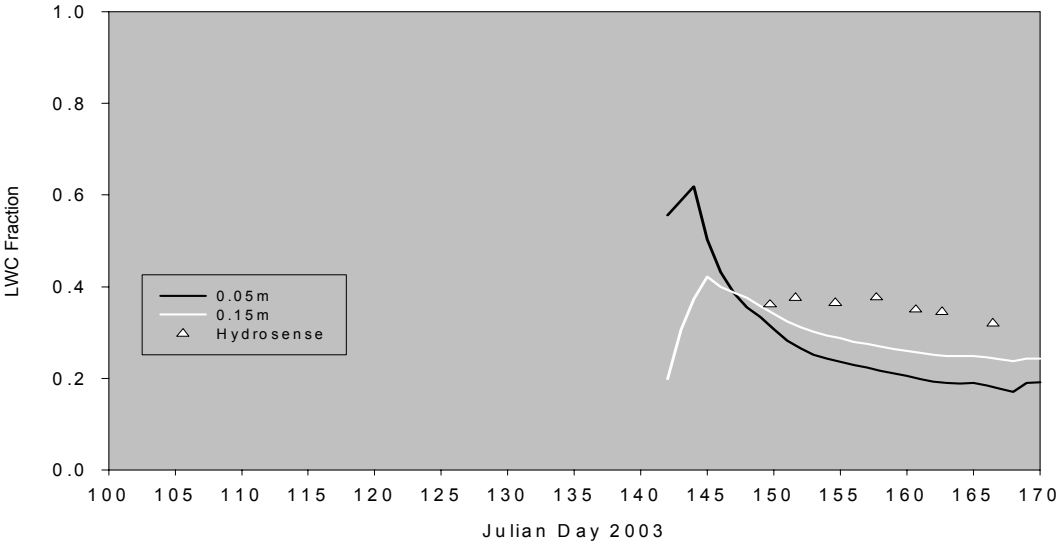

Figure 5.11 UX Proxy Mean Daily Liquid Soil Moisture Fraction and UX Hydrosense measurements (upper 0.15m).

5.1.4 PRE-MELT SNOW DEPTH

The deepest snow at the end of the accumulation period was measured in the tall shrubs (mean 0.70 m), on the north-facing slope (0.72 m), and in the LX LU (0.62 m) (Table 5.1). Shallower depths were observed in the short shrubs (mean 0.40 m), UX (0.52 m), and the south-facing slope (0.57 m). Using the coefficient of variation, *cv*, as an indication of variability, TS3 exhibited the greatest variability in snow depth (*cv* = 0.60), while TS1 exhibited the least variability (*cv* = 0.27) among all LUs. Snow depth was similar among the short shrub LUs with considerably less variation in depth than two of the three tall shrub sites (Table 5.1). Snow density was greatest at the UX, the tall shrubs, and NF, yielding greater SWEs than the other sites, while density was lowest in the Short Shrubs, LX, and South Facing slope (Table 5.1). Snow density was less variable than snow depth.

Table 5.1 Snowpack characteristics for basin LUs.

	Density (kg/m^3)	***c.v.***	**Depth (m)**	***c.v.***	**SWE**	***c.v.***
SS 1	293+/-3	0.01	0.38+/-0.16	0.43	98+/-47	0.48
SS 2	285+/-74	0.25	0.42+/-16	0.38	107+/-13	0.12
TS 1	322+/-13	0.04	0.66+/-0.17	0.27	203+/-49	0.24
TS 2	300+/-46	0.15	0.63+/-0.34	0.55	207+/-144	0.7
TS 3	334+/-14	0.04	0.81+/-0.48	0.60	279+/-186	0.67
LX	260+/-26	0.1	0.62+/-0.25	0.42	167+/-91	0.54
UX	365+/-57	0.16	0.53+/-0.26	0.50	204+/-140	0.69
SF	285+/-15	0.05	0.57+/-0.18	0.32	164+/-59	0.36
NF	310+/-28	0.09	0.72+/-0.26	0.37	201+/-129	0.64

There was an observed relation between snow accumulation and vegetation. The height of the closest shrub within a 1 m radius of the snow survey point was measured in fall 2003 (Table 5.2). Greater SWE was generally associated with taller

vegetation. The notable exception to this trend was the UX LU where greater SWE was likely attributed to denser wind-packed snow.

Table 5.2 Shrub height and snow depth for basin LUs

	Shrub Height (m)	Snow Depth (m)	SWE (mm)
SS 2	0.39+/-0.38	0.42	107
TS 1	0.78+/-0.45	0.64	203
TS 2	0.62+/-.670	0.63	206
TS 3	0.74+/-0.70	0.81	279
UX	0.12+/-0.20	0.52	204
South	1.01+/-0.44	0.57	164
North	1.10+/-0.46	0.62	201

5.1.5 SNOW WATER EQUIVALENT

At the end of the accumulation period, snow-water equivalent was greatest in the tall shrub LUs (TS1, TS2, TS3), the higher elevation headwater area (UX), and on the north-facing (NF) LU near the stream outlet (Table 5.1). The lowest SWE was measured in the short shrubs (SS1, SS2), while intermediate SWE was measured in the other two LUs, (LX and SF). The mean SWE for the three tall shrub sites was 229 mm, almost 2.3 times greater than the mean SWE of 102 mm for the two short shrub sites. The large accumulation at NF (201 mm) was attributed in part to an extensive snow drift that forms annually at the site. Accumulation here was 1.2 times greater than the contrasting SF LU (SWE = 164) across the river valley. SWE and snow density were 1.2 and 1.4 times greater respectively at the UX compared with LX.

5.1.6 SNOW DEPTH DECLINE

Snow depth decline was determined as the change in mean snow depth between successive snow depth measurements. Snow depth decline was negligible prior to JD 112 (Figure 5.12). The greatest decline in depth in all sites occurred between JD 112 and JD 122, the warmest period of the spring. As a fraction of the pre-melt value, depth declined by 90% and 72% at SS1 and SS2; 58%, 50%, and 37% in TS1, TS2, TS3; 66% and 51% in LX and UX; and 89% and 42% in SF and NF respectively during this period.

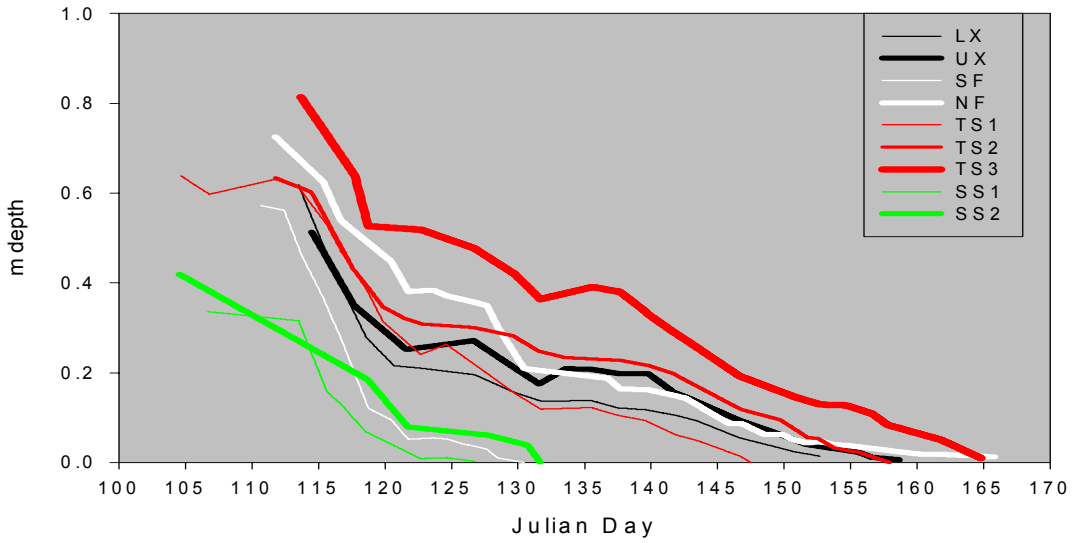

Figure 5.12 Average snow depth (m) for basin LUs.

The average rate of depth decline was calculated by averaging the rate of depth decline between successive measurements for the entire study period and used for comparison between and within LUs (Table 5.3; Figure 5.13). The average depth decline in SF was nearly 30 mm per day, while all other LUs varied between *ca* 11 and 16 mm per day. The mean rate of depth decline was nearly twice as great

for the SF as compared to the contrasting NF; UX had a slower rate than LX. The average depth decline in SS1 and SS2 was only greater than TS1 and TS2.

Table 5.3 Mean rate of snow depth decline in mm/hour and mm/day for all LUs

	SS 1	SS 2	TS 1	TS2	TS3	LX	UX	SF	NF
mm/hr	0.69	0.64	0.62	0.57	0.65	0.64	0.47	1.2	0.54
mm/day	16.6	15.4	14.8	13.7	15.7	15.4	11.4	28.9	13.1

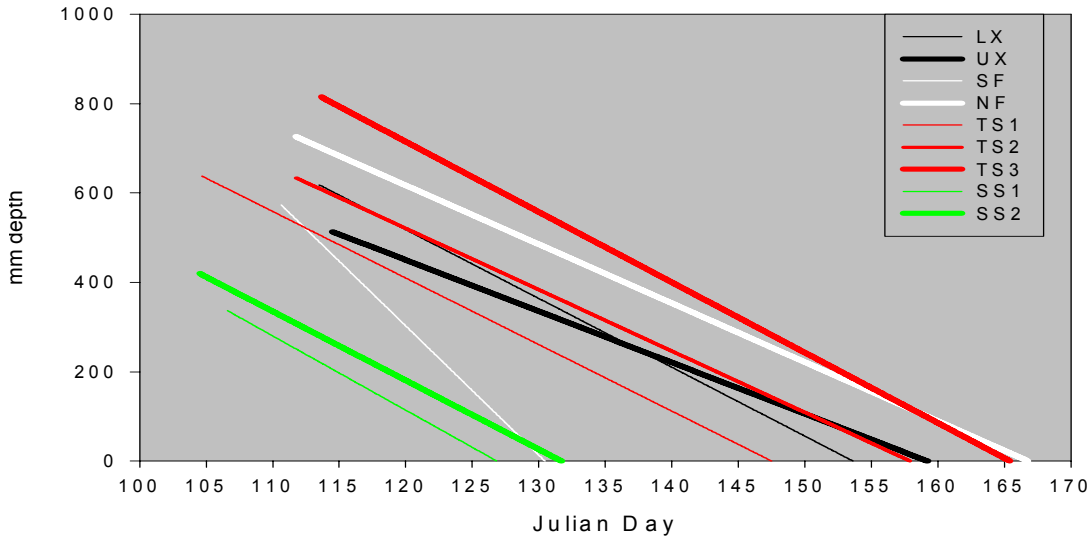

Figure 5.13 Average snow depth decline for basin LUs.

5.1.7 SNOW WATER EQUIVALENT DECLINE

The first sustained melting period of the 2003 season began on JD 113 and lasted for one week until JD 120 and during this time the greatest decline in SWE (Figure 5.14) occurred. The largest ablation as a percentage of total SWE took place at the SF, SS1, and SS2 LUs, where SWE was depleted by 79% (131 mm), 90% (89 mm) and 74% (79 mm) respectively (Figures 5.14, 5.15). In contrast, SWE depleted 34 % (68 mm) at NF, 45 % (92 mm) at TS1, 42% (86 mm) at TS2

and 23 % (63 mm) at TS3 during this period. From JD 121 to JD 126, the weather cooled dramatically and mean daily temperatures fell below 0^{o}C (Figure 5.3). During this time melt was suppressed throughout the entire basin. From JD 127 to JD 131, conditions changed and sufficient energy was available to melt the remaining snow in the SF and SS1, SS2 sites. Geographically, snow remained at higher elevations longer as evidenced by the gradual decrease in remaining SWE in the Tall Shrub sites, and the UX site. By the time the Short Shrubs were completely devoid of snow (JD 130) 29% of SWE remained at TS1 (58 mm), 51% at TS2 (105 mm), and 60% (167 mm) at TS3 (Figures 5.14, 5.15). The NF site had only lost 53% (107 mm) of its SWE by the time SF was completely ablated on JD 131 (Figure 5.14, 5.15). At the end of the second melt period on JD 131, ca 35% (61 mm) SWE remained at LX, while close to 40% (81 mm) remained at UX (Figures 5.14, 5.15). From JD 132 to 136 melt was suppressed again, but following JD 137 snowmelt persisted for the remainder of the study period. Temperatures in the upper basin were consistently cooler than areas lower down which likely contributed to less available energy and a more persistent snow pack. As a result, TS1 ablated by JD 147, more than 3 weeks after it declined to 50% of its pre-melt SWE. TS2 was snow-free by the end of JD 157 and TS3 persisted until JD 165. The LX site became snow-free on JD 152 while UX persisted until JD 158. The North site, due to the presence of a large snow-drift, had a small amount of snow that persisted just after JD 165.

Table 5.4 Mean rate of SWE decline in mm/hour and mm/day for all LUs

	SS 1	SS 2	TS 1	TS2	TS3	LX	UX	SF	NF
mm/hr	0.21	0.17	0.20	0.19	0.22	0.18	0.19	0.35	0.16
mm/day	5.1	4.1	4.8	4.4	5.3	4.2	4.5	8.2	3.8

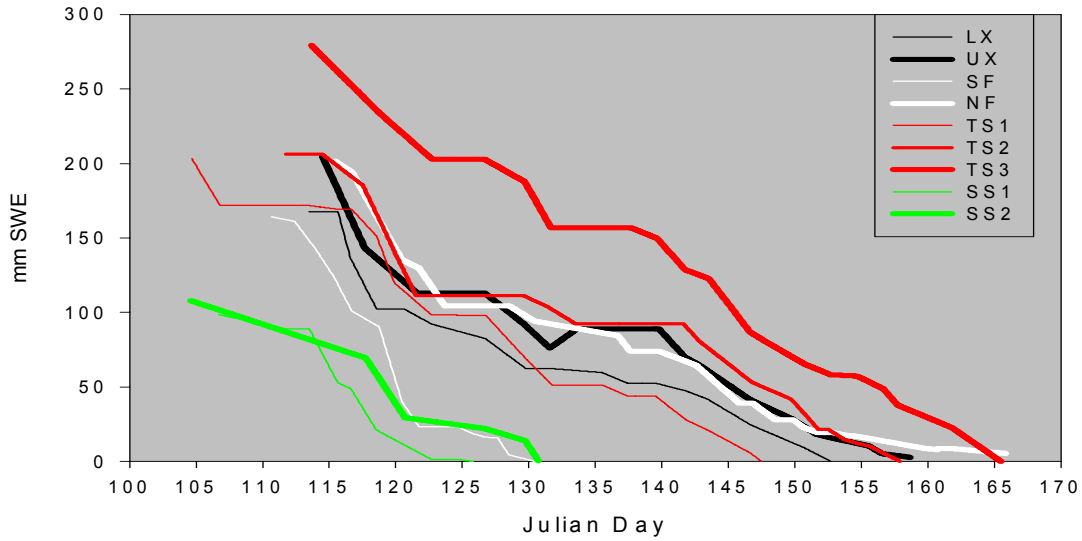

Figure 5.14 SWE decline for basin LUs.

Snowmelt at the Short Shrub sites was rapid and exhibited similar behaviour (Figure 5.14, 5.15). Both LUs started with the lowest SWE; SS1with 98 mm and SS2 with 107 mm. SS1 maximum SWE was measured on JD 106 and by JD 113, SWE had declined to approximately 89 mm, with 87 % of the transect remaining snow-covered. By JD 115, SWE dropped to 51 mm, with less than 50 % snow-covered area remaining. Ablation continued rapidly after JD 115 as SWE declined to 22 mm by JD 118 and 2 mm by JD 122. One persistent small snow-patch remained until JD 126. At SS2, maximum SWE (107 mm) was measured on JD

104. Logistical constraints prevented this site from being measured again until JD 117, when SWE decreased to 69 mm. Between JD 117 and JD 120, 37 mm (34 % of the initial SWE) was depleted and an estimated 77% of the total snow-covered area had depleted. On JD 126, 21 mm (<20%) of SWE remained, and by JD 130, SS2 was completely snow-free (Figure 5.14; 5.15).

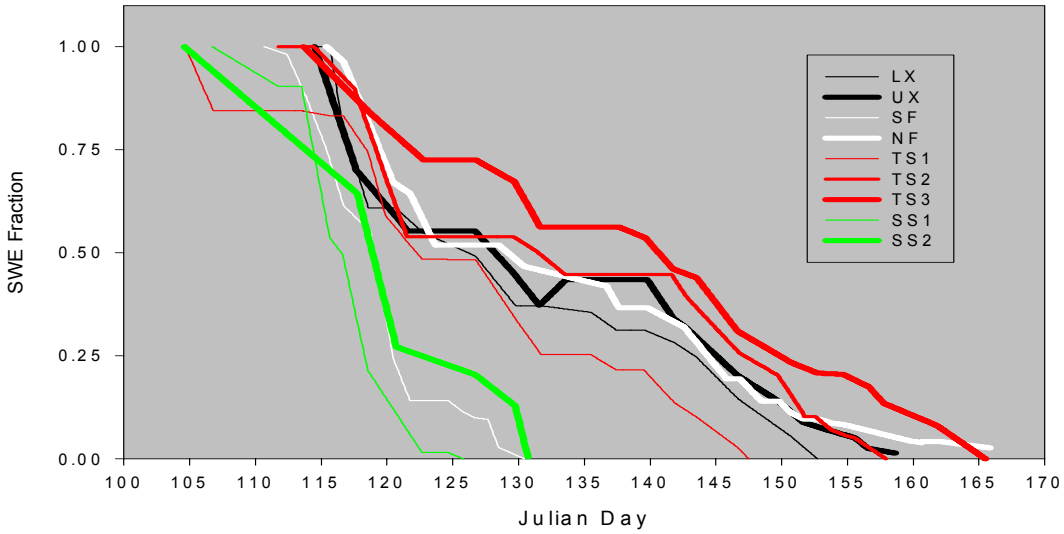

Figure 5.15 SWE Fraction for basin LUs.

The Tall Shrub sites had the largest SWE of all LUs, with TS3 being the largest. Maximum SWE at TS1 was measured on JD 104 and depleted from 203 mm to 171 mm by JD 111, and remained fairly constant until JD 113. The decline in SWE between JD 113 and JD 120 for TS1 and SS1 was similar when comparing the volumetric decline (60 mm for TS1 and 71 mm for SS1 respectively). However, as a fraction of the initial SWE, SS1 was depleted 72% compared to 30% in TS1. By JD 122, 98 % of SS1 SWE had depleted, whereas 50 % remained at TS1. Snow persisted at TS1 until JD 147, where the remaining half depleted at a relatively steady rate (Figure 5.14; 5.15).

TS2 maximum SWE was measured on JD 111 and by JD 121, SWE had been reduced to 58 % (121 mm) of the original SWE (Figure 5.14, 5.15). The timing of melt in TS2 was similar to TS1 during the first phase of the melt season. By JD 121, 46% (95 mm) of the SWE was ablated from TS2 compared to 49 % (100 mm) of the SWE at TS1. After this time, the depletion of SWE took much longer at TS2 where almost 25 % of the SWE remained after TS1 was completely snow-free.

Maximum SWE at TS3 was 279 mm on JD 113. By the end of JD 122, SWE had depleted only 27 % compared to 46 % at TS2, and 52 % at TS1 (Figure 5.14, 5.15). Volumetrically, this was 71 mm of liquid water which was close to the decline of 100 mm in TS1 and 95 mm in TS2. Melt at this site was also suppressed by the cool conditions between JD 122 and JD 126, and SWE did not decline again until JD 129 when SWE decreased from 202 mm to 183 mm. Like TS2, melt in TS3 was suppressed from JD 132 to 136, and no decline in SWE was measured until JD 139. By this time, only 48 % (134 mm) of the SWE was ablated from TS3, compared to 80% at TS1, and 55% at TS2. After JD 139, SWE depletion was steady but slow and by JD 161, approximately 10% of the SWE remained at TS3, two weeks after TS1 and 4 days after TS2 were snow-free.

The maximum SWE for the Upper and Lower sites measured on JD 114 were 204 mm and 167 mm respectively. Both sites exhibited a similar melt response to the first week between JD 113 and JD 120, and SWE at LX and UX decreased by 40% (67 mm) and 43% (88 mm) respectively (Figure 5.14, 5.15). By JD 141, SWE was depleted to less than 30 % (47 mm) at LX and 34 % (68 mm) at

UX of pre-melt SWE. Over the next week, more melt occurred at LX compared to UX, and by the end of JD 146 SWE was reduced to 24 mm at LX and 41 mm at UX. However, as a fraction of the initial SWE each site had very similar amounts remaining with 14% and 19% for LX and UX respectively (Figures 5.14, 5.15). There was one snow-precipitation event that increased the UX SWE by 9 mm on JD 134. LX became snow-free by the end of JD 152, while UX became snow-free by the end of JD 159.

The greatest contrast in the depletion of SWE was observed at the NF and SF LUs (Figure 5.13, 5.14). Maximum SWE for SF (167 mm) was measured on JD 110 and maximum SWE for NF (201 mm) was measured on JD 115. By JD 121, 86% of the SWE (141mm) had melted from SF compared to 31% (70mm) from NF. After JD 121, conditions deteriorated and no further decline occurred at the SF until JD 124. Over the next 5 days, the remaining 23 mm SWE depleted and by JD 130, SF was snow-free, which was close to the time the Short Shrub sites became snow-free. Although melt was suppressed on the South-face from JD 121 until JD 124, the SWE on NF continued to decline from 127 mm on JD 121 to 104 mm on JD 124. Considering the large SWE at NF, it took more time and energy to warm the snowpack, but as a result it took more time to cool. By JD 130 when SF was snow-free, 94 mm, or slightly less than 50% of the SWE, remained on NF. By this time, the snowpack was once again ripe at NF and melt continued for the next 5 weeks. A large drift was responsible for the persistent behaviour of SWE at this site. While other parts of NF melted the drift did not fully ripen and melt until JD 142. At the end of JD 165 only 5 mm of SWE remained.

Ablation differences are enhanced for the SF and NF LU when comparing the average decline in SWE among LUs (Figure 5.16). With respect to the timing and magnitude of snowmelt in the SF LU, SWE declined much earlier and at an accelerated rate in comparison to the NF LU. The timing of snowmelt in the Short shrubs precedes that of the Tall shrubs in most cases by three weeks; however the rate of SWE depletion was very similar. The average SWE decline for LX and UX was also similar (Figure 5.16).

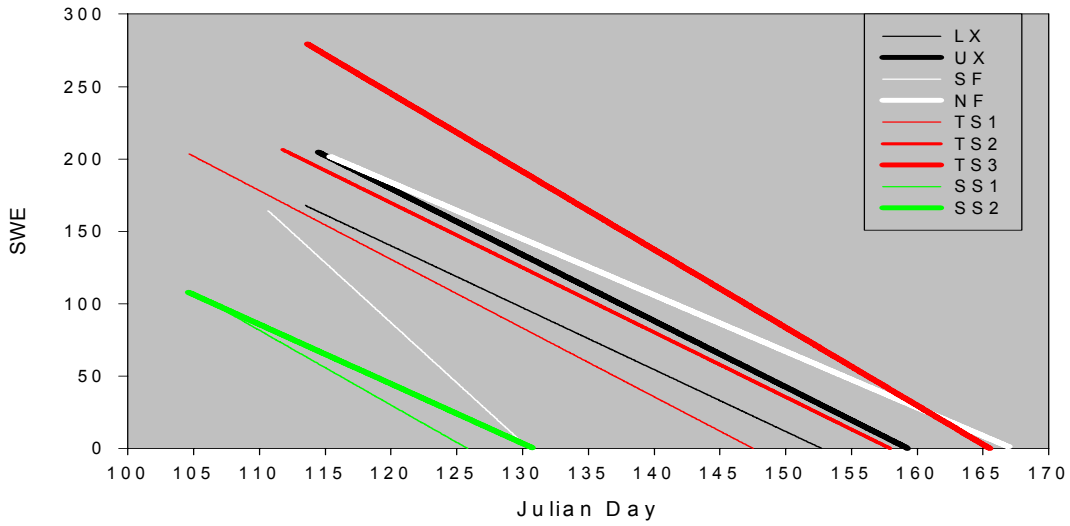

Figure 5.16 Mean SWE decline for basin LUs.

5.1.8 SNOW COVERED AREA DEPLETION

Two methods were used to compare the depletion of snow-covered area. The first method assumed each survey transect represented a fraction of the total area and as points became snow-free, snow-covered area depleted by that amount. The second method outlined in Equation [4.2] (Essery and Pomeroy 2004) was used for comparative purposes. Each method of snow covered area (SCA) depletion ends at approximately the same time. The tangent function algorithm model shows a

more rapid depletion in SCA later in the melt period when SWE was approaching it's lowest (Figure 5.17; Figure 5.18).

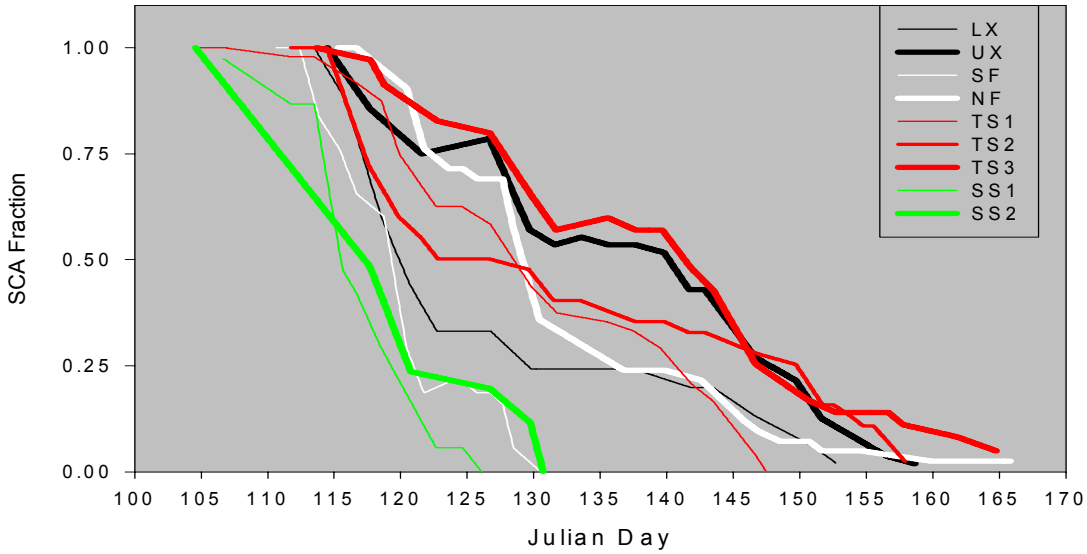

Figure 5.17 Point Survey SCA Fraction.

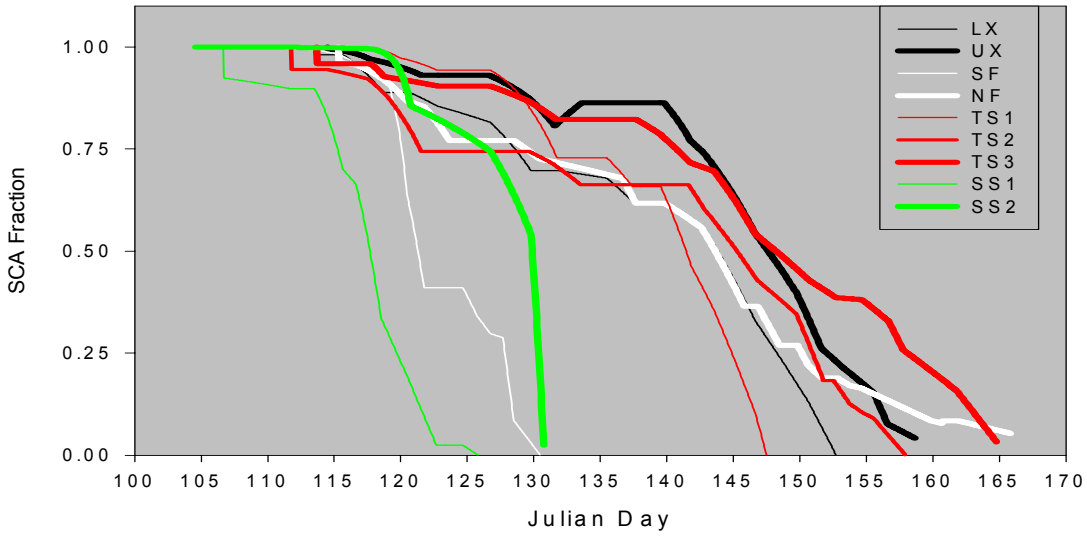

Figure 5.18 Tan Function SCA Fraction.

5.1.9 STREAMFLOW

Streamflow measurements began on JD 110 prior to any known snowmelt (Figure 5.19). Baseflow measurements were extrapolated backward as the average of the first three measurements (JD 110, 111, and 112) for the preceding 9 days (JD 100 to 109). During the study period, there are 5 distinct increased flow events that were attributed to enhanced periods of melt. Discharge increased from values of 0.008 m^3/sec prior to melt to a maximum 0.445 m^3/sec (445 L sec^{-1}) on JD 157. The sudden spike on JD 157 was attributed to the release of a large amount of water retained in the upper portion of the basin known as the "Drift" adjacent to the Upper transect. Two additional peaks on JD169 and JD 180 are attributed to rainfall events.

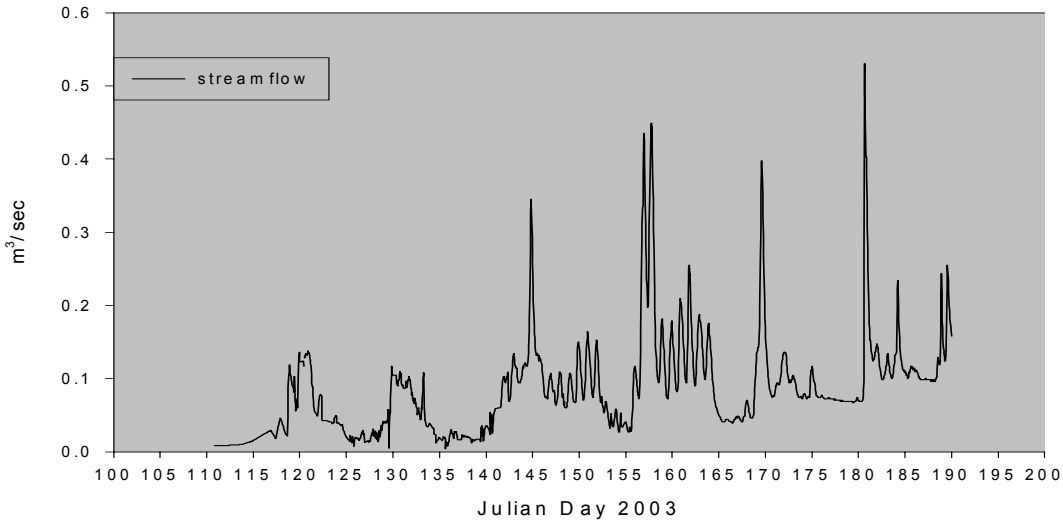

Figure 5.19 Streamflow discharge (m^3/s^{-1}) measured at the Granger Basin outlet.

Stream conductivity (SpC) is inversely related to discharge and can be used as a proxy to estimate when dilute snowmelt water is contributing to the stream (Kobayashi 1996; Kobayashi et al. 1999) (Figure 5.20). Considering that baseflow

conductivity is much higher than that of meltwater, declines in SpC can be used to evaluate when dilute meltwater reaches the stream channel. Conversely, when melt is suppressed, SpC returns to near baseflow conditions as indicated from JD 123-128 and JD 134-140. The release of the snow-dammed lake (GB Lake) and rapid meltwater release from Mount Granger (JD 157) and two precipitation events between JD 168 and JD 171) are also reflected in the stream conductivity as the event water results in a rapid dilution. The Hydrolab DataSonde 4a failed between JD 159 to JD 169 and no SpC data was obtained during this period.

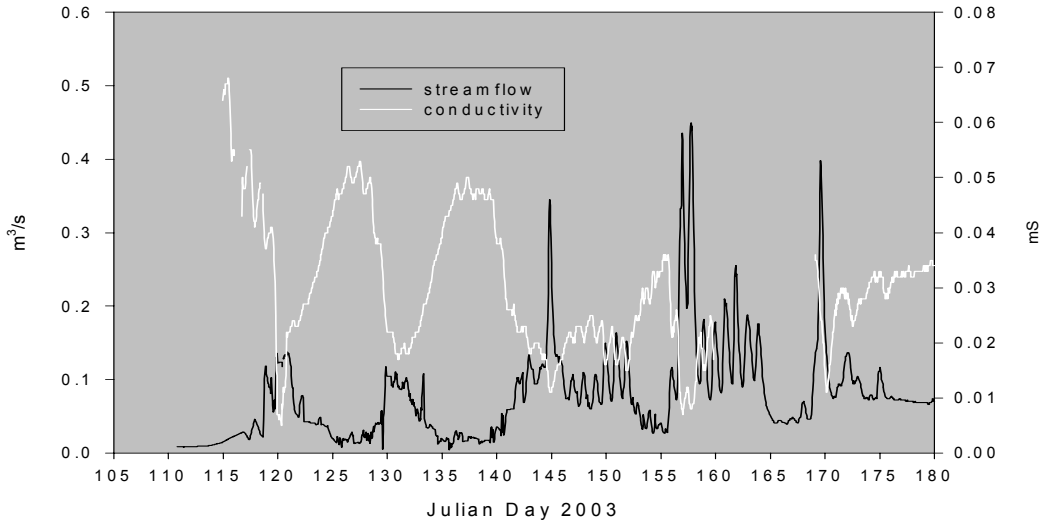

Figure 5.20 Streamflow discharge and specific conductivity measured at the Granger Basin outlet.

5.1.10 PRECIPITATION

The only rainfall event began late JD 168 and continued intermittently until JD 172 (Figure 5.21). The approximate daily amounts in millimetres are as follows: 0.7, 7.0, 1.5, and 0.4 for JD 168, 169, 170, and JD 171 respectively.

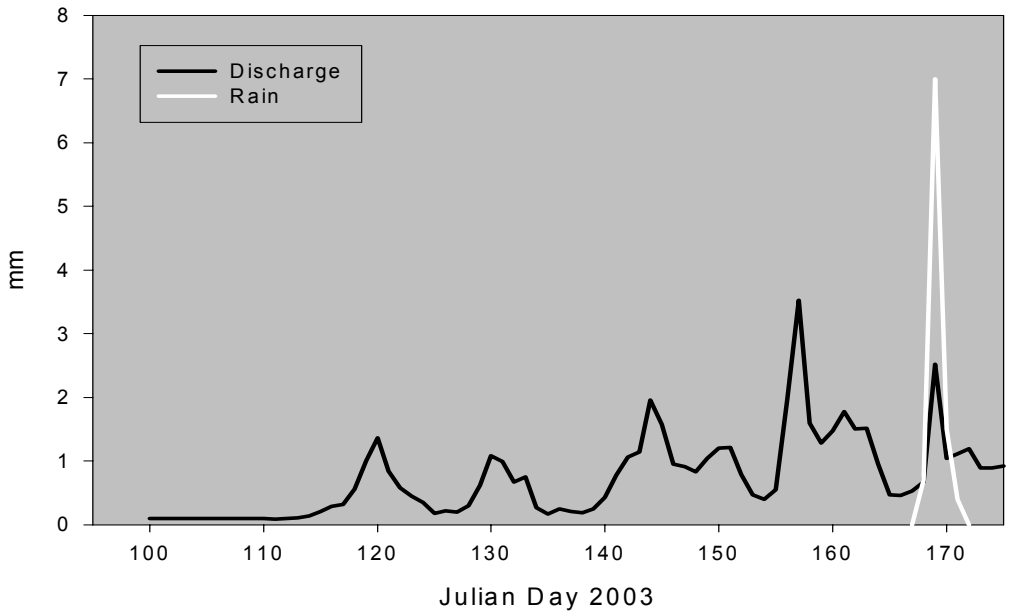

Figure 5.21 Basin discharge and rain events.

5.1.11 GB LAKE

A large surface depression, referred to as GB Lake, within the UX LU collects annual snowmelt runoff. This was the largest and most significant surface storage during the snowmelt period. Manual stage measurements began JD 121. Programmed stage measurements at GB Lake stage were recorded every 3 hours from JD 141 to JD 235. Lake stage increased steadily from the start of measurements to JD 154, followed by a rapid increase to the time of peak stage on JD 157. From the first measurement to the time of greatest storage surface area increased from *ca* 2062 m^2 to 12727 m^2. Field observations and the stage record showed a rapid release of water on JD 157 from GB Lake which coincided with the release of water retained by snow-dams in the headwater zone of the catchment.

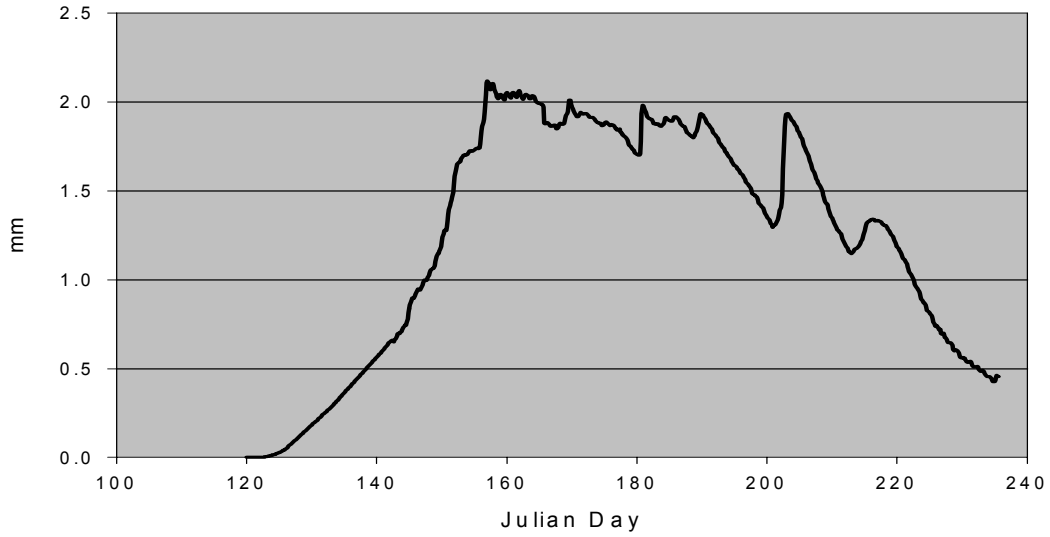

Figure 5.22 Change in Lake Storage (mm depth over Granger Basin).

While the release of melt water from GB Lake corresponded well with the hydrograph event of JD 157, the volumetric contribution to the daily discharge was approximately 0.025 mm of 3.5 mm for this particular day (Figure 5.23).

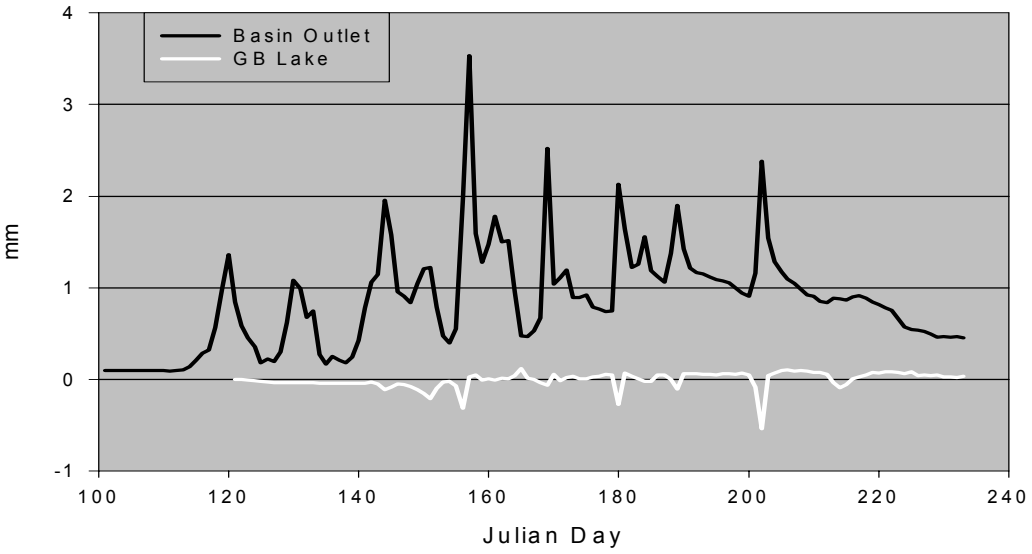

Figure 5.23 Daily Discharge showing GB Lake contribution.
(Negative values represent increase in lake storage).

5.2 WATER BALANCE RESULTS

The following sections outline the results for the snowmelt water balances of the individual LUs and the distributed basin water balance. The water balance equation [4.3] is presented again;

$$SWE - SUB = INF + ORG + Q$$

where SWE is the initial snow water equivalent of the snowpack, SUB is sublimation, INF is infiltration into frozen mineral soils, ORG is organic soil storage and Q is discharge. First, the above terms were determined for each LU, and then weighted based on their catchment area to provide a water balance for Granger Basin.

At the end of the snowmelt study period on JD 170, 189 mm of snowmelt occurred and 50 mm was observed as discharge from Granger Creek (Figure 5.24). Calculations of water balance components indicate that of the 189 mm, 108 mm infiltrated the mineral soils, 21 mm was stored in near surface organic soils, 3 mm sublimated and 57 mm of infiltration-excess occurred. At the onset of snowmelt, rapid melt overwhelmed the ability of organic and frozen mineral soils to store water, creating saturated conditions across much of the basin and generating infiltration-excess runoff, either at the surface in tundra environments or within the organic layer where travel time velocities are similar to surface flow (Quinton et al. 2001). The discrepancy in timing between the calculated runoff from Eq 4.3 and the measured discharge at the basin outlet is unsurprising considering the assumption that all excess meltwater immediately is transferred to the stream on the

same day, and that snow-choked channel processes are neglected (see discussion) and there are unknown measurement and model errors.

The water balances of the individual LUs show large variability in the timing and magnitude of water balance components (Figures 5.25 to Figures 5.28; Table 5.5). Differences in total SWE and the meltrate have a notable impact on the partitioning of meltwater within LUs. The Short Shrubs and SF LU had the earliest onset of melt and the shortest melt period, ending by JD 131 (Figures 5.25). At SS1 and SS2, almost all water was able to infiltrate frozen soils as predicted from Eq 4.3, providing a runoff ratio of less than 0.1 for both LUs. In the contrasting Tall Shrubs (Figure 5.26), INF by volume was between ca 30 and 40% greater than the Short Shrubs, and was the largest portion of the snowmelt water balance. However, as a fraction of SWE, INF was only 64, 56 48% of TS1, TS2, TS3 respectively. The organic layer contained nearly one quarter of the SWE at the end of the study period the Tall Shrubs. Sublimation from the snowpack was minimal in the Tall Shrubs and accounted for only less than 2% (3-4 mm) of the LU water balances. Given the measured discharge of TS1 (75 mm), the initial SWE (203 mm) and the water stored in the organic layer (45 mm) at the end of the study period, it is likely that Equation 4.3 overestimated INF and the water balance residual is attributed to a large overestimate in INF and will be discussed in Chapter Six.

The Tall Shrub LUs had water balances that reflected their greater SWE and prolonged melt. At TS1, melt commenced first, providing 20 mm of water to organic storage before infiltration into the mineral substrate and runoff generation began. At the end of the snowmelt period on JD 154, INF (128 mm) was

approximately 2.5 times greater than Q (53 mm). Runoff observed at the outlet of TS1 (78 mm) was greater than predicted by Eq 4.3, and was delayed with regards to timing, which can again be attributed to differential runoff travel times and model uncertainty. At TS2 and TS3, melt was prolonged, ending on JD 159 and JD 165 respectively. Differences in runoff ratios and water balance components among Tall Shrubs were due to the greater SWE at TS3, which surpassed the ability of soils to infiltrate additional water. The LX LU had a similar water balance to TS1, although snow persisted slightly longer despite smaller accumulation (Figure 5.27). The UX LU had a prolonged melt period until JD 158, with runoff occurring rapidly at the onset of melt as snowmelt overwhelmed the frozen soils ability to infiltrate water (Figure 5.27). On the SF, increased meltrates overwhelmed the ability of the frozen soils to infiltrate water, and 30 mm of runoff occurred, providing a runoff ratio of 0.19 (Figure 5.28). The NF LU had the greatest ORG and smallest INF of any site due to the ability of the overlying organic soils to store significant quantities of meltwater and the high water content of the mineral substrate. Runoff ratios were the highest of any LU at 0.46 (Figure 5.28).

In terms of total runoff contribution to basin runoff, the UX LU contributed 70% and the Tall Shrubs 18% of calculated Q. The large contribution of these LUs is in part attributed to their total basin areas (64%), yet in total they were responsible for 88% of Q. In contrast, the Short Shrub LUs contributed an estimated 1% of runoff despite 12% of the basin area. The SF and LX LUs had intermediate contributions based on area, whereas the NF LU had a very small area and a negligible total impact on basin runoff.

Table 5.5 Water balance components and runoff ratios for all LUs

	SWE (mm)	SUB (mm)	ORG (mm)	INF (mm)	Q (mm)	Runoff Ratio
SS1	98 (5.4)	3 (0.1)	0 (0)	88 (5.2)	8 (0.4)	0.08
SS2	107 (6.7)	3 (0.2)	0 (0)	94 (5.7)	10 (0.5)	0.09
TS1	203 (8.1)	5 (0.2)	45 (1.8)	138 (5.5)	15 [78] (0.6) [3.1]	0.07 [0.38]
TS2	206 (14.4)	4 (0.3)	47 (3.5)	129 (9.0)	26 (1.8)	0.13
TS3	279 (19.3)	5 (0.4)	65 (4.6)	133 (9.3)	75 (5.2)	0.26
UX	204 (93.0)	4 (1.8)	0 (0)	113 (51.9)	87 (40.0)	0.43
LX	167 (23)	2 (0.3)	50 (6.7)	101 (13.6)	14 (1.9)	0.09
NF	201 (4.0)	3 (0.1)	55 (1.1)	52 (1.0)	92 (1.8)	0.46
SF	164 (14.7)	2 (0.2)	47 (4.0)	98 (8.8)	19 (1.7)	0.12
Granger Basin	189	3	21	110	54 [50]	0.29

All values are in millimetres. Values in rounded brackets are the estimated amount from each LU contributing to the GB water balance. Values in square brackets are observed values of discharge. SWE is snow water equivalent, SUB is sublimation, ORG is organic layer storage, and Q is runoff.

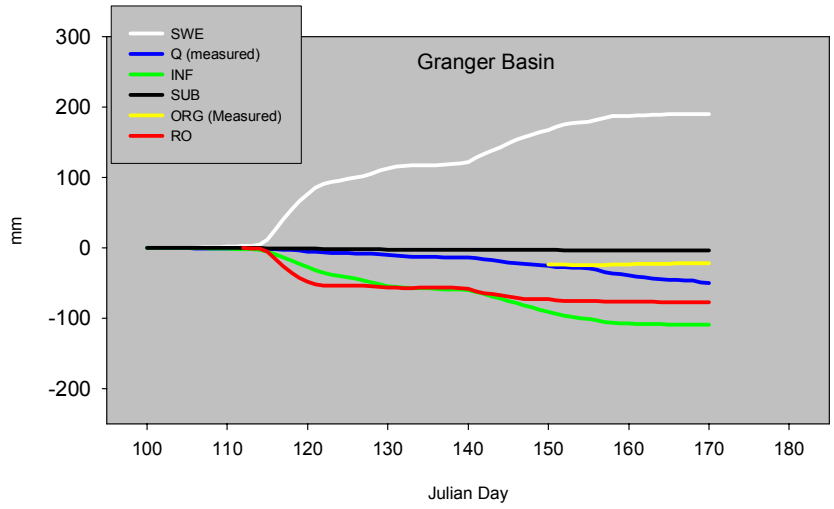

Figure 5.24 Cumulative water balance for Granger Basin.

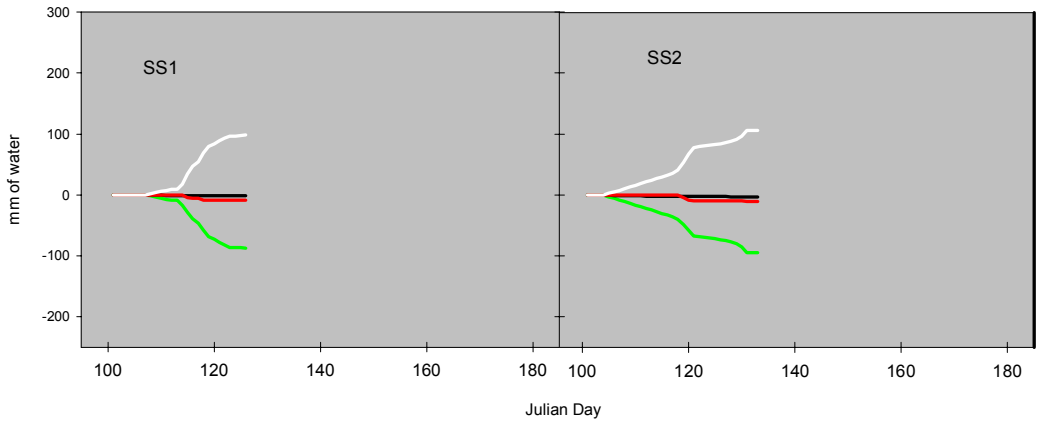

Figure 5.25 Cumulative water balances for SS1 and SS2 Landscape Units.

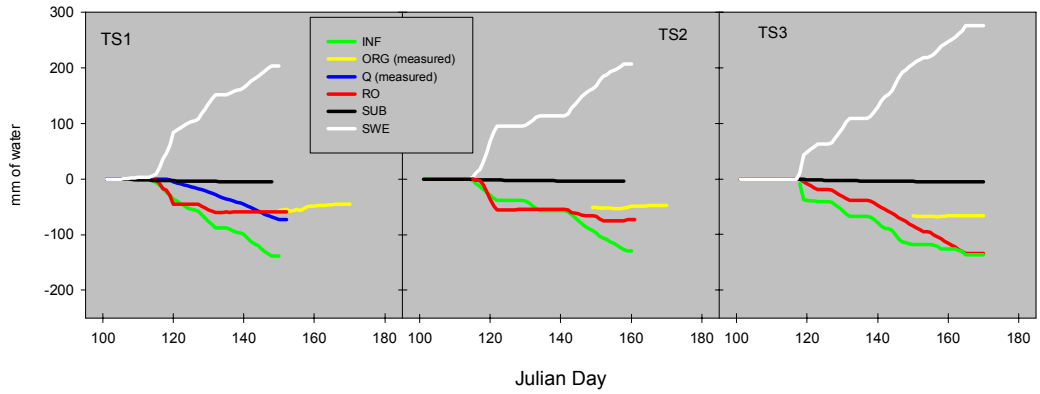

Figure 5.26 Cumulative water balances for TS1, TS2, and TS3 Landscape Units.

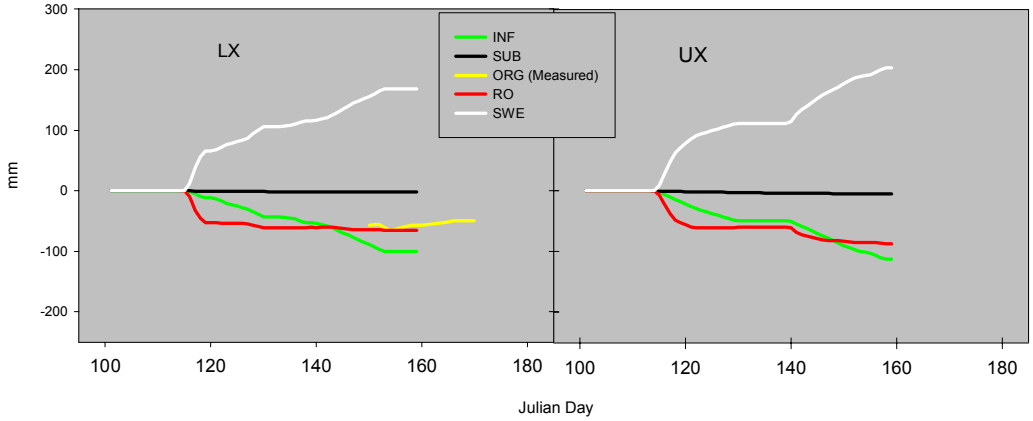

Figure 5.27 Cumulative water balances for LX and UX Landscape Units.

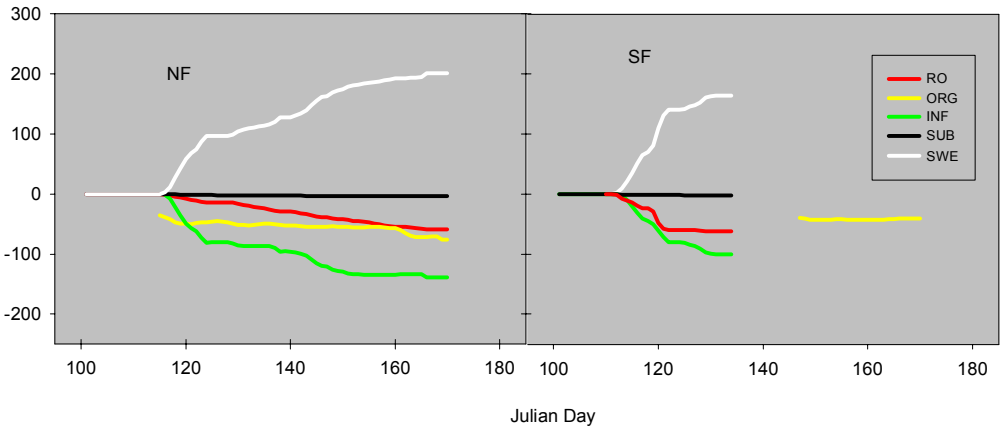

Figure 5.28 Cumulative water balances for NF and SF Landscape Units.

CHAPTER 6
6.0 DISCUSSION

This study examines the snowmelt hydrology of a discontinuous permafrost catchment of subarctic, Yukon. By partitioning the basin into LUs based on their directly observed physiographic and vegetation characteristics and determining water balances for each, practical information on the differential storages and pathways of water during melt and the most influential controlling factors controlling freshet response are identified. This study is unique in that it explores hydrological processes and interactions of landscapes typical to subarctic north-western Canada just beyond the traditional headwater scale. While similar hydrological investigations have divided basins into specific areas or landcover types (i.e. Marsh and Pomeroy 1996; Woo and Young 1997) and/or determined water balances during the snowmelt period (i.e. Kane et al 1991; Woo and Young 1997; Carey and Woo 2001; Spence 2000), this study combines both approaches while linking freshet discharge events to distinct areas of the basin, referred to here as Landscape Units. Identifying the spatial variability in pre-melt SWE has been cited as more important than capturing spatial variability in melt (Anderton et al. 2002; Pohl et al. 2005, 2006a, 2006b, 2006c; Luce et al. 1998; 1989; Hartman et al. 1999). This collective body of literature highlights the importance of identifying the spatial variation in pre-melt SWE and subsequent temporal and spatial differences in meltwater release from different landcover types. This a-priori

identification is critical for the development and/or application of distributed hydrological models in cold regions for predicting snowmelt runoff (Pietroniro and Soulis 2003). However, it is evident that the factors controlling pre-melt SWE and melt energy are not consistent among catchments. Furthermore, the pathways and mechanisms that affect meltwater delivery from the catchment to the drainage networks at larger scales have not been intensively studied.

This study provides new and additional insight into the process of snowmelt runoff hydrology at the meso-scale by documenting the effect of snowmelt water balance variability among different geographic regions on the streamflow hydrograph of a discontinuous permafrost basin. In this study, pre-melt SWE was closely associated with landscape attributes such as topographic depressions, leeward slopes, and taller shrub vegetation stands. For example, the north face LU consistently had a greater SWE than the south face LU despite their close proximity, which was largely attributed to prevailing winds that form a large drift at the top of the NF LU. Differences in SWE between SF and NF may also be attributed to greater pre-melt sublimation losses on the SF (Carey and Woo 1998, 1999; Pomeroy et al. 2003). The Tall Shrub SWE was more than twice that of the Short Shrubs which was attributed to the net loss of wind blown snow from the exposed flatter areas to the adjacent low-lying shrub areas (Pomeroy et al. 1999). This highlights the importance of shrub vegetation in reducing wind speed and preferentially accumulating wind-blown snow (Essery and Pomeroy 2004; Liston et al. 2002; McFadden et al. 2001; Pomeroy et al. 1999; Sturm et al. 2001a). There has been increased investigation into the role of shrub vegetation and it's impact on

cold region hydrology because of its expansion in the subarctic and arctic (Sturm 2001b; Sturm et al. 2005). Consequently, this expansion of shrubs will likely increase snow accumulation to a limit controlled by the blowing snow regime (Essery and Pomeroy 2004). Although not as pronounced, the LUs in the upper basin had a greater SWE than LUs in the lower basin. Snowmelt rates exhibited little variability among LUs. Aside from the NF and SF LUs that had strong contrasts in their radiation regime, all other LUs had an average meltrate between 4.1 and 5.3 mm d^{-1} (Table 5.4). Furthermore, there was no relation between elevation and meltrate. This suggests that aside from LUs with strong aspects, variability in snow accumulation has a greater influence on the partitioning of water balance components than variability in meltrate in this basin.

During melt, water infiltrates into the frozen soil beneath the snowpack. In cases where there is an organic soil layer atop mineral soils, water infiltrated the organic soils unimpeded and raised the soil moisture to its approximated drainable porosity. Where present, the volume of water stored in the organic layer was between 10 and 25% of SWE, and controlled by the thickness of the organic horizon. At the NF and Tall Shrub LUs, organic soil storage delayed runoff by several days after the onset of melt until its moisture deficit was satisfied. Additional meltwater inputs percolated through the organic layer and encountered the sharp discontinuity in hydraulic properties at the organic-mineral interface. As water encountered this discontinuity, INF rates were at a maximum, and then rapidly declined as the capillary gradient decreased (Zhao et al. 1997). In this study, it was assumed that percolation from organic to mineral layers was controlled

by the parameters outlined in the Zhao and Gray (1999) frozen soil infiltration/percolation equation (Eq. 2.2). Of these parameters, INF is most sensitive to pre-melt soil water content and porosity, with soil temperature, initial SWE, and infiltration opportunity time providing secondary controls. In areas with high pre-melt soil water contents (NF), infiltration was impeded as the saturation deficit is quickly satisfied when melt begins. In contrast, when soil water contents are low, large fractions of SWE can infiltrate into the mineral substrate (SS1 and SS2). In these cases, vertical water fluxes predominate as the high infiltration capacity suppresses runoff (i.e. Carey and Woo 1998; Kane et al 1981; Slaughter and Kane 1979). An unexpected result was the runoff ratio of 0.29 predicted for the permafrost-free SF LU as previous studies on this LU (Carey and Quinton 2005; Pomeroy et al. 2003) indicated limited runoff contribution. However, in 2003, the rapid nature of melt compared with other years likely overwhelmed the ability of the frozen soil to infiltrate water.

The areas responsible for the bulk of springtime streamflow were the Tall Shubs and the UX LUs. Discharge (Q) from these LUs accounted for 81% of the total discharge for the basin and was synchronized most closely with measured streamflow discharge. The UX LU was a large contributor to total flow because of its large area and lack of organic soil, which combined with a large SWE, resulted in substantial runoff production. At the Tall Shrub LUs, large SWE and rapid melt exceeded the ability of the soils to infiltrate meltwater. Despite the presence of thick organic soils, their high antecedent wetness prior to melt (particularly TS3) resulted in soil storage being quickly satisfied, reducing INF and enhancing Q.

Furthermore, Tall Shrub areas were observed to have well developed drainage networks, with near-surface drainage pathways that facilitated runoff. The timing of melt in all three Tall Shrub transects was timed well with basin discharge (Figure 6.1).

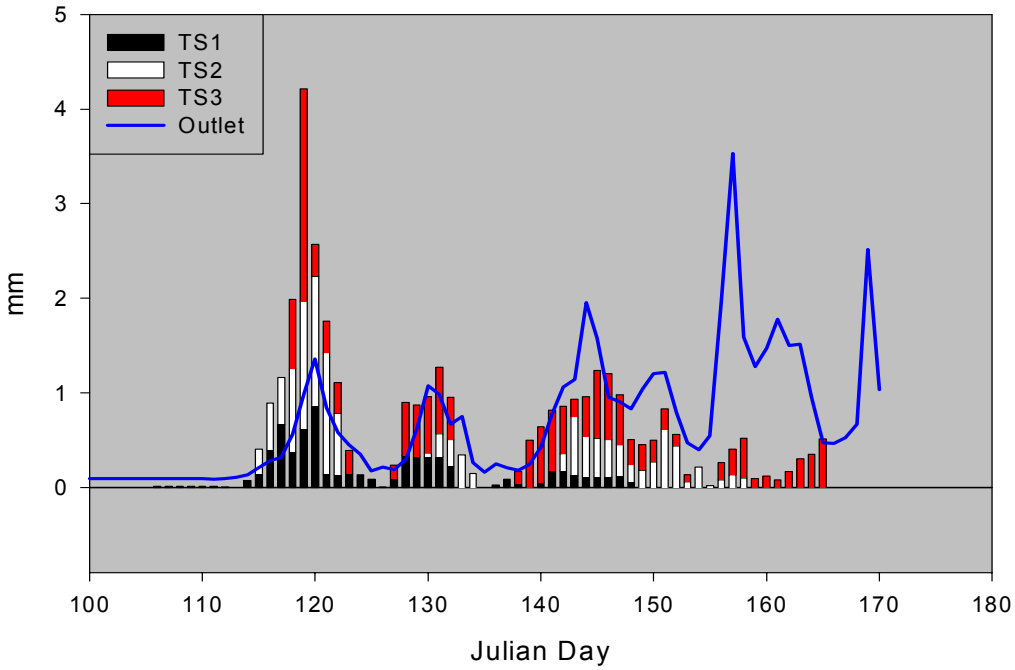

Figure 6.1 Basin discharge and daily snowmelt for TS1, TS2 and TS3.

Measurements from TS1 provide supporting evidence documenting the important role that tall shrub areas have on freshet discharge. Discharge from TS1 was first measured on JD 119 (Figure 6.2) and it is unlikely that a significant quantity of water left this LU before that time and measurements ended on JD 153 with only trace amounts of flow occurring thereafter. The estimated contribution from TS1 was on average 19% (max 55%, min 3%) of the daily discharge for the measurement period. By the end of JD 154 when TS1 measurements were stopped, it had contributed 11% (3 mm) of total discharge (28 mm) while comprising an

estimated 4% of total basin area. As stated, just under 40% of the SWE from this LU discharge. While contribution from the other two tall shrubs could not be measured, observations indicate that they exhibited similar hydrological behaviour as did TS1. Based on the premise that close to 40% of the SWE was partitioned to discharge, these three areas contributed more than 30% of the basin discharge while occupying less than 20% of the area.

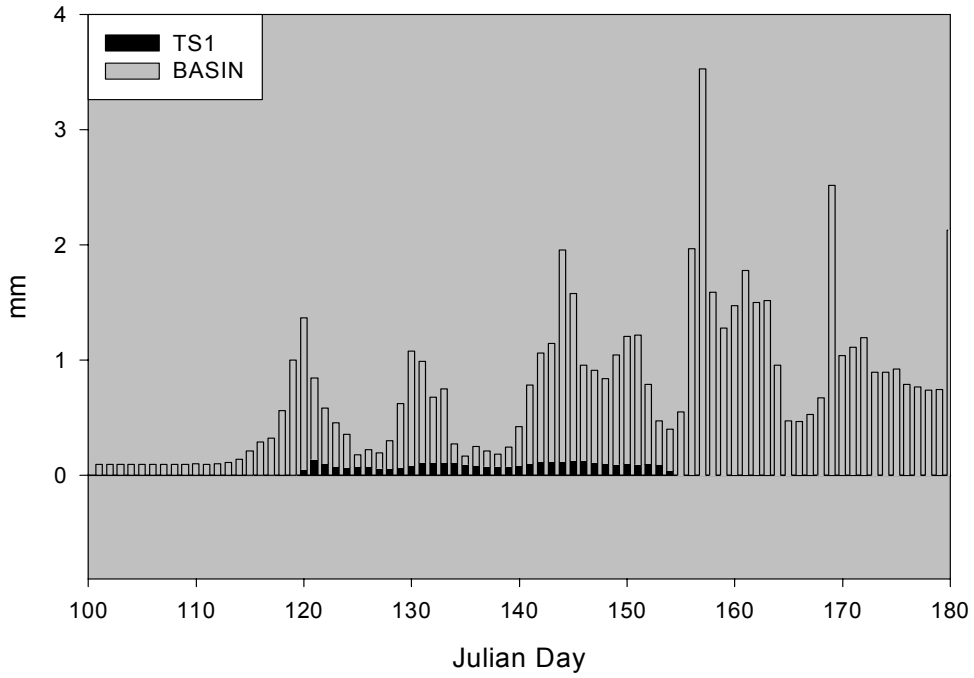

Figure 6.2 Granger Basin daily discharge and TS1 measured contribution.

The combined effect of the large SWE, proximity to the drainage network, active water-tracks and runoff pathways strongly affected basin hydrology during the snowmelt period. Furthermore, where organic soils are widespread, they are able to store a significant volume of meltwater. However, the timing of freshet appears most closely associated with the timing of saturation excess generated from

when mineral soil infiltration capacity is exceeded. This observation agrees with hillslope and plot-scale investigations of runoff processes that show water rapidly percolates to the organic/mineral interface, and due to the less transmissive nature of mineral soils, a zone of saturation forms at this interface and wets-up toward the surface (Hinzman et al. 1993; Carey and Woo 2001a). When this saturated zone develops at the organic/mineral interface, lateral runoff is initiated and near-surface pathways such as soil pipes (Carey and Woo 2000), water tracks (McNamara et al. 1998) and inter-hummock flow (Quinton and Marsh 1998; 1999) become active.

In contrast, Short Shrub LUs had little influence on streamflow due to their small SWE, large INF and lack of a developed drainage network. Whereas previous research examined runoff processes in detail (Carey and Woo 2001b; McNamara et al. 1998; Quinton et al. 2004), these results demonstrate that catchment properties such as vegetation and soil profiles control the volume of vertical and lateral water fluxes. In areas with high SWE, soil moisture and rapid melt, lateral hydrological fluxes are enhanced. In Granger Basin, the alpine (UX) area augment lateral fluxes due to increased accumulation and reduced soil moisture storage. While the tall shrubs augment lateral fluxes due to increased accumulation and their connectivity to the main channel via well developed drainage networks.

While a small fraction of the SF LU was adjacent to the main channel, any lateral runoff originating within the organic layer was small compared with other streamflow contributors. This corresponds with the notion that permafrost-free south facing slopes rarely generate runoff in this environment (i.e. Carey and Woo 1998; 2001a; Slaughter and Kane 1979; Santeford 1978). The NF had small

streamflow contributions despite large SWE, minimal INF and storage and proximity to the stream because of its small catchment area.

6.1 SOURCES OF ERROR

One of the greatest challenges and most poorly documented processes in snowmelt dominated basins of the subarctic is channel development. Because of this, snowmelt discharge events may exhibit delayed and diminished relations, where meltwater reaches the stream but is retained before flows reach the outlet (Russell et al. 2004; Woo and Sauriol 1980). In GB, flow downstream is inhibited by dense snow in the channel and aufeis. Meltwater accumulates behind snow dams until a more discrete channel is carved. This temporary storage complicates the analysis, particularly early in the melt season, as changes in the hydrograph may be indicative of channel not catchment processes as water retained within the channel may suddenly release at any time due to the failure of the retaining snowpack or snow dam (Xia and Woo 1992).

Channel freezing occurred between JD 121 and 126, creating an additional temporary channel storage that could not be quantified (Figure 6.3). This lead to a delay suggesting that water attributed to early season melt events was being measured much later in the study period. Also with regards to channel processes, a large amount of aufies was unexpectedly found near the headwater region of the catchment (Figures. 6.4, 6.5) which altered the timing and pathways of meltwater once it had reached the stream. While the water equivalent of the aufies was unknown it would have contributed to flow near the end of the study period and

afterwards since a portion of the aufies remained after JD 170. The influence of aufies on the runoff hydrograph is largely unknown (Reedyk et al. 1995).

Figure 6.3 Frozen runoff in channel near LX LU (JD 122).

Figure 6.4 Aufies in Granger Creek (JD 117).

Figure 6.5 Aufies in Granger Creek (JD 153).

Accurate quantification of the pre-melt accumulation is undoubtedly one of the most important aspects of any hydrometric mass balance investigation involving snowmelt. One of the largest difficulties preventing this is overcoming the logistical hurdles associated with basin-scale process studies. Errors associated with the extrapolation of point source data to an area increases with increasing area of the LU to which the data is being applied to (Woo 1997). There is uncertainty as to the representativeness of the snow-survey transects, most significantly for the UX LU which covers 40% of the basin. A large perennial snowpack exists in the upper reaches of this LU on the lee-side of Mount Granger that was inaccessible. It was anticipated that any meltwater contributions from this area would not have occurred until after the study period and that the small area of the perennial snow patch would result in a small contribution to streamflow.

However, the discharge events on JD 156 and 157 were attributed to release of water retained at the base of the slope and the near catastrophic the release of Granger Lake (Figures 6.6, 6.7, 6.8). Another factor leading to the uncertain approximation of SWE was not considering the large snowpack on the lee-side of Mt. Granger. It was assumed that snow-melt contributions from this area would have not occurred until much later in the season. However, because of a lack of measurements it is speculated that its role in the overall basin hydrology was likely underestimated. Discharge measurements slightly down stream of the catchment headwaters recorded for the summer period indicate that on average 80% of daily flow is attributed to upstream sources that account for a small fraction of the basin (Figure 6.9).

Figure 6.6 Release of snow-dammed GB Lake JD 157

Figure 6.7 Water retained in saturated channel snowpack; base of Mt. Granger (JD 156).

Figure 6.8 Release of water retained in channel snowpack: Base of Mt. Granger (JD 157).

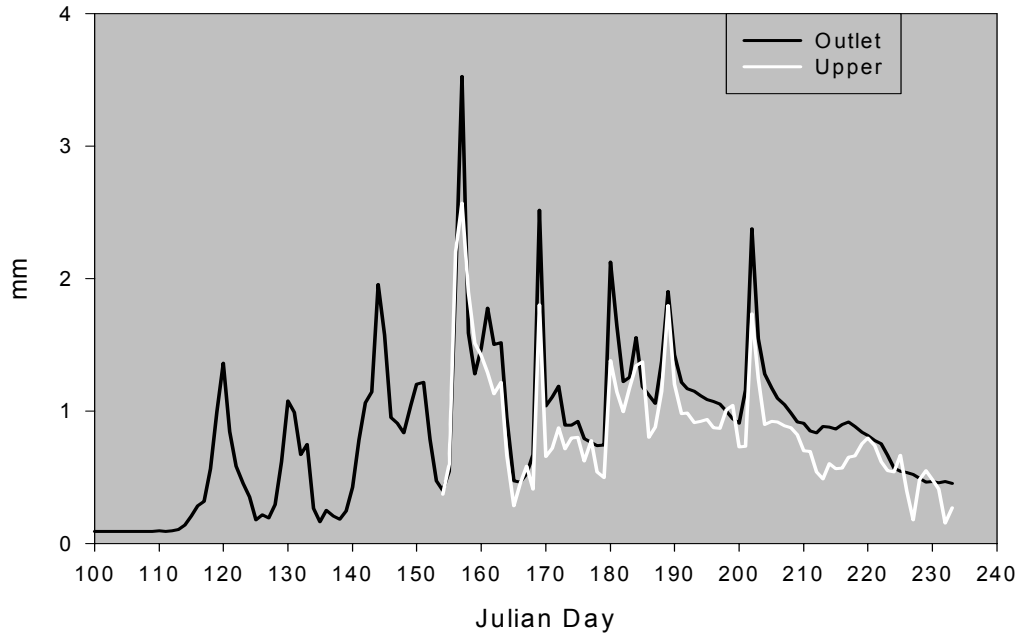

Figure 6.9 Daily discharge from the upper basin compared to Granger Basin.

The infiltration equation of Zhao and Gray (1999) has only received limited application for this environment (Janowicz et al. 2002) and no testing on slopes. Janowicz (2000) used the twin probe gamma attenuation method to measure cumulative infiltration into frozen ground in the Wolf Creek area, which was then compared to Equation [2.2]. The closest agreement between measured and modeled INF was found at SWEs greater than 80 mm where estimated infiltration was on average 1.27 times greater than measured. The results of that study also showed measured INF exceeding the initial SWE. It was suggested that in situations where observed INF exceeded the SWE, other processes in addition to infiltration were involved.

Comparing infiltration-excess predicted runoff and observed discharge Eq. 2.2 appears to underestimate INF from the perspective of GB while overestimating

INF for TS1. By intensively studying all other water balance components of TS1, it was possible to estimate INF as a water balance residual and compare it with Equation [2.2]. Of the 204 mm pre-melt SWE approximately 75 mm was discharged by JD 153, while 45 mm was contained in the organic soils. This suggests that no more than 83 mm of the original SWE could have infiltrated frozen mineral soils assuming no evaporation or sublimation. The estimated INF from Equation [2.2] was 130 mm, overestimating by a factor of 1.6, which is likely attributed to inaccurate estimates the equation parameters, and potentially, problems with the equation as applied to this environment. Marsh and Woo (1993), using an empirical simplified form of Eq. 2.2 overestimated frozen soil when comparing to in-situ measurements. Their study predicted INF of 79 and 116 mm for a snowpack of 150 and 289 mm respectively, yet observed INF was only 9 and 38 mm, (6 and 13 % of the initial SWE). While that study took place in the high-arctic, it is one of the few studies that compares predicted INF to observed INF. Marsh and Woo (1993) suggest that an equation similar to Eq. 2.2 overestimates infiltration in a high-arctic environment because of surface sealing upon freezing of meltwater. The occurrence of soil macropores could increase apparent infiltration dramatically from the predicted infiltration into the frozen soil matrix. A large potential source of model error is the uncertainty in equation parameters and variables because of extrapolation across LUs. The brief sensitivity analysis for INF in TS1 below shows how it varies with small changes in the equation parameters. At the observed values, a 1% error in initial soil water content results in a 2.2% error in INF (Figure 6.10); a 1% change in S_0 (surface saturation) will result in a 2 % change in INF

(Figure 6.11); a 5% over/underestimate in porosity will affect INF by 10% (Figure 6.12); and if temperature is over or underestimated by 0.5°C INF would be in error of just over 20% (Figure 6.13).

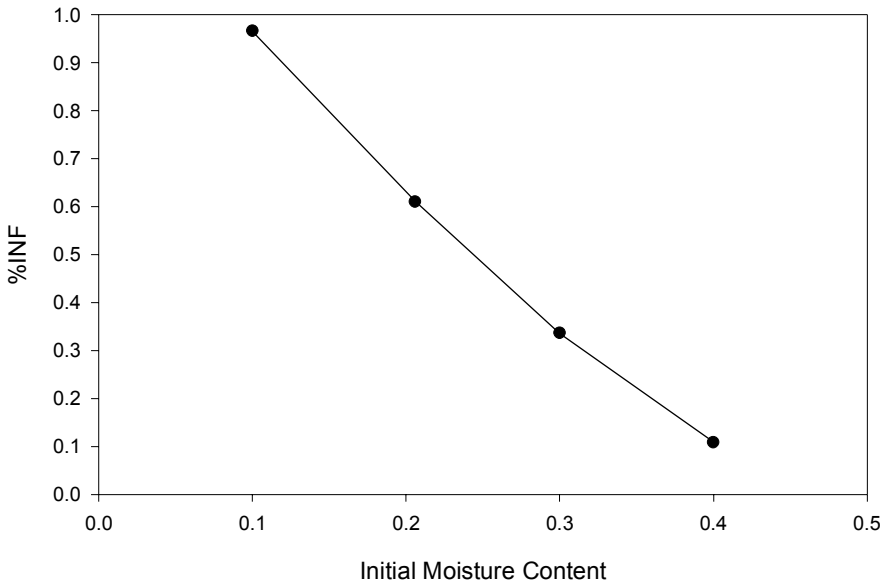

Figure 6.10 Response to increasing initial soil moisture content (Figure F1). X axis represents the equation parameter and the response is plotted as a percentage of the SWE.

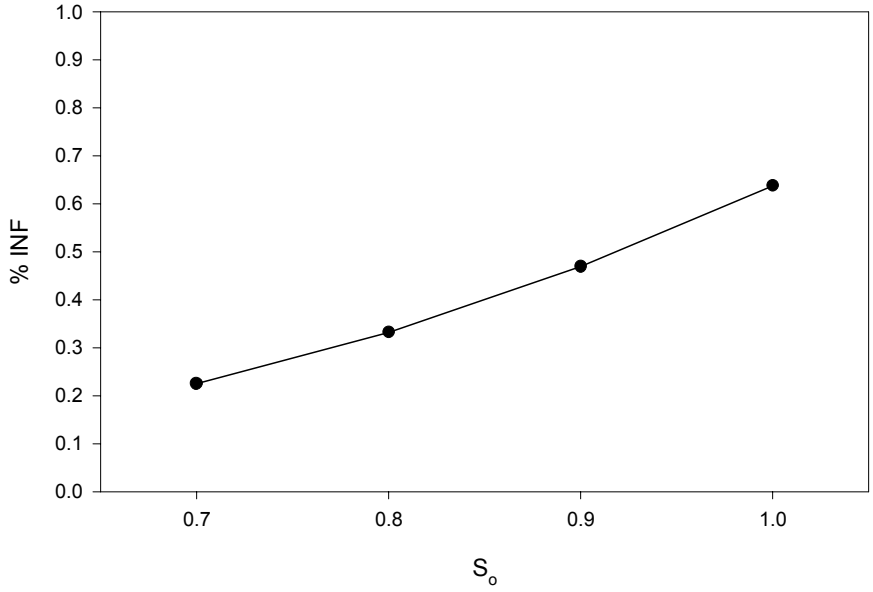

Figure 6.11 Response to increasing surface saturation (Figure F2). X axis represents the equation parameter and the response is plotted as a percentage of the SWE.

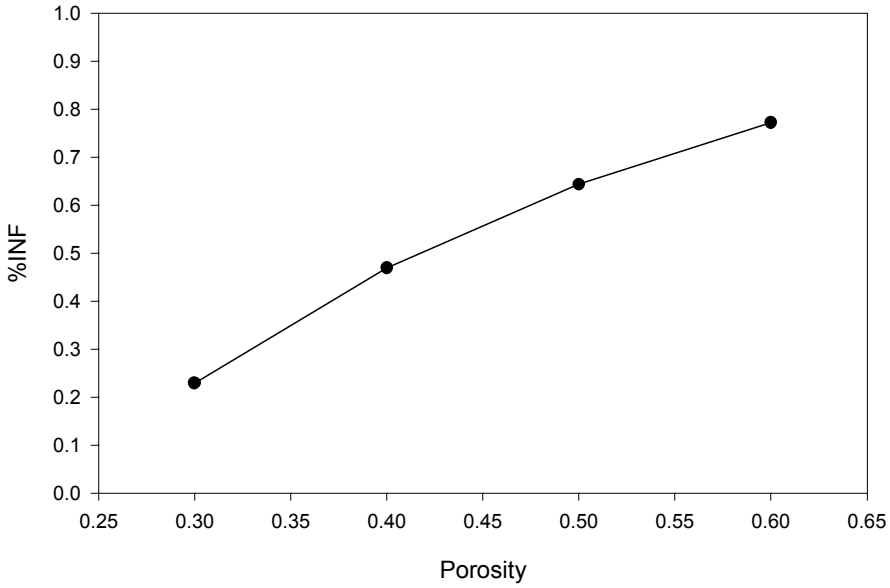

Figure 6.12 Response to increasing soil porosity. X axis represents the equation parameter and the response is plotted as a percentage of the SWE.

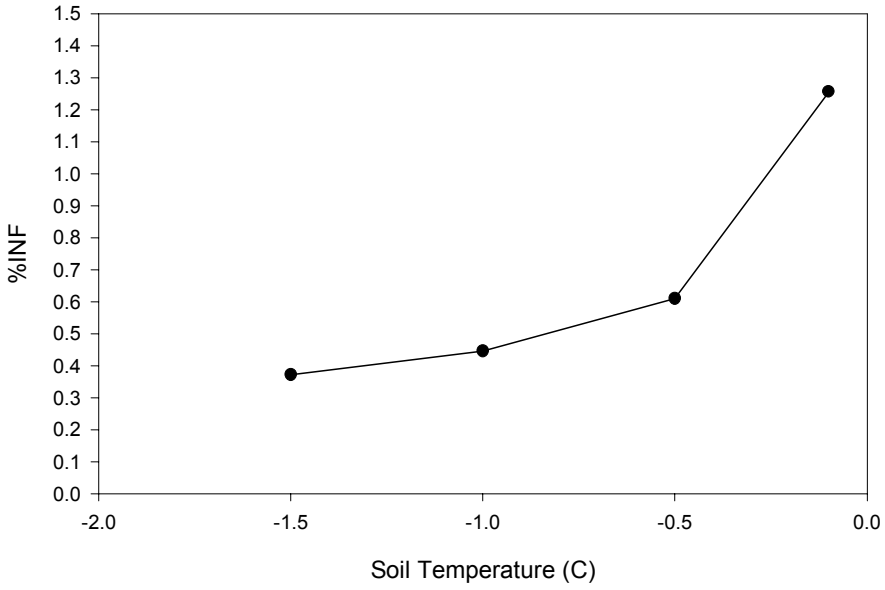

Figure 6.13 Response to increasing initial soil temperatures. X axis represents the equation parameter and the response is plotted as a percentage of the SWE.

The basin snow water equivalent was the summation of the maximum SWE for each area multiplied by the LU area as a fraction of the total basin area. The greatest range of SWE occurred in TS2, TS3, UX, and NF, some of the largest areas of the basin. Standard error estimates of SWE range from 3% (SS2) to 20% (TS3), with an average mean standard error of 10%. This may have resulted in an over-estimated SWE for each LU leading to cumulative errors in the water balance.

In Eq. 2.2, all errors are accumulated in Q, which is calculated as a residual. If all errors are cumulative and in the same direction, Q has an absolute uncertainty of more than 50%. However, considering the differences in the absolute value of measured discharge at TS1 (78 mm) and the residual Q (15 mm) as determined by Eq. 2.2, an inaccuracy of almost 80% exists.

CHAPTER 7
7.0 CONCLUSIONS

This study examined the meltwater hydrology of an 8 km^2 subarctic basin by segmenting the catchment into contrasting Landscape Units (LUs). The comparison of the water balance variability and hydrologic properties of each Landscape Unit indicated that certain areas have related characteristics or hydrologic responses before and during the snowmelt period. While areas with greater snow accumulation were associated with taller shrub vegetation, leeward slopes and increasing elevation, the only appreciable difference in accumulation were in the Short Shrubs and TS3 areas. SS1 and SS2 were approximately 43% below the mean SWE, while TS3 was 53% above average. All others were within 15%. As such the absence of shrub vegetation on the wind-swept plateaus had a much greater impact on pre-melt accumulation when compared to elevation, aspect, or the presence of shrub vegetation.

At the end of the snowmelt study period on JD 170, 189 mm of snowmelt occurred and 50 mm was observed as discharge from Granger Creek. Calculations of water balance components indicate that of the 189 mm, 108 mm infiltrated the mineral soils, 21 mm was stored in near surface organic soils, 3 mm sublimated and 57 mm of infiltration-excess occurred.

The amount of accumulation had little effect on the average melt rate as all LUs displayed similar melt rates. The timing of melt varied among LUs and was

controlled by available energy. Melt rates averaged over the entire period were similar among LUs, except for those with contrasting aspects (SF, NF), where both the SF average rate of depth decline and rate of SWE decline was more than twice that of the NF.

Runoff was enhanced at the expense of infiltration in LUs with: i) high SWE, ii) rapid meltrates, iii) thin or no organic soil covers, iv) high antecedent moisture in the mineral soil, and v) cold soil temperatures. For Granger Basin, the Tall Shrub and UX LUs accounted for 88% of the computed runoff while accounting for 64% of total area.

The observed differences in snowmelt water balances at the headwater scale has significance to the structure of hydrological models that attempt to predict basin freshet in this environment (i.e. Pietroniro and Soulis 2003). Models that try to lump landscape at too coarse of a spatial scale will miss the primary runoff generating zones of the catchment. Quantification and incorporation of sub-grid variability based on landscape attributes is a first step towards improved hydrological prediction. Futhermore, the observation that areas with increasing shrub vegetation height trap more snow in alpine basins has important climate change impacts for increasing runoff volume considering the widespread expansion of shrubs in the past century (Sturm et al. 2001).

Results from this study indicate that areas with preferential flow pathways and connectivity to the stream network are vital to the spring freshet. These areas, which are typically associated with higher accumulations, exceed the recharge capacities of the soil resulting in a greater fraction of the SWE contributing to

streamflow during the snowmelt period. Measurements made from TS1 indicated that almost 40% of SWE made it to the stream shortly after ablation. The absence of direct discharge measurements from TS2 and TS3 served to reduce the empirical support of the combined influence of all Tall Shrub areas. Future investigations attempting to predict the timing and magnitude of early season streamflow in subarctic basins should focus more on areas like these because of the larger fraction of SWE that consistently accumulates there and the subsequent rapid transmission of meltwater to the stream network.

Literature Cited

Anderton, S.P., White, S.M., and Alvera, B. 2003. Evaluation of spatial variability in snow water equivalent for a high mountain catchment *Hydrological Processes.*18: 435-453.

Benson, C.S. and Sturm, M. 1993. Structure and wind transport of seasonal snow on the Arctic slope of Alaska. *Annals Glaciology.* 18: 261-267.

Bevin, K. How far van we go in distributed hydrological modeling? *Hydrology and Earth Systems Sciences.* 5: 1-12.

Bloschl, G. 1999. Scaling issues in hydrology. *Hydrological Processes.* 13: 2149-2175.

Bloschl, G. and M. Sivapalan. 1995. Scale Issues in Hydrological Modelling: A Review. *Hydrological Processes.* 9: 251-290.

Bloschl, G. 2001. Scaling in hydrology. *Hydrological Processes.* 15: 709–711.

Burn, C.R. 1990. Snowmelt infiltration into frozen soils at sites in discontinuous permafrost near Mayo, Yukon Territory. In Prowse and Ommanney (Eds), Northern Hydrology 445-459.

Buttle, J.M. and J.J. McDonnel, 1987. Modelling the areal depletion of snowcover in a forested catchment. *Journal of Hydrology*. 90: 43–60.

Carey SK. 2003. Dissolved organic carbon fluxes in a discontinuous permafrost subarctic alpine catchment. *Permafrost and Periglacial Processes.* 14: 161-171.

Carey, S.K., and Woo, M.K., 1998. Hydrology of two subarctic slopes. Southern Yukon, Canada. *Nordic Hydrology.* 29:331-446.

Carey, S.K., and Woo, M.K., 1999. Hydrology of two slopes in subarctic Yukon, Canada. *Hydrological Processes.* 13: 2549-2562.

Carey, S.K., and Woo, M.K., 2000. The role of soil pipes as a slope runoff mechanism, Subarctic Yukon, Canada. *Journal of Hydrology.* 233: 206-222.

Carey, S.K., and Woo, M.K., 2001a. Spatial variability of hillslope water balance, wolf creek basin, subarctic Yukon. *Hydrological Processes.* 15: 3113-3132.

Carey, S.K., Woo, M.K., 2001b. Slope runoff processes and flow generation in a subarctic, subalpine catchment. *Journal of Hydrology.* 253: 110-219.

Carey SK, and Quinton WL. 2004. Evaluation of runoff generation during summer using hydrometric, stable isotope and hydrochemical methods in a discontinuous permafrost environment. *Hydrological Processes.* 19: 95-114.

Chacho, E.F. and Bredthauer, S. 1983. Runoff from a small subarctic watershed, Alaska. In *Permafrost, Fourth International Conference.* National Academy Press, Washington D.C. 115-120.

Curry, R., Dickson, B., and Yashayaev, I. 2003. A change in the freshwater balance of the Atlantic Ocean over the past four decades. *Nature.* 426: 836-839.

Davar, K. 1970. Peak flow snowmelt events. In (Eds) Gray. D.M. *Handbook on the Principles of Hydrology*.National Research Council of Canada, Ottawa.

de La Casiniere, A. C., 1974: Heat exchange over a melting snow surface. *Journal of Glaciology.* 13: 55–72.

Dingman, S.L. 1973. Effects of permafrost on streamflow characteristics in the discontinuous permafrost zone of central Alaska. In *Permafrost, Second International Conference, National Academy of Sciences. Wasthington, D.C.* 447-453.

Dingman, S. L. 1994. *Physical Hydrology.* McConnin, R. (Ed) 575p.

Dunne, T. and Black, R.D. 1971. Runoff processes during snowmelt. *Water Resources Research.* 7: 1160-1172.

Dunne, T., Price, A., and Colbeck, S.C., 1976. The generation of runoff from subarctic snowpacks. *Water Resources Research* 12: 677-685.

Dye, D.G., 2002. Variability and trends in the annual snowcover cycle in the northern hemisphere land areas, 1972-2000. *Hydrological Processes.* 16: 3065-3077.

Engelmark, H. and Svensson, U. 1993. Numerical modelling of phase change in freezing and thawing unsaturated soil. *Nordic Hydrology.* 24: 95-110.

Essery, R. 1997. Modelling fluxes of momentum, sensible heat and latent heat over heterogeneous snow cover. *Quarterly Journal of the Royal Meteorological Society.* 123: 1867-1883.

Essery, R. 1999. Parameterization of heterogeneous snowmelt. *Theoretical and Applied Climatology.* 62: 25-30.

Essery, R. and Pomeroy, J.W. 2004. Implications of spatial distributions of snow mass and melt rate on snowcover depletion: theoretical considerations. Annals of Glaciology: International Symposium on snow and avalanches, Davos Switzerland.

Faria, D.A., Pomeroy, J.W. and R.L.H. Essery, 2000. Effect of covariance between ablation and snow water equivalent on depletion of snow-covered area in a forest. *Hydrological Processes.* 14: 2683–2695.

Flerchinger, G.N. and Saxton, K.E. 1989a. Simultaneous heat and water model of a freezing snow-residue-soil system I. Theory and Development. *Transactions of the ASAE.* 32 565-571.

Flerchinger, G.N. and Saxton, K.E. 1989b. Simultaneous heat and water model of a freezing snow-residue-soil system II. Field verification. *Transactions of the ASAE.* 32 573-578.

Giesbrecht, M. and Woo, M.K. 2000. Simulation of snowmelt in a subarctic spruce woodland: 2. open woodland model. *Water Resources Research*. 36: 2287-2295.

Granger, R.J., D.M. Gray and G.E. Dyck. 1984. Snowmelt infiltration to frozen prairie soils. *Canadian Journal Earth Sciences.* 21: 669-677.

Granger, R.J., Pomeroy, J.W., and Parvianen, J. 2002. Boundary-layer integration approach to advection of sensible heat to a patchy snow cover. *Hydrological Processes.* 16: 3559-3569.

Gray, D.M., R.J. Granger and G.E. Dyck. 1985. Overwinter Soil Moisture Changes. *Transactions, ASAE*, 28: 442-447.

Gray D.M. and Landine P.G. 1987 Albedo model for shallow Prairie snow covers. *Canadian Journal Earth Sciences.* 24: 1760-1768.

Gray, D.M., Toth, B., Zhao, L., Pomeroy, J.W., and Granger, R.J., 2001. Estimating areal infiltration into frozen soils. *Hydrological Processes.* 15: 3095-3111.

Harding, R.J. and J.W. Pomeroy. 1996. The energy balance of the winter boreal landscape. *Journal of Climate.* 9: 2778-2787.

Hartman, M. D., J. S. Baron, R. B. Lammers, D. W. Cline, L. E. Band, G. E. Liston, C. Tague, Simulations of snow distribution and hydrology in a mountain basin. *Water Resources Research*. 35(5): 1587-1604.

Hinzman, L.D., Kane D.L., and Everett, K.R., 1993, Hillslope hydrology in an arctic setting: 6th International Conference on Permafrost, Beijing, China, 5-9 July, 1993, Proceedings (R-155).

Janowicz, J.R., Gray, D.M., and Pomeroy, J.W. 1997. Snowmelt and runoff in a subarctic mountain basin. In Millburn, D. (Eds). *Proceedings of the Hydro-ecology Workshop on the Arctic Environmental Strategy,* Symposium No. 16, National Hydrology Research Institute, Saskatoon: 303-320.

Janowicz, J.R. 2000. Spatial variability of snowmelt infiltration to frozen soil within the Yukon boreal forest. In; *Proceedings AWRA Conference Water Resources in Extreme Environments,* Anchorage, Alaska, May 1-3, 2000. Edited by D.L. Kane, 121-127.

Janowicz, J.R., Gray, D.M., and Pomeroy, J.W. 2002. Characterisation of snowmelt infiltration scaling parameters within a mountainous subarctic watershed. In *Proceedings, 59th Eastern Snow Conference*. Stowe Vermont.

Kane, D.L., Bredthauer, S.R., and Stein, J., 1981, Subarctic snowmelt runoff generation in Vinson, T., ed., The Northern Community: A Search for a Quality Environment, Proceedings, American Society of Civil Engineers, New York, p. 591-601.

Kane, D.L. and J. Stein, 1983. Field evidence of groundwater recharge in Interior Alaska. *Proc. 4th Int. Conf. Permafrost, Fairbanks:* National Academy Press, Washington, D.C., 572-577.

Kane, D.L., Hinzman, L.D., Benson, C.S., and Liston, G.E., 1991. Snow hydrology of a headwater Arctic basin 1. Physical measurements and process studies. *Water Resources Research.* 27:1099-1109.

Kane, D.L., Hinzman, L.D., Woo, M.K., and Everett, K.R., 1992. Arctic hydrology and climate change. In Chapin, F.S., Jefferies, R.L., Reynolds, J.F., Shavers, G.R., and Svoboda, J. (Eds). *Arctic Ecosystems in a Changing Climate: an Ecophysical Perspective* 35-57.

Kobayashi, D. 1985. Separation of the snowmelt hydrograph by stream temperatures. *Journal of Hydrology.* 76:155-162.

Kobayashi, D. 1986. Separation of a snowmelt hydrograph by stream conductance. *Journal of Hydrology.* 84:57-165.

Komarov VD, Makarova TT. 1973. Effect of the ice content, segmentation and freezing depth of the soil on meltwater infiltration in a basin. *Soviet Hydrology Selected Papers* 3: 243-249.

Kuchment, L.S. and Gelfan, A.N., 1996. The determination of the snowmelt rate and the meltwater outflow from a snowpack for modelling river runoff generation. *Journal of Hydrology.* 179:23-36.

Kuzik IA, Bezmenov AI. 1963. Infiltration into seasonally frozen soils. Soviet Soil Science. 7: 59-65.

Laudon H., J. Seibert, S. Köhler, K. Bishop. 2004. Hydrological flow paths during snowmelt: Congruence between hydrometric measurements and oxygen 18 in meltwater, soil water, and runoff. *Water Resources Research*. 40: W03102

Lewkowicz, A.G. and Ednie, M. 2004. Probability mapping of mountain permafrost using the BTS method, Wolf Creek, Yukon Territory, Canada. *Permafrost and Periglacial Processes.* 15:67-80.

Lindstrom, G., Bishop, K., and Lofvenius, M.K. 2002. Soil frost and runoff at Svartberget, northern Sweden-measurements and model analysis. *Hydrological Processes.* 16:3379-3392.

Liston, G. E. 1995. Local advection of momentum, heat, and moisture during the melt of patchy snow covers. *Journal of Applied Meteorology.* 34:1705-1715.

Liston, G.F. and Sturm, M. 1998. A snow-transport model for complex terrain. *Journal of Glaciology.* 45: 273-285.

Liston, G. E., 1999: Interrelationships among snow distribution, snowmelt, and snow cover depletion: Implications for atmospheric, hydrologic, and ecologic modeling. *Journal of Applied Meteorology*. 38:1474-1487.

Liston, G.E., McFadden, J.P., Sturm, M. and Pielke, R.A., 2002. Modelled Changes in arctic tundra snow, energy and moisture fluxes due to increased shrubs. *Global Changes Biology.* 8:17-32.

Luce, C.H., Tarboton, D.G., and Cooley, K.R., 1998. The influence of the spatial distribution of snow on basin-averaged snowmelt. *Hydrological Processes.* 12:1671-1683.

Luce, C.H., Tarboton, D.G., and Cooley, K.R. 1999. Sub-grid parameterization of snow distribution for an energy and mass balance snow cover model. *Hydrological Processes.* 13:1921-1933.
Male, D. H., 1980: The seasonal snowcover. *Dynamics of Snow and Ice Masses,* S. H. Colbeck, Ed., Academic Press, 305–395.

Male, D.H. and Gray, D.M. 1981. Snowcover ablation and runoff. In (Eds) Male, D.H. and Gray, D.M, *Handbook of Snow: Principles, Processes, Management and Use.* Pergamon Press, Toronto.

Marsh, P., and Woo, M.K., 1981. Snowmelt, glacier melt, and high arctic streamflow regimes. *Canadian Journal of Earth Science.* 18:1380-1384.

Marsh, P. and Woo, M.K., 1984. Wetting front advance and freezing of meltwater within a snowcover. 1. Observations in the Canadian Arctic. *Water Resources Research.* 20:1853-1864.

Marsh, P., and Woo, M.K., 1993. Infiltration of meltwater into frozen soils in a continuous permafrost environment. In *Proceedings, 6th International Conference on Permafrost, Beijing China* 443-448.

Marsh, P. and Pomeroy, J.W. 1996. Meltwater fluxes at an arctic forest-tundra site. *Hydrological Processes.* 10: 1383-1400.

Marsh, P., 1999. Snowcover formation and melt: recent advances and future prospects. *Hydrological Processes.* 13: 2117-2134.

Marsh, P., N. Neumann, R. Essery and J. Pomeroy. 1999. Model estimates of local scale advection of sensible heat over a patchy snow cover, p. 103-110. In M.R. Tranter, E. Armstrong, E. Brun, G. Jones, M. Sharp and M. Williams (ed.), Interactions between the cryosphere, climate and greenhouse gases. IAHS Publication No. 256, July 1999, Birmingham, UK.

McCann, S.B. and Cogley, J.G. 1972. Hydrological observations on a small arctic catchment, Devon Island. *Canadian Journal of Earth Science.* 9: 361-365.

McFadden, J.P., Liston, G.E., Sturm, M., Pielke, R.A., and Chapin, F.S. 2001. Interactions of shrubs and snow in arctic tundra: measurements and models. In *Soil-Vegetation-Atmosphere Transfer Schemes and Large-Scale Hydrological Models* (Proceedings of a symposium held during the Sixth IAHS Scientific Assembly at Maastricht, The Netherlands) Publ. No. 270, 2001 pg. 317-325.

McGlynn, B.L., McDonnell, J.J., Shanley, J.B., and Kendall, C. 1999. Riparian zone flowpath dynamics during snowmelt in a small headwater catchment. *Journal of Hydrology.* 222: 75-92.

McGlynn, B., McDonnell, J., Stewart, M., and Seibert, J., 2003. On the relationships between catchment scaled and streamwater mean residence time. *Hydrological Processes*. 17: 175-181.

McGlynn, B.L., McDonnell, J.J., Siebert, J., Kendall, C. 2004. Scale effects on headwater catchment runoff timing, flow sources, and groundwater-streamflow relations. *Water Resources Research.* 40: W07504.

McNamara, J.P., Kane, D.L., and Hinzman, L.D. 1997. Hydrograph separations in an Arctic Watershed using mixing model and graphical techniques. *Water Resources Research.* 33:1707-1719.

McNamara, J. P., Kane, D.L, Hinzman, L.D., 1998. An analysis of streamflow hydrology in the Kuparuk River Basin, Arctic Alaska: a nested watershed approach. *Journal of Hydrology.* 206:39-57.

Metcalfe RA, Buttle JM. 1999. Semi-distributed water balance dynamics in a small boreal forest basin. *Journal of Hydrology.* 226: 66–87.

Neumann, N. and Marsh, P. 1998. Local advection of sensible heat in the snowmelt landscape of Arctic tundra. *Hydrological Processes.* 12: 547-1560.

Pietroniro, A. and Soulis, E.D. 2003. A hydrology modelling framework for the Mackenzie GEWEX programme. *Hydrological Processes.* 17:673-676.

Pohl, S., Davison, B., Marsh, P. and Pietroniro, A. 2005. Modelling spatially distributed snowmelt and meltwater runoff in a small arctic catchment with a hydrology - land surface scheme (WATCLASS). *Atmosphere-Ocean,* 43: 193-211.

Pohl, S. and Marsh, P. 2006a. Small-scale modelling of spatially variable snowmelt in an arctic catchment. Paper accepted at *Hydrological Processes* (Publication Date March 2006).

Pohl, S., Marsh, P. and Pietroniro, A. 2006b. Spatial – temporal variability in solar radiation during spring snowmelt. Paper accepted at *Nordic Hydrology*.

Pohl, S., Marsh, P. and Liston, G. E. 2006c. Spatial – temporal variability in turbulent fluxes during spring snowmelt. Paper submitted to *Arctic, Antarctic and Alpine Research.*

Pomeroy, J. W., and D. M. Gray, 1995: Snowcover accumulation, relocation and management. National Hydrology Research Institute Science Rep. 7, Environment Canada, Saskatoon, SK, Canada, 134 pp.

Pomeroy, J.W., Marsh, P., and Gray, D.M. 1997. Application of a distributed blowing snow model to the arctic. *Hydrological Processes.* 11: 1451-1464.

Pomeroy, J.W. and Goodison, B.E. 1997. Winter and Snow. In Bailey, W.G., Oke, T.R., Rouse, W.R. (Eds). *The surface climates of Canada.* McGill-Queen's University Press, Montreal.

Pomeroy, J.W, Gray, D.M., Shook, K.R., Toth, B., Essery, R.L.H., Pietroniro, A. and Hedstrom, N. 1998. An evaluation of snow accumulation and ablation processes for land surface modelling. *Hydrological Processes.* 15: 2339-2367.

Pomeroy, J.W., R. Essery, D.M. Gray, K.R. Shook, B. Toth and P. Marsh, 1999a. Modelling snow-atmosphere interactions in cold continental environments. In, (ed. M. Tranter et al.) Interactions between the Cryosphere, Climate and Greenhouse Gases. IAHS Publ. No. 256. IAHS Press, Wallingford, UK. 91-102.

Pomeroy, J.W., N. Hedstrom and J. Parviainen. 1999b. The snow mass balance of Wolf Creek. In, (eds. J. Pomeroy and R. Granger) *Wolf Creek Research Basin: Hydrology, Ecology, Environment*. National Water Research Institute. Minister of Environment: Saskatoon. 15-30.

Pomeroy, J. W., Toth, B., Granger, R. J., Hedstrom, N. R., Essery, R. L. H. 2003: Variation in Surface Energetics during Snowmelt in a Subarctic Mountain Catchment. *Journal of Hydrometeorology.* 4: 702–719.

Pomeroy, J.W., Essery, R., Toth, B. 2004. Implications of spatial distributions of snow mass and melt rate for snow-cover depletion: observations in a subarctic mountain catchment. *Annals of Glaciology.* 38: 195-201.

Price, A. G. and Dunne, T. 1976. Energy balance computations of snowmelt in a subarctic area. *Water Resources Research.* 12:686–694.

Quinton, W.L. and Marsh, P. 1998. The influence of mineral earth hummocks on subsurface drainage in the continuous permafrost zone. *Permafrost and Periglacial Processes.* 9:213-228.

Quinton, W.L. and Marsh, P. 1999. A conceptual framework for runoff generation in a permafrost environment. *Hydrological Processes.* 13: 256-2581.

Quinton, W.L., Gray, D.M., and Marsh, P. 2000. Subsurface drainage from hummock-covered hillslopes in the Arctic tundra. *Journal of Hydrology.* 237: 113-125.

Quinton, W.L., and Gray, D.M. 2001. Estimating subsurface drainage from organic-covered hillslopes underlain by permafrost: toward a combined head and mass flux model. *Soil-Vegetation-Atmosphere Transfer Schemes and Large-Scale Hydrological Models* (Proceedings of a symposium held during the Sixth IAHS Scientific Assembly at Maastricht, The Netherlands. IAHS Publ. no. 270: 333-341.

Quinton, W.L., Carey, S.K., Goeller, N.T. 2004. Snowmelt runoff from northern alpine tundra hillslopes: major processes and methods of simulation. *Hydrology and Earth System Sciences.* 8:877-890.

Quinton, W.L. 2005 Personal Communication.

Reedyk, S., Woo, M., and Prowse, T. 1995. Contribution of icing ablation to streamflow in a discontinuous permafrost area. *Canadian Journal of Earth Sciences.* 32: 13-20.

Roulet, N.T., and Woo, M.K., 1988. Runoff generation in a low arctic drainage basin. *Journal of Hydrology.* 101: 213-226.

Russell, M., Marsh, P., and Onclin, C. 2004. A continuous dye injection system for estimation discharge in snow-choked streams. *Arctic, Antarctic, and Alpine Research.* 36:539-554.

Santeford, H.S. 1978. Snow soil interactions in interior Alaska. In *Proceedings, Modelling of Snow Cover Runoff.* Cold Regions Research and Engineering Laboratory, Hanover, NH. pg. 311-318.

Seyfried, M.S. and Wilcox, B.P., 1995. Scale and the nature of variability: Field examples having implications for the hydrologic modeling. *Water Resources Research.* 31: 173-184.

Shanley, J.B. and Chalmers, A. 1999. The effect of frozen soil on snowmelt runoff at Sleepers River, Vermont. *Hydrological Processes.* 13:1843-1857.

Shook, K. 1995. Simulation of the Ablation of Prairie Snowcovers, Ph.D. thesis, Department of Agricultural and Bioresource Engineering, University of Saskatchewan, Saskatoon, Saskatchewan, Canada, p. 189.

Shook, K., Gray, D.M., 1997. Snowmelt resulting from advection. *Hydrological Processes.* 11:1725-1736.

Seibert, J. and McDonnell, J.B160 2002. The quest for an improved dialog between modeler and experimentalist. *In Qingyun Duan, Hashin V. Gupta, Soroosh Sorooshian, Alain N. Rousseau, and Richard Turcotte (Eds.), Calibration of Watershed Models, AGU Water Science and Application Series, 346 pp.*

Shipak I.S. 1969. Relationship between the runoff coefficient and moisture content and depth of freezing of the soil. *Soviet Soil Science.* 1: 702-706.

Sivapalan, M.2003. Prediction in ungauged basins:A grand challenge for theoretical hydrology, *Hydroligal Processes.* 17:3163–3170.

Sklash, M.G. and Farvolden, R.N. 1979. The role of groundwater in storm runoff. *Journal of Hydrology*. 43:45-65.

Slaughter, C.W. and D.L. Kane, 1979. Hydrologic role of shallow organic soils in cold climates. In Canadian Hydrology Symposium '79 Cold Climate Proceedings: National Research Council of Canada, Ottawa, pg 380-389.

Soulsby, C., Helliwell, R.C., Ferrier, R.C., Jenkins, A., and Harriman, R., 1997. Seasonal snowpack influence on the hydrology of a sub-arctic catchment in Scotland. *Journal of Hydrology.* 192: 17-32.

Soulsby, C., Rodgers, P., Smart, R., Dawson, J. and Dunn, S. 2003. A tracer-based assessment of hydrological pathways at different spatial scales in a mesoscale watershed in NE Scotland. *Hydrological Processes*. 17:759-777.

Stewart, I.T., Cayan, D.R., and Dettinger, M.D. 2004. Changes in snowmelt runoff timing in western North America under a 'business as usual' climate change scenario. *Climatic Change.* 62: 217-232.

Sturm, M., J. P. McFadden, G. E. Liston, F. S. Chapin, III, C. H. Racine, and J. Holmgren, 2001. Snow-shrub interactions in Arctic tundra: a hypothesis with climatic implications. *Journal of Climate*. 14: 36-344.

Tarboton, D.G., Bloschl, G., Cooley, K.R., Kirnbauer, R., and Luce, C.H. 2000. Spatial snow cover processes at Kuhtai and Reynolds Creek. In (Eds) Grayson, R., and Bloschl, G., *Spatial Patterns in Catchment Hydrology: Observations and Modelling*. University Press, Cambridge. pg 158-186.

Uhlenbrook S, Frey M, Leibundgut C, and Maloszewski P. 2002. Hydrograph separations in a mesoscale mountainous basin at event and seasonal timescales. *Water Resources Research.* 38 (6): Art. No. 1096.

Weisman, R.N. 1977. Snowmelt: a two-dimensional turbulent diffusion model. *Water Resources Research*. 13:337-342.

Westerstrom, G., Singh, V.P., 2000. An investigation of snowmelt runoff on experimental plots in Lulea, Sweden. *Hydrological Processes.* 14: 1869-1885.

Williams, P. J., and Smith, M. W. 1989. *The Frozen Earth: Fundamentals of Geocryology, Cambridge Univ. Press, New York.*

Woo, M.K., 1986. Permafrost Hydrology in North America. *Atmosphere and Ocean*. 24: 201-234.

Woo, M.K. 1997. A guide for ground based measurement of arctic snow cover. Publication for Canadian Cryospheric Information Network. p. 30.

Woo, M.K. and Sauriol, J., 1980. Channel development in a snow-filled valley, Resolute, N.W.T. Canada. *Geografiska Annaler.* 62:37-56.

Woo, M.K. and Young, K.L. 1997. Hydrology of a small drainage basin with a polar oasis environment, Fosheim Peninsula, Ellesmere Island, Canada. 1997. *Permafrost and Periglacial Processes.* 8: 257-277.

Woo, M.K. and Giesbrecht, M. 2000. Simulation of snowmelt in a subarctic spruce woodland: 1. tree model. *Water Resources Research.* 36: 2275-2285.

Woo, M.K., Marsh, P., and Pomeroy, J.W., 2000. Snow, frozen soils and permafrost hydrology in Canada, 1995-1998. *Hydrological Processes* 14: 1591-1611.

Woo, M.K., and Marsh, P. 2005. Snow, frozen soils and permafrost hydrology in Canada, 1999-2002. *Hydrological Processes* 19:215-229.

Wu, P., R. Wood, and P Scott, 2005. Human influence on increasing Arctic river discharges. *Geophysical Research Letters.* 32, L02703, doi:10.1029/2004GL021570.

Xia, Z.J. and Woo, M.K. 1992. Theoretical analysis of snow-dam decay. *Journal of Glaciology.* 38:191-199.

Zhao, L. and Gray, D.M. 1997. A parametric expression for estimating infiltration into frozen soils. *Hydrological Processes.* 11:1761-1775.

Zhao, L. and Gray, D.M. 1999. Estimating snowmelt infiltration into frozen soils. Hydrological Processes 13:1827-1842.

Zhao, L., Gray, D.M., and Male, D.H. 1997. Numerical analysis of simultaneous heat and mass transfer during infiltration into frozen ground. *Journal of Hydrology.* 200 345-363.

Zoltai, S.C., Tarnocai, C., Mills, G.F. and Velduis, H. 1988. Wetlands of Canada. Ecological Land Classification Series No. 24. Environment Canada, Ottawa, and Polyscience Publications Inc., Montreal.

APPENDIX A

	Transect Start		Transect End		Elevation Range (NTS)	
	North	**West**	**North**	**West**	**Lower**	**Upper**
SS1	60˚32.882’	135˚11.804’	60˚33.094’	135˚12.111’	1440	1480
SS2	60˚32.991’	135˚12.892’	60˚33.027’	135˚13.010’	1500	1540
TS1	60˚32.757’	135˚11.761’	60˚32.882’	135˚11.804’	1400	1480
TS2	60˚32.640’	135˚12.339’	60˚32.679’	135˚12.534’	1500	1600
TS3	60˚33.000’	135˚13.235’	60˚32.967’	135˚13.044’	1540	1600
NF	N/A	N/A	N/A	N/A	1350	1400
SF	N/A	N/A	N/A	N/A	1350	1520
UX	60˚32.818’	135˚13.952’	60˚32.945’	135˚13.131’	1600	2080
LX	60˚32.986’	135˚11.964’	60˚33.093’	135˚12.111’	1440	1500

Geographic co-ordinates of Landscape Unit transects and elevation range

APPENDIX B

Photographs of NF LU (Figure B1 left) and SF LU (Figure B2 right).

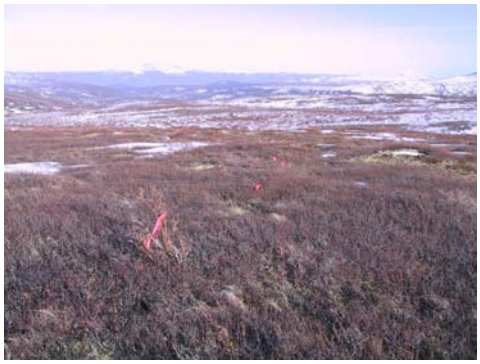

Photographs of SS1 LU (Figure B3 left) and SS2 LU (Figure B4 right).

Photographs of TS1 LU (Figure B5 left) and TS2 LU (Figure B6 right).

Photograph of TS3 LU (Figure B7).

Photograph of UX LU (Figure B8 left) and LX LU (Figure B9 right).

APPENDIX C

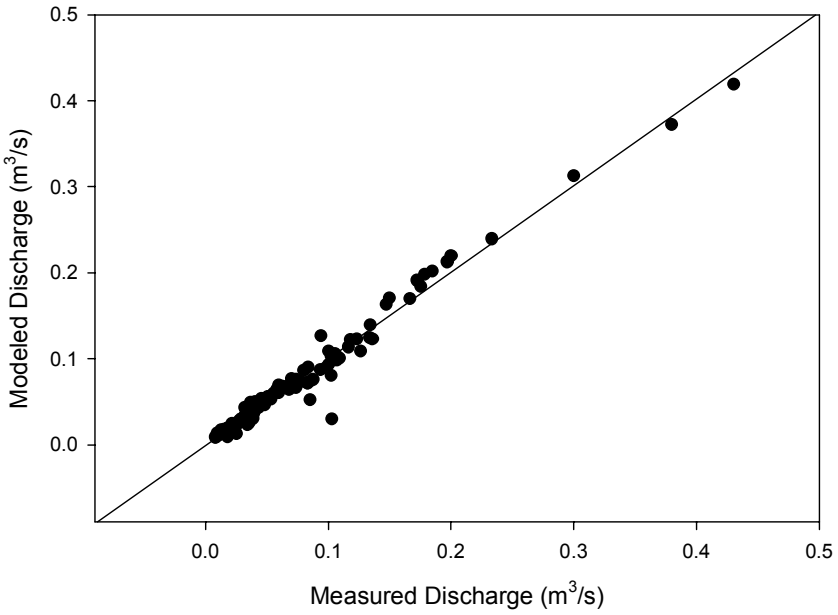

Regression of measured discharge versus the modeled discharge using the stage discharge relationship (Figure C1).

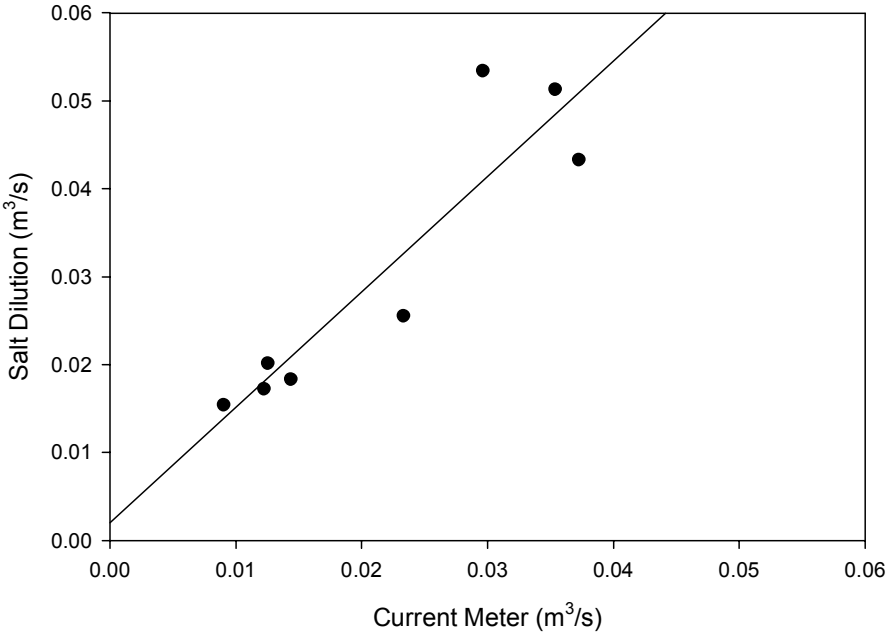

Regression of discharge measurements comparing the current meter to the salt dilution method (Figure C2).

APPENDIX D

In depth discussion of net radiation results.

Net radiation data was available for SF, NF, SS1 and the TS1 proxy site. Data presented consists of daily net-radiation and cumulative net radiation to the ground surface from JD 100 to JD 170. During this time, SF, TS1 Proxy and SS1 each had similar daily mean net radiation values. Net radiation was positive for these three sites with the exception of SF on JD 100 and JD 105. The TS1 Proxy site followed a pattern very similar to that of SF with the following exceptions: 1) on a daily basis, net radiation was positive for the entire study period, and 2) there was no drop in net radiation on JD 138 as observed at the NS and SF towers. Net radiation was obtained near SS1 for only a short period, between JD 108 and 131. SS1 followed a pattern similar to that of the SF and TS1 proxy site but did not have the same high daily peaks exhibited by SF because of the reduced aspect. After JD 110, daily average net radiation approximately tripled from less than 5 MJ day^{-1} to nearly 15 MJ day^{-1} by JD 115. It was by JD 115 when the average daily net radiation was no longer negative for NF. Although the north and south towers were less than 300 meters apart, their contrasting aspects yielded pronounced differences with respect to net radiation, which had implications on the total energy available for melt. From JD 100 to JD 132, daily net radiation for SF was significantly greater than NF LU. For each of the four sites there were similar patterns in the day to day radiation regimes, but the large contrast in the early part of the snowmelt season had implications on the cumulative radiation. By the time the NF cumulative net radiation was no longer negative (JD 123) the other sites had already accumulated more than *ca* 100 MJ.

APPENDIX E

In depth discussion of air temperature results.

Mean daily air temperatures were available for SF, NF, SS1, UX, and the TS1 Proxy site. All sites followed a similar trend in temperature patterns throughout the study period. The only exception was that UX was on average 2.1 ºC (+/- 1.01 ºC) colder than the other sites in the basin for the duration of study. While the actual TS1 LU was adjacent to SS1 and air temperature could be extrapolated to it, the data obtained from the TS1 Proxy site, located slightly outside the basin, was included for comparative purposes. Mean daily air temperature was above 0 ºC for all locations from JD 113 to 120, the same period when net radiation for SF, SS1, and the TS1 Proxy site first became positive. Temperatures for all locations, except UX, remained below freezing from JD 121 until JD 127. UX remained below freezing until JD 128. Following this, air temperature increased, and was above freezing from JD 127 to 131 for NF and SF, JD 127 to 130 for SS1, and JD 128 to 130 for UX. The TS1 proxy site also experienced warmer temperatures from JD 126 to 132. This second period for all locations was not as warm as observed during the JD 113 to 120 time period. The second and final freezing events of the study period occurred between JD 132 and 136 for SF and NF, JD 133 to 136 for SS1 and the TS1 Proxy site, and JD 131 to 137 for UX.

The mean daily air temperatures were similar for SF, NF, SS1, and the TS1 Proxy site, and while the diurnal pattern for UX was also similar, this LU was on average 2.1 ºC (+/- 1.01 ºC) colder than the lower portion of the basin for the duration of study. Air temperature at the UX LU typically declined earlier and remained colder longer than all other sites. With respect to NF and SF, the SF typically had a slightly higher mean daily temperature and was on average 0.45 ºC (+/- 0.28) greater on all but 13 days after JD 125. This similarity in air temperature despite large differences in net radiation has been observed previously at this site and elsewhere within the basin (Carey and Woo, 1998; Pomeroy et al. 2003).